

**DEVELOPMENT OF METAL AND METAL OXIDE  
NANOSTRUCTURES FOR SURFACE ENHANCED  
RAMAN SCATTERING**

*Thesis submitted to*  
***Cochin University of Science and Technology***  
*in partial fulfillment of the requirements*  
*for the award of the degree of*  
***Doctor of Philosophy***

**Hasna K**

**Department of Instrumentation**  
**Cochin University of Science and Technology**  
**Cochin - 682022, Kerala, India**

**August 2016**

Development of metal and metal oxide nanostructures for surface enhanced Raman scattering

*Ph.D. thesis in the field of surface enhanced Raman spectroscopy*

*Author:*

Hasna K.  
Nanophotonic and Optoelectronic Devices Laboratory  
Department of Physics  
Cochin University of Science and Technology  
Cochin - 682 022, Kerala, India.  
Email: hasnaprovidence@gmail.com

*Supervisors:*

Dr. K. Rajeev Kumar  
Associate Professor  
Department of Instrumentation  
Cochin University of Science and  
Technology  
Cochin - 682 022, Kerala, India.  
Email: rajeev@cusat.ac.in

Dr. M. K. Jayaraj  
Professor  
Department of Physics  
Cochin University of Science and  
Technology  
Cochin - 682 022, Kerala, India.  
Email: mkj@cusat.ac.in

August 2016

Dedicated to my Vappichi and Ummachi





**Department of Instrumentation,  
Cochin University of Science and Technology,  
Kochi-682022, India**

---

**Dr. K. Rajeev Kumar**  
Associate Professor

---

17<sup>th</sup> August 2016

## *Certificate*

Certified that the work presented in this thesis entitled ***“Development of metal and metal oxide nanostructures for surface enhanced Raman scattering”*** is based on the authentic record of research carried out by Hasna K. under the joint guidance of myself and Prof. M. K. Jayaraj, at Department of Instrumentation, Cochin University of Science and Technology & at Nanophotonic and optoelectronic devices laboratory, Department of Physics, Cochin University of Science and Technology, and has not been included in any other thesis submitted for the award of any degree. All the relevant corrections and modifications suggested by the audience during the pre-synopsis seminar and recommendations by doctoral committee of the candidate have been incorporated in the thesis.

**Dr. K. Rajeev Kumar**  
(Supervising Guide)

---

Phone: +91 484 2862359 Email: rajeev@cusat.ac.in





**Department of Physics,  
Cochin University of Science and Technology,  
Kochi-682022, India**

---

**Dr. M. K. Jayaraj**  
Professor

---

17<sup>th</sup> August 2016

## *Certificate*

Certified that the work presented in this thesis entitled ***“Development of metal and metal oxide nanostructures for surface enhanced Raman scattering”*** is based on the authentic record of research carried out by Hasna K. under my co-guidance at Nanophotonic and optoelectronic devices laboratory, Department of Physics, Cochin University of Science and Technology and at Department of Instrumentation, Cochin University of Science and Technology, and has not been included in any other thesis submitted for the award of any degree. All the relevant corrections and modifications suggested by the audience during the pre-synopsis seminar and recommendations by doctoral committee of the candidate have been incorporated in the thesis.

**Dr. M. K. Jayaraj**  
(Co-guide)

---

Phone: +91 484 2577404 extn. 33 Email: [mkj@cusat.ac.in](mailto:mkj@cusat.ac.in)



## ***Declaration***

I hereby declare that the work presented in this thesis entitled **“Development of metal and metal oxide nanostructures for surface enhanced Raman scattering”** is based on the original research work carried out by me under the joint supervision and guidance of Dr. K. Rajeev Kumar, Associate Professor, Department of Instrumentation, Cochin University of Science and Technology, Cochin-682022 and Dr. M. K. Jayaraj, Professor, Department of Physics, Cochin University of Science and Technology, Cochin-682022 and has not been included in any other thesis submitted previously for the award of any degree.

Kochi- 22  
17<sup>th</sup> August 2016

**Hasna K.**



## Acknowledgements

*My dream of attaining doctorate in Physics was made possible only through the lasting support and collaborative work of many people. I would like to write a few words to thank all of them.*

*First and foremost, I express my sincere gratitude to my supervisor, Prof. M. K. Jayaraj, for his generous guidance and support. He always inspired and encouraged my spirit to move into diverse fields of research. I appreciate that he led me in the right direction in research and gave sufficient freedom to try my ideas. Even though we were new in the area of Raman spectroscopy, we could generate a thesis in the field only due to the great effort, support and wise guidance given by Jayaraj sir during the various phases of research. I always wondered about his acumen to utilize various opportunities to achieve our goal. I could conduct experiments at Universitat Politècnica de Catalunya (UPC), Spain and at Nanyang Technological University, Singapore, all of which made my thesis fruitful, only because of his well-timed effort. Besides research, interaction with him helped to learn mentorship and professionalism, which in turn strengthened my personality. His words helped me to move forward with a positive outlook during the difficult and trying times of research. Sir, I thank you for the opportunity given to become a member of the OED family that made my research life enjoyable.*

*I would also like to extend my deepest gratitude to Dr. K. Rajeev Kumar, Department of Instrumentation, CUSAT, under whom I joined for research. I am thankful for the freedom that he gave to conduct my research study at the department of Physics, CUSAT and for his support, help and patience during different phases of my research. I always appreciate his way of interaction with people and the respect that he showed even during his interaction with students.*

*I owe my special thanks to Dr. Aldrin Antony, whose innovative ideas along with unconditional help and support helped me a lot during nanofabrication work at IBEC Barcelona and at UPC, Barcelona. I am also thankful for the memorable*

moments during my stay in Barcelona. Words cannot express my feelings for the encouragement given for travelling alone to Catania which turned into an everlasting beautiful experience in my life.

I express my hearty thanks to Prof. Joaquim Puigdollers, UPC, Spain, for the endless support to conduct experiments at IBEC Barcelona and at UPC, Barcelona. Without any hesitation, he always spent time for creative ideas and supported me financially for the successful completion of the experiments. I also appreciate the hard work and dedication shown by Ms. Judith Linacero, Ms. Yolanda and Ms. Maria Jesus, IBEC, Barcelona to complete nanofabrication successfully.

I express my sincere gratitude to Prof. V. M. Murugesan, Nanyang Technological University, Singapore who gave an opportunity to conduct simulation work at School of mechanical and Aerospace engineering, Nanyang Technological University, Singapore which in turn contributed a lot to my research work. I gratefully remember the freedom and support that I had in his lab. I am thankful to Dr. James who helped me to learn the FDTD simulation and also for the help and support given during my stay at Singapore. I am also thankful to Dr. V. K. Shinoj for his affection, support and care that made my life more beautiful at Singapore.

I am thankful to Dr. Padma Nambisan, Department of Biotechnology, CUSAT, for her valuable suggestions and to Ms. Kiran Lakshmi who put in great effort to prepare biological sample for me during her busy schedule.

I would like to thank Dr. Manzoor. K, Amrita Viswa Vidyapeetham University, Kochi, for valuable discussions and support. Special thanks to Dr. Girish C M, who spent the time to conduct experiments for me in his busy time schedule and also for his valuable suggestions.

I thank former and present heads of the department of Instrumentation, members of doctoral committee and research committee and the entire faculty at the department of Instrumentation for their support.

*I thank all my teachers at the department of Physics for their kind words and support. Special thanks to Prof. Ramesh Babu, who inspired and influenced me a lot as a teacher. I also thank Prof. M. R. Antharaman and Prof. S. Jayalakshmi for their encouragement and support given during my Ph.D. work.*

*I thankfully remember my Plus Two tuition teacher, Sreeraj Sir who inspired me to enter the exciting world of Physics which in turn transformed into a good turning point in my life. I also thank other teachers during my school days and college days who added to my knowledge in Physics and Mathematics.*

*I thank Mr. Morisson, Laser Spectra, Bangalore for his dedicated support and service to maintain microRaman spectrometer in working condition so that I could successfully complete my work. His dedication to the job is really appreciating and inspiring.*

*I acknowledge UGC, Govt. of India for the research fellowship. I am also thankful to CSIR, India, and DST, India for the international travel grant. I thank Ministerio de Economía y Competitividad (MICINN), Spain for the financial support during my short stay at Universitat Politècnica de Catalunya, Barcelona*

*I thank STIC CUSAT, IISc Bangalore, IIT Bombay and MG University, Kottayam for the characterization facilities provided.*

*Nonacademic support is always an essential part to complete a course. It is my pleasure to thank all office staff at Department of Instrumentation and at Department of Physics, CUSAT for their help during my Ph.D. Special thanks to Antony Sir for his patience, support and friendship. I am also thankful to Mani Ram Sir and Mathew Sir for their dedicated work and help.*

*I express my thanks to all the staffs of Academic Section, especially Ms. Praseetha, Administrative Office, CUSAT, for their help and service.*

*Friendships are always the special gifts in our life. Thanks to Deepu, Anju, Subha and Sarithechi for their true friendship, unconditional care, encouragement, support and beautiful memories that I am going to cherish for a lifetime. Their advices, loving words and criticisms helped me to acquire all the positive personality attributes.*

*Research life at OED lab has endowed me with a wealth of experiences and beautiful memories. I thank all my dear friends at OED lab, who shared an enjoyable period of my life and created a homely atmosphere in the lab. Special thanks to Vikas for the care and support during various stages of research and for the bright moments we shared. I remember the help and support by Anjana, Shijeesh and Jasna during the last stage of my research. I thank Kurias, Abhayjith and Manu for the relaxing and funny moments in and outside the lab. I also thank Dr. James for his care and affection towards me. I thank Dr. Krishna Prasad, Dr. Aneesh, Dr. Arun Aravind, Dr. Sasanka Kumar, and Dr. Sreeja for their help and support at various stages of research. I also thank other members of OED family for their support.*

*I also thank Savitha and Dr. Subin Thomas for their open friendship, endless help and support.*

*I happily remember my life at Athulya hostel and my hostel mates who added colorful memories to my life. I also thank all my friends at the department of Physics and department of Chemistry for their support.*

*No words to thank my Vappichi and Ummachi, who are always with my dreams. They allowed unbounded freedom so that I could think, dream and move freely to reach up to here. It is only because of their support that I could lead a beautiful research life and I am fortunate to get all achievements in my life. I specially thank my sister Mrs. Seenath for motherly love and support. Special thanks to my brother in law- Mr. Noushad, for his friendship, affection, and care in my life. I also thank my sister in law Mrs. Shamseera for adjusting my laziness in home and sisterly care. My lovable thank to my brothers- Mr. Dulkkifli and Mr. fazil, my sisters- Mrs. Sajitha and Mrs. Rashida, my brothers in law- Mr. Shereef and Mr. Suhail for their affection and support throughout. I thank to all my nephews and nieces -Sarfaz, Aju, Minnu, Hamna, Safa, Akku, Annu, Munna and Paathu for the cute moments.*

*Thank you very much, everyone!*

*Hasna K*

## ||| Preface |||

Raman spectroscopy is a non-destructive technique that provides molecular fingerprint, an information which is highly desired in the fields of chemistry, environmental science, biology, medicine, and nanotechnology. The low scattering cross section of Raman effect hindered its applicability to a large extent and this led to the development of a new technique with extreme sensitivity and selectivity. In this new technique known as surface enhanced Raman spectroscopy (SERS), molecules are attached to nanometer sized metallic structures, and results in strongly enhanced Raman signals. The order of Raman signal enhancement is up to  $10^{12}$ - $10^{14}$  which enables detection of even a single molecule. The inherent ability of Raman spectra to identify specific molecules along with the advantages of SERS such as narrow spectral bandwidths, ability for fluorescence quenching, capacity to be used with or without optical labels, etc., make it a good choice for cellular imaging and biosensing, detection of chemical and bioanalytes, explosives, etc.

Enhancement mechanism in SERS is mainly divided into two: electromagnetic enhancement (EM) and chemical enhancement (CE), EM enhancement being the dominant. EM enhancement is due to the enhanced electric field produced in the vicinity of metal nanostructure during localized surface plasmon resonance (LSPR). Generally, SERS substrates include nanocolloids, roughened electrodes and periodic nanostructures, made of coinage metals like silver, gold and copper that exhibit LSPR in visible spectra region. The SERS efficiency dramatically increases when molecules are adsorbed to "hot spots" in SERS substrates. Although this can be achieved through sophisticated lithographic methods, these approaches face difficulties such as time consumption, cost and scale-up issues. The field lacks fabrication of cost-effective SERS active substrate over a large area with uniform array of "hot spots" in a reproducible way, to be implemented in practical applications.

First part of the thesis comprises the fabrication of an efficient and reproducible SERS substrate in a cost-effective way using silver nanotriangular arrays via nanoimprinting technique. Also a recyclable SERS substrate has been developed by decorating silver nanoparticles onto titanium dioxide nanorods. The second part of the thesis is about investigation of electromagnetic and chemical enhancement mechanisms. Correlation between excitation wavelength and surface plasmon resonance wavelength for observing SERS is investigated using gold nanotriangular arrays. Photo-induced charge-transfer mechanism in TiO<sub>2</sub> nanostructures is also investigated. Last part of the thesis is the demonstration of bio and chemical sensing applications of SERS. Label-free DNA detection and food adulterant detection by SERS is successfully demonstrated.

**Chapter 1** is devoted to the basic principles of Raman spectroscopy, its instrumentation and an overview of surface enhanced Raman scattering (SERS). The various enhancement mechanisms, evolution of SERS active substrates and its application in various fields are described in detail.

**Chapter 2** deals with the development of colloidal SERS active substrate using silver nanocubes synthesized via solvothermal method. Finite-difference time-domain simulation is carried out in detail to visualize dipole generation in nanocube during localized surface plasmon resonance and to locate the respective "hot spots" in silver nanocubes responsible for the huge Raman enhancement. The prediction is verified by the SERS analysis of the synthesized nanocubes using Rhodamine 6G molecule. An excellent sensitivity with a detection limit of  $10^{-17}$  M and an enhancement factor of  $1.2 \times 10^8$  confirm "hot spots" in the nanocubes. SERS activity is also performed for crystal violet and for food adulterant Sudan I molecule.

**Chapter 3** highlights the fabrication of patterned or periodic SERS substrates with uniformly distributed "hot spots". These substrates possess spatial reproducibility as well as sample to sample reproducibility. The silicon

master with inverted pyramidal structure is fabricated via photolithography and SERS substrate is replicated from the silicon master using a commercially available replication kit. In addition to the reproducibility in SERS enhancement, the method also offers fabrication of an economic SERS substrate. But the sensitivity is low due to the lesser number of "hot spots" in the detection volume. To fabricate a patterned substrate with very high sensitivity, nanotriangular array based SERS substrate is designed. Large area arrays of nanotriangular pits are successfully fabricated via electron beam lithography (EBL). To conquer drawback related to expense of EBL, nanoimprinting technique is employed to fabricate nanotriangular arrays. Based on the fabricated nanotriangular arrays, highly competent SERS active substrates with advantages such as cost effectiveness, uniformity over large area, reproducibility and excellent sensitivity with enhancement factor of  $2.9 \times 10^{11}$  is introduced. This enhancement factor is the highest compared to reported values for patterned SERS substrates.

**Chapter 4** discusses fabrication of multifunctional recyclable Ag-TiO<sub>2</sub> based 3D hybrid SERS active substrates by a simple and novel method. The TiO<sub>2</sub> nanorods are grown on fused silica in a single step by hydrothermal method and Ag nanoparticles are assembled simultaneously, merely by chemical reduction. The inclined growth of TiO<sub>2</sub> nanorods leads to the formation of different types of "hot spots". As prepared substrates exhibit enhancement factor of about  $7 \times 10^8$  with single molecule detection capability. The recycling capacity of Ag-TiO<sub>2</sub> based SERS substrate is verified, which unlock a new opportunity to get rid of single-use problem with traditional SERS substrates. The substrate can be a promising multifunctional sensor for detection of food adulterants, organic pollutants, pesticides, etc.

**Chapter 5** summarizes the results on the investigation of SERS enhancement mechanism such as correlation between excitation wavelength, LSPR wavelength to produce EM enhancement mechanism and role of surface

state energy level in producing chemical enhancement effect in metal oxide nanostructures. With the help of gold nanotriangular arrays, it is observed that SERS effect is observable only if the position of LSPR and excitation wavelength of laser are within a range. In order to investigate photo-induced charge-transfer mechanism, TiO<sub>2</sub> nanorods are synthesized by hydrothermal method and TiO<sub>2</sub> nanoparticles are synthesized by chemical precipitation method. It is observed that surface state energy level mediate the charge-transfer in TiO<sub>2</sub> nanostructures.

**Chapter 6** describes the possibility of SERS technique in bio and chemical sensing applications. In order to demonstrate SERS as an inexpensive and an easily processable food adulterant sensor, the fabricated SERS substrate is employed for the detection of Sudan I and melamine. Sudan I with a concentration of 10<sup>-6</sup> M and melamine with a concentration of 10<sup>-10</sup> M are detected via SERS. To investigate the applicability of SERS technique as a biosensor, label-free detection of DNA of salmon fish and E. coli are also demonstrated. The DNA detection by SERS opens up a new technique for cancer cell detection and also for DNA barcoding.

**Chapter 7** summarizes the entire work along with future prospects.

## Contents

### Chapter 1

#### An overview of surface enhanced

#### Raman spectroscopy ..... 01 - 55

1.1 Raman spectroscopy.....	02
1.1.1 Introduction.....	02
1.1.2 Classical theory of Raman scattering .....	05
1.1.3 Limitations of normal Raman spectroscopy .....	07
1.2 Surface enhanced Raman scattering/spectroscopy.....	07
1.2.1 Historical background.....	08
1.2.2 Enhancement mechanism in surface enhanced Raman scattering.....	10
1.2.2.a Electromagnetic enhancement mechanism (EM enhancement).....	11
1.2.2.b Chemical enhancement mechanism (CE).....	22
1.2.3 Factors influencing EM enhancement .....	25
1.2.4 Factors influencing the SERS enhancement .....	28
1.3 Advancement of SERS substrates.....	29
1.4 Interpretation of SERS spectra.....	32
1.5 Enhancement factor.....	33
1.6 Applications of SERS.....	34
1.6.1 Applications of SERS in biosensing.....	35
1.6.2 Applications of SERS in electrochemical systems.....	36
1.6.3 Applications of SERS in environmental analysis.....	36
1.6.4 Applications of SERS in bioimaging .....	37
1.7 Raman instrumentation.....	38
1.7.1 Laser source.....	39
1.7.2 Sample-illumination system.....	41
1.7.3 Filters.....	41
1.7.4 Charge coupled devices .....	42
1.8 Advancements in surface enhanced Raman scattering.....	42
1.8.1 Extension of SERS to transition metals .....	43
1.8.2 Fabrication of versatile SERS active substrates .....	44
1.8.3 Single molecule SERS .....	45
1.8.4 Tip enhanced SERS.....	45
1.9 SERS probes .....	46
References.....	48

## *Chapter 2*

### **Development of colloidal SERS substrates**

<b>using silver nanocubes.....</b>	<b>57 - 83</b>
2.1 Introduction .....	58
2.2 Literature review on colloidal SERS substrates .....	59
2.3 Synthesis of silver nanocubes by solvothermal method.....	63
2.4 Characterization of silver nanocubes .....	65
2.4.1 Morphological characterization.....	65
2.4.2 Optical characterization.....	68
2.4.3 Electric field enhancement studies in silver nanocubes.....	72
2.4.4 SERS characterization of silver nanocubes .....	74
2.5 Conclusion .....	80
References.....	80

## *Chapter 3*

### **Development of patterned SERS substrates using pyramidal arrays and**

<b>nanotriangular arrays.....</b>	<b>85 - 115</b>
3.1 Introduction.....	86
3.2 Experimental details .....	89
3.2.1 Fabrication of inverted pyramidal structures by photolithography .....	89
3.2.2 Fabrication of pyramidal array based SERS substrate .....	91
3.3 Results and discussion.....	92
3.3.1 Morphological characterization.....	92
3.3.2 SERS studies on pyramidal arrays .....	93
3.4 Fabrication of nanotriangular array based SERS substrate.....	97
3.4.1 Fabrication of silicon master substrates with nanotriangular pits via EBL .....	98
3.4.2 Fabrication of nanotriangular pillars via NIL .....	102
3.5 Results and discussion.....	104
3.5.1 FDTD simulation .....	104
3.5.2 SERS characterization .....	106
3.7 Conclusion .....	112
References.....	112

## *Chapter 4*

### **Development of recyclable SERS substrates using TiO<sub>2</sub> nanorods decorated**

#### **with Ag nanoparticles ..... 117 - 136**

4.1	Introduction.....	118
4.2	Experimental details.....	120
4.2.1	Synthesis of TiO <sub>2</sub> nanorods.....	120
4.2.2	Deposition of silver nanoparticles on TiO <sub>2</sub> nanorods.....	121
4.3	Results and discussion.....	122
4.4	Conclusion.....	135
	References.....	136

## *Chapter 5*

### **Investigation on electromagnetic and**

#### **chemical enhancement mechanism of SERS ..... 137 - 158**

5.1	Investigation on SERS electromagnetic enhancement mechanism.....	138
5.1.1	Experimental details.....	139
5.1.2	Results and discussion.....	140
5.2	Investigation on SERS chemical enhancement mechanism in metal oxide nanostructures.....	144
5.2.1	Experimental details.....	147
5.2.2	Results and discussion.....	148
5.4	Conclusion.....	156
	References.....	157

## *Chapter 6*

### **Detection of bio and chemical analytes by surface enhanced Raman**

#### **Spectroscopy ..... 159 - 171**

6.1	Detection of food adulterants by SERS.....	160
6.1.1	Experimental details.....	162
6.1.2	Results and discussion.....	162

6.2	Label-free detection of DNA by SERS .....	165
6.2.1	Experimental details .....	166
6.2.2	Results and discussion.....	166
6.3	Conclusion .....	169
	References.....	170

*Chapter 7*

<b>Concluding remarks .....</b>	<b>173 - 176</b>
---------------------------------	------------------

## Abbreviations

AFM	Atomic force microscope
Ag-TiO <sub>2</sub>	TiO <sub>2</sub> nanorods decorated with silver nanoparticles
Ag NC	Silver nanocube
AgNP	Silver nanoparticles
a.u.	Arbitrary unit
BT	Benzene thiol
CT	Charge-transfer
CB	Conduction band
CCD	Charge coupled device
CE	Chemical enhancement
cps	Counts per second
3D	Three dimension
2D	Two dimension
DNA	Deoxyribo nucleic acid
E. coli	Escherichia coli
EF	Enhancement factor
EG	Ethylene glycol
EBL	Electron beam lithography
EM	Electromagnetic
FDTD	Finite-difference time-domain
FESEM	Field emission scanning electron microscope
He-Ne laser	Helium neon laser
HOMO	Highest occupied molecular orbital
hr	Hour
hrs	Hours
min	Minute(s)
HPLC	High performance liquid chromatography
HRTEM	High resolution TEM
ICDD	International centre for diffraction data
ICP	Inductively coupled plasma
IPA	Isopropanol

IR	Infra red
LSPR	Localized surface plasmon resonance
LUMO	Lowest unoccupied molecular orbital
4-MBA	4-mercapto benzoic acid
4-Mpy	4-mercapto pyridine
NIR	Near-infrared
NIL	Nanoimprint lithography
NPs	Nanoparticles
NSL	Nanosphere lithography
nTP	Nanotransfer printing
PATP	4-aminothiophenol
PICT	Photo-induced charge-transfer mechanism
PL	Photoluminescence
PML	Perfectly matched layers
PMMA	Polymethylmethacrylate
PVP	Polyvinylpyrrolidone
R6G	Rhodamine 6G
RIE	Reactive ion etching
RRS	Resonance Raman scattering
s	Seconds
SERS	Surface enhanced Raman scattering
SERRS	Surface enhanced resonance Raman scattering
SPP	Surface plasmon polaritons
SPR	Surface plasmon resonance
STM	Scanning tunnelling microscope
TEM	Transmission electron microscope
TERS	Tip enhanced SERS
TMAH	Tetramethyl ammonium hydroxide
TTIP	Titanium tetra isopropoxide
UV	Ultra violet
Vis	Visible
VB	Valence band
XRD	X-ray diffraction

## Publications

### Journal publications

- [1] Fabrication of cost effective, highly reproducible large area arrays of nanotriangular pillars for surface enhanced Raman scattering substrate, **Kudilatt Hasna**, Aldrin Antony, Joaquim Puigdollers, Kumaran Rajeev Kumar, and Madambi Kunjukuttan Jayaraj, *Nano Research*, DOI 10.1007/s12274-016-1190-y.
- [2] Development of High-Sensitive, Reproducible Colloidal Surface-Enhanced Raman Spectroscopy Active Substrate Using Silver Nanocubes for Potential Biosensing Applications, **Kudilatt Hasna**, Kiran Lakshmi, Madambi Kunjukuttan Ezhuthachan Jayaraj, Kumaran Rajeev Kumar and Murukeshan Vadakke Matham, *Journal of Nanophotonics*, 2016, 10 (2), 026020.
- [3] Development of highly sensitive recyclable surface enhanced Raman scattering substrates using TiO<sub>2</sub> nanorods decorated with Ag nanoparticles, **K. Hasna**, P. P. Subha, M. K. Jayaraj and K. Rajeev Kumar, *Nanotechnology* (under review).

### Other publications to which author has contributed

- [1] Synthesis of chemically pure, luminescent Eu<sup>3+</sup> doped HAp nanoparticles: a promising fluorescent probe for in vivo imaging applications, **K. Hasna**, S. Sasanka Kumar, Manoj Komath, Manoj Raama Varma, M. K. Jayaraj and K. Rajeev Kumar, *Physical Chemistry Chemical Physics*, 2013,15, 8106.
- [2] On the structural and optical properties of gold-polyaniline nanocomposite synthesized via a novel route, P. B. Anand, **K. Hasna**, K. M. Anilkumar and S. Jayalekshmi. *Polymer International*, 2012 61(12), 1733.
- [3] Magnetic and Raman scattering studies of Co-doped ZnO thin films grown by pulsed laser deposition, Arun Aravind, **K. Hasna**, M.K. Jayaraj, Mukesh Kumar Ramesh Chandra, *Applied Physics A*, 2014, 115(3), 843.

- [4] Linear and Nonlinear Optical Properties of Multi Walled Carbon Nanotubes with Attached Gold Nanoparticles, R. Sreeja, P. M. Aneesh, **K. Hasna**, and M. K. Jayaraj, *Journal of Electrochemical Society*, 2011, 158 (10), K187.
- [5] Structural and optical properties of La-doped BaSnO<sub>3</sub> thin films grown by PLD, K. K. James, P.S. Krishnaprasad, **K. Hasna**, M. K. Jayaraj, *Journal of Physics and Chemistry of Solids*, 2015, 76, 64.

#### **Conference presentations**

- [1] “Synthesis of SERS active gold colloids for bio sensing application”, **K. Hasna**, P. P. Subha, A. C. Saritha, L S Vikas, M. K. Jayaraj, K. Rajeev Kumar, ICMAT 2013, Suntec, Singapore.
- [2] “Synthesis of SERS active silver nanocubes via solvothermal method”, **K. Hasna**, Saranya Babu, M. K. Jayaraj and K. Rajeev Kumar, ICORS 2012, IISC, Bangalore.
- [3] "Synthesis of biocompatible fluorescent HAp quantum dots", **K. Hasna**, Manoj Komath, Manoj Raama Varma, M. K. Jayaraj and K. Rajeev Kumar, ANGEL 2012, Toarmina, Italy.
- [4] “SERS studies of carbon nanotubes with attached gold Nanoparticles”, **K. Hasna**, R. Sreeja, P. P. Subha, K. Rajeev Kumar and M. K. Jayaraj, Cochin Nano-2011, Kochi.
- [5] “Metal nanoparticles for SERS applications”, **K. Hasna**, M. K. Jayaraj, CT NANO 2012, Kochi.
- [6] “Synthesis and characterization of ZnO nanotubes”, **K. Hasna**, R. Sreeja, P. P. Subha, NSNT 2011, IIT Delhi.

# Chapter 1

## **An overview of surface enhanced Raman spectroscopy**

The chapter is devoted to the basic principles of Raman spectroscopy, its instrumentation and an overview of surface enhanced Raman scattering (SERS). Various SERS enhancement mechanisms, the evolution of SERS active substrates and its application in various fields are also discussed in detail.

Surface enhanced Raman scattering (SERS) has emerged as a powerful vibrational spectroscopic technique through overcoming the most the most significant drawback of inherently weak scattering cross section of normal Raman spectroscopy (RS) in analytical applications<sup>1</sup>. SERS enhances Raman scattering cross section by exciting the sample in contact with a ‘plasmonic’ surface with an appropriate laser line. In turn, Raman signal intensity is extraordinarily enhanced to a detection limit down to the single molecule<sup>2</sup>. Thus, the advancement in SERS detection is strongly associated with the progress in synthesis and optical characterization of new plasmonic nanostructured materials. The main reason why SERS technique has not been established as a routine analytical tool, despite its high specificity and sensitivity, is the low reproducibility of the SERS signal. In addition, the recording of SERS spectra is affected by a number of parameters, such as laser power, integration time, and analyte concentration.

## 1.1 Raman spectroscopy

### 1.1.1 Introduction

The inelastic scattering of electromagnetic radiation was first proposed theoretically by A. Smekal *et al.*<sup>3</sup> in 1923 and first observed experimentally by Indian physicist Sir Chandrasekhara Venkata Raman and his student Kariamanickam Srinivasa Krishnan in 1928. The effect was observed in liquid using sunlight as a source of light and using some basic optical filters<sup>4</sup>. Prof. C. V. Raman was awarded Nobel prize in Physics in the year 1930 for this discovery. Originally, the effect was visible to human eyes because of the measurement from highly concentrated pure organic solvents. However, the effect was too weak to observe for dilute solutions or solids. Therefore, many applications of Raman scattering were narrowed for several decades until the discovery of the laser along with development of more efficient detection systems (e.g. notch filter, holographic gratings, high throughput monochromators, photomultipliers, multi-channel charge coupled devices etc.).

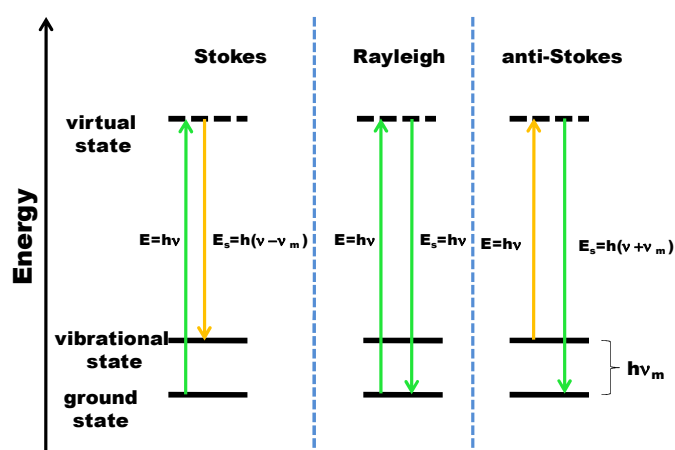


**Figure 1.1:** Simplified Jablonski diagram of Stokes process, anti-Stokes process and Rayleigh process

The scattering process involves instantaneous absorption of an incident photon and subsequent emission of another photon or scattered photon by phonons<sup>5</sup>. During the scattering process, three different types of scattering are possible and is shown in figure 1.1. When the emitted photon is elastically scattered with the same frequency as absorbed photon, the process is called as Rayleigh scattering. In contrast, Raman scattering is a process in which emitted photon is inelastically scattered and emitted with different frequency as compared to absorbed photon. Raman scattering is a consequence of the interaction of optical and vibrational oscillations and its probability is small but finite. When the molecule moves to a more vibrationally excited state of the ground electronic state, photon is emitted with energy lower by an amount equal to a vibrational transition and are called Stokes scattered photons. If the molecule makes a transition to a less vibrationally excited state, emitted photons are termed as anti-Stokes scattered photons. Anti-Stokes scattering occurs at higher energy than the Rayleigh scattering, and Stokes scattering has lesser energy than the Rayleigh scattering, while both Stokes and anti-Stokes are equally displaced from the Rayleigh line in spectra. Usually, Stokes line is followed in Raman spectroscopy since anti-Stokes scattering is less intense. Since vibrational spectra are unique to each molecule, the Raman spectra are referred as a chemical fingerprint of scattered molecules. Raman scattering process can be mathematically represented as

$$h\nu + E = h\nu' + E' \quad \dots\dots\dots (1.1)$$

$$\Delta E = h(\nu - \nu') \quad \dots\dots\dots (1.2)$$

where  $\nu$  and  $\nu'$  are incident and scattered frequencies respectively. On the basis of definition, the elastic and inelastic scattering can be classified as,

- a) Rayleigh scattering,  $\Delta E = 0$ , when  $\nu = \nu'$
- b) Stokes line of Raman scattering,  $\Delta E < 0$ , when  $\nu > \nu'$
- c) Anti-Stokes line of Raman scattering,  $\Delta E > 0$ , when  $\nu < \nu'$

In Raman experiments, the primary parameter that express Raman shift is wave number and it is defined as follows

$$\text{Raman shift, } \Delta\lambda(\text{cm}^{-1}) = \left(\frac{1}{\lambda_0} - \frac{1}{\lambda_1}\right) \times \frac{10^7}{\text{cm}} \dots\dots\dots (1.3)$$

where  $\lambda_0$  is the excitation wavelength and  $\lambda_1$  is the Raman scattered wavelength in nm.

The efficiency of Raman process is quantified as Raman scattering cross section,  $\sigma$  and it relates the incident light with Raman scattered light. So Raman intensity  $P$  relative to incident power  $S_0$  at the molecular position is defined as

$$P = \sigma S_0 \dots\dots\dots (1.4)$$

Since scattered radiation is collected through a specific direction, one can define absolute differential Raman cross section,  $\frac{d\sigma_{RS}}{d\Omega}$  as

$$\langle I_{RS}^{SM} \rangle = \frac{d\sigma_{RS}}{d\Omega} S_0 \delta\Omega \dots\dots\dots (1.5)$$

where  $S_0$  is incident laser intensity at molecular position and  $\delta\Omega$  is the small solid angle which in turn relates to numerical aperture of the

collecting optics.  $\langle I_{RS}^{SM} \rangle$  is Raman scattered intensity and is average of the signal obtained for a given vibrational mode of a single molecule over all orientations<sup>6,7</sup>. Suppose the collection of signal over all solid angle direction is possible, then total absolute Raman scattering cross-section can be defined as

$$\sigma = \int \frac{d\sigma_{RS}(\Omega)}{d\Omega} d\Omega \quad \dots\dots\dots (1.6)$$

Intensity of Raman scattered photons  $I_R$  is proportional to the induced dipole moment of the molecule by the excitation light source

$$I_R = |P_{ind}|^2 \propto \left| \overset{\rightarrow}{\alpha} \overset{\rightarrow}{E_0} \right|^2 \quad \dots\dots\dots (1.7)$$

where  $\alpha$  is the molecular polarizability tensor, which describes molecule's responsiveness to the electric field  $E_0$  (here the excitation source). Raman spectra unveil the energy transfer between the photons and molecules during their interaction. Hence a molecule exhibits Raman scattering only if there is a change in the molecular polarization potential or deformation of the electron cloud with respect to the vibrational coordinates. Since almost all molecules are Raman active, Raman spectroscopy is a powerful spectroscopic tool for studying any types of materials<sup>8</sup>.

### 1.1.2 Classical theory of Raman scattering

The standard approach to Raman effect is by classical theory and it consists of two steps (i) the perturbation of the molecule by the incident electric field and (ii) the modification of the molecule's polarizability through its vibration. Thus, Raman scattering process can

be depicted as the polarization of electron cloud of molecules. When a molecule is placed in an electric field, it gets polarized and as a result dipoles are generated<sup>5</sup>. Then the magnitude of induced dipole moment can be written as

$$P = \alpha E \dots\dots\dots (1.8)$$

An electromagnetic wave oscillating with a frequency  $\nu$  and amplitude  $E_0$  can be written as

$$E = E_0 \cos 2\pi\nu t \dots\dots\dots (1.9)$$

However, the polarizability changes with small displacement due to molecular vibration in response to the applied electromagnetic radiation and is given by

$$\alpha = \alpha_0 + (r - r_{eq}) \frac{\partial \alpha}{\partial r} \dots\dots\dots (1.10)$$

where  $\alpha_0$  is equilibrium polarizability;  $r_{eq}$  and  $r$  are bond lengths at equilibrium position and at any instant, respectively. If the molecule executes simple harmonic oscillations, then

$$r - r_{eq} = r_0 \cos 2\pi\nu_j t \dots\dots\dots (1.11)$$

On substituting equations 1.9, 1.10 and 1.11 into 1.8,

$$\mu = \left[ \alpha_0 + (r_0 \cos 2\pi\nu_j t) \frac{\partial \alpha}{\partial r} \right] E_0 \cos 2\pi\nu t \dots\dots\dots (1.12)$$

Equation (1.12) on expansion ends up in three terms as given below

$$\mu = \alpha_0 E_0 \cos 2\pi\nu t + \frac{E_0 r_0}{2} \frac{\partial \alpha}{\partial r} \cos 2\pi(\nu - \nu_j)t + \frac{E_0 r_0}{2} \frac{\partial \alpha}{\partial r} \cos 2\pi(\nu + \nu_j)t \dots (1.13)$$

The first term in equation 1.13 represents Rayleigh scattering and second and third terms correspond to Stokes and anti-Stokes scattering respectively. The existence of a given vibrational frequency in a molecule is not always Raman active and this leads to Raman selection rules. From the equation (1.13), it is clear that Raman activity could be observed if the polarizability of the molecule changes with molecular vibration.

### **1.1.3 Limitations of normal Raman spectroscopy**

Even though Raman spectrum provides a vibrational fingerprint of scatterer molecule and have potential applications in different fields such as chemistry, physics and biology, its practical applications are limited. It is because of very low scattering cross section of about  $10^{-29} \text{ cm}^2 \cdot \text{sr}^{-1}$ . Even if a molecule is Raman active, the intensity of Raman spectra may not be within the measurable count. Therefore, in order to exploit the benefit of Raman spectroscopy, a new method is essential to enhance Raman scattering cross section enhancement. Surface enhanced Raman spectroscopy, resonance Raman spectroscopy, coherent anti-Stokes scattering technique, etc., are some of the methods used to overcome the limitations of normal Raman spectroscopy.

## **1.2 Surface enhanced Raman scattering/spectroscopy**

Surface enhanced Raman scattering/spectroscopy (SERS) spectroscopy provide enhanced Raman signal and it offers many advantages over other spectroscopic or spectrometric techniques such as Fourier transform infrared (IR) spectroscopy, near infrared (NIR) absorption, UV-Vis absorption, fluorescence, nuclear magnetic

resonance (NMR), X-ray diffraction, X-ray photoelectron spectroscopy and mass spectrometry. The advantage of SERS includes, it can extract a significant amount of information directly from complex environments such as biological fluids, living tissues and cells without any need for prior sample preparation. SERS also offers high sensitivity for small structural changes in macromolecules, non-invasive sampling capability, minimum sample preparation and high spatial resolution. Simply, it can be said that surface-enhanced Raman spectroscopy (SERS) combines molecular fingerprint specificity with potential single-molecule sensitivity. Therefore, SERS technique is an attractive tool for sensing molecules in trace amount within the field of chemical and biochemical analytics.

### 1.2.1 Historical background

In 1974, the group Fleischmann, Hendra and McQuillan<sup>1</sup> accidentally discovered anomalously large enhancement of Raman intensity for pyridine molecule adsorbed onto a roughened silver electrode and later it was termed as surface enhanced Raman scattering. It was Jean Maire and Van Duyne<sup>9</sup> and Albrecht and Creighton<sup>10</sup> who showed that the anomalously enhanced intensity is not attributed to increased surface area, but due to new phenomena giving rise to the idea of the SERS cross section. It was discovered that enhancements in Raman intensity is attributed to strong electromagnetic fields induced by excitation of surface plasmon polaritons (SPP) on nanoscale noble metal structures (Au, Ag and Cu) at wavelengths in the visible spectrum<sup>11</sup>. In order to enhance the Raman signal, the molecule must typically be adsorbed on the metal surface, or at least be very close to it (typically  $\leq 10$  nm)<sup>12</sup>. The energy

produced due to the enhanced electromagnetic field is transferred to the molecules located near the surface of the nanostructures. Then the magnitude of the induced molecular dipole is increased, and therefore, the intensity of the inelastically scattered photons increases and greatly enhances the Raman scattering efficiency. It is seen that the electromagnetic model is not the only effect that accounts for all of the SERS effects, the contribution from molecular resonances and charge-transfer transitions can contribute to Raman enhancement. However, it is commonly accepted that the dominant effect in SERS is due to the unique property of metal nanostructures and is termed as electromagnetic (EM) enhancement effect. Raman signal enhancement in SERS spans several orders of magnitude as compared to normal Raman scattering enables the detection limit down to single molecule level.

The discovery of SERS widened the applications of Raman spectroscopy for molecular identification and detection at very low concentrations. This offers a unique capability for the label-free detection and identification of a variety of analytes<sup>8,13</sup>. Applications of SERS for quantitative chemical analysis primarily depend on properties of metallic nanostructures with nanometer-scale precision and high reproducibility of Raman enhancement over the substrate. The unique optical property that the metal surface can support is dependence on the size and geometry of the nanostructure, and the dielectric function of the material. These all have an intense effect on the overall capability of the metal nanostructure to enhance the Raman scattering cross section of molecules adsorbed on the metal surface.

### 1.2.2 Enhancement mechanism in surface enhanced Raman scattering

Based on the theory that intensity of Raman signal is proportional to change in dipole moment and the electric field in the vicinity of the molecule, two ways are possible to enhance Raman signal<sup>6</sup>. Consequently, there are two primary mechanisms for SERS enhancement: an electromagnetic (EM) enhancement and a chemical enhancement (CE)<sup>14</sup>. In the EM enhancement, the molecule is adsorbed onto or it is held in close proximity to the metal surface and an interaction between the molecule and the surface plasmons occurs<sup>6</sup>. In the case of CE, the molecule is adsorbed and chemically bonded to the metal surface. Excitation is through the transfer of electrons from the metal to the molecule and back to the metal again. This chemical enhancement is also called charge-transfer enhancement and is less dominant as compared to EM enhancement. It is commonly accepted that the electromagnetic enhancement effect is the dominant factor. But the relative importance of the two effects is still being scrutinized. The integrated photon flux from a SERS experiment can be estimated as<sup>15</sup>

$$\phi_{\text{SERS}} = \frac{I_0}{\hbar\omega_0} \sigma \sum_{i=1}^N G_i^{\text{EM}} G_i^{\text{CM}} \dots\dots\dots (1.14)$$

Here  $I_0$  and  $\hbar\omega_0$  are the laser intensity and laser energy.  $G_i^{\text{EM}}$  and  $G_i^{\text{CM}}$  are the electromagnetic and chemical parts of the overall enhancement factor, respectively,  $\sigma$  is the Raman scattering cross section of the scatterer and  $N$  is the number of scatterers in the probe volume. Here it is also assumed that two enhancement factors are independent.

**1.2.2.a Electromagnetic enhancement mechanism (EM enhancement)**

EM enhancement mechanism is a direct consequence of roughness present on the noble metal surface. When an electromagnetic radiation of frequency  $\nu$  interact with a molecule, oscillating Raman dipoles are generated and the corresponding induced dipole moment can be written as,

$$\mu_R = \alpha_R E \dots\dots\dots (1.15)$$

This oscillating Raman dipole radiates a power proportional to  $|\mu_R|^2$  at a frequency  $\nu_R$ , which is the frequency of Raman scattered photon. With the same phenomenological concept, SERS can also be explained. But here, presence of metal nanostructures alter SERS effect by generating local field enhancement at the metallic surface and consequently radiation properties of Raman dipole gets affected which in turn results in a possible radiation enhancement.

Let  $E_L$  be the field enhancement at the metallic surface due to localized surface plasmon resonance (LSPR)<sup>16</sup> which is much larger than the incident field  $E$  in magnitude and opposite in direction to  $E$ . Thus the induced Raman dipole,  $\mu_R = \alpha_R E$  is enhanced by a factor  $M_L(\nu_L) = \frac{|E_L(\nu_L)|}{|E|}$ . Hence the power radiated by Raman dipoles,  $P_{Rad}$  will be enhanced by  $\frac{|E_L(\nu_L)|^2}{|E|^2}$ . The Raman dipole radiation is also altered due to the presence of metallic nanostructures<sup>8</sup> and the radiation enhancement can be represented as

$$M_{Rad} = \frac{P_{Rad}}{P_0} \dots\dots\dots (1.16)$$

Hence fundamental mechanism behind electromagnetic enhancement is the amplification of the incident electric field  $E$  on the nanotextured metal surface and the total electromagnetic enhancement effect can be described as a consequence of the enhancement of both the incident electric field and the Raman scattered electric field.  $M_L(\nu_L)$  can be estimated by solving Maxwell equation under specific incident electric field. But the calculation of  $M_{Rad}$  is very complicated. Hence the electromagnetic enhancement factor for a Raman scattering process can be approximated as<sup>17</sup>

$$G^{EM}(\vec{r}, \omega) = M_L(\nu_L)M_{Rad} = \left[ \frac{E_{Loc}(\vec{r}, \omega)}{E_o(\vec{r}, \omega_0)} \right]^2 \left[ \frac{E_{Loc}(\vec{r}, \omega_0 - \omega_1)}{E_o(\vec{r}, \omega_0 - \omega_1)} \right]^2 \dots (1.17)$$

Here it is assumed that enhancement is independent of the absolute photon fluxes and polarizations.  $E_o$  and  $E_{Loc}$  are the magnitude of the incident electric field and the total local field generated in the metal nanostructure. The incident radiation has frequency  $\omega_0$  and the scattered radiation has vibrational frequency  $\omega_1$ . The equation 1.17 can be approximated as

$$G^{EM}(\vec{r}, \omega) = \left[ \frac{E_{Loc}(\vec{r}, \omega)}{E_o(\vec{r}, \omega_0)} \right]^4 \dots (1.18)$$

The above equation implies that significant factor determining electromagnetic enhancement factor is  $E_{Loc}$ , the enhanced electric field in the vicinity of metal nanostructure surface. The local field generated in the vicinity of the metal nanostructure can be expressed as the sum of the incident field and the induced field, which is generated during surface plasmon resonance in the metal nanostructure. The most important components of the EM models include the excitation of a

localized surface plasmon resonance in an isolated metal nanoparticle or in a void or in the aggregate of metal nanostructures. The localized surface plasmon resonance positions are determined by the optical properties such as dielectric constant of the material, the size and shape of the nanostructure or roughness and other variables like small gaps as in bimetallic structures, nanoshells or nanowires. Maximum local field enhancement is obtained for a molecule directly attached to the metal surface (first-layer effect) and its effect also extends up to about 10 nm away from the metal molecule interface. The effect of multiple plasmon resonances is important for the treatment of aggregates or closely packed nanostructures.

### ***Plasmonics***

The basic physical phenomena behind electromagnetic enhancement in surface enhancement Raman scattering/spectroscopy (SERS) is the unique optical properties of metal nanostructures. It has been established that the surface plasmons which are collective light-induced electronic excitations present in metals, act as optical antennas that have the capacity to capture and concentrate light waves<sup>18</sup>. Various nanofabrication method to engineer metallic nanostructures with well-defined dimensions and separations advances the application of metal nanostructures in the field of plasmonics.

Plasmons are classified into surface plasmon polariton and localized surface plasmons<sup>8</sup>. They are illustrated as quantised elementary excitation present in solid and are associated with the high-frequency collective motion of the valence electrons in a solid

The plasmon energy is termed as

$$\hbar\omega_p = \hbar \left( \frac{Nq^2}{\epsilon_0 m_0} \right)^{\frac{1}{2}} \dots\dots\dots (1.19)$$

where  $\omega_p$  is the plasma frequency,  $N$  is the number of valence electrons per unit volume,  $\epsilon_0$  is the permittivity of free space, and  $m_0$  is the free electron mass. Plasmons described in coinage metals such as silver, gold, copper etc are oscillations of conduction electron density about fixed positive ions at a natural frequency termed as plasma frequency  $\omega_p$ . The illumination of metal with visible and infrared range produce a dominant interaction between photons and the free electron plasmons. The interaction excite the valence electrons occupied near the Fermi surface into different energy and momentum. These mixed photon–plasmon modes are called plasmon polaritons. The dielectric function of metal is given by simplified Lorentz harmonic oscillator model

$$\epsilon(\omega) = 1 - \frac{\omega_p^2}{\omega^2 + i\gamma\omega} \dots\dots\dots (1.20)$$

where  $\gamma$  is a damping constant as a result of electron-electron and electron phonon scattering in the metal. Theses dielectric functions are complex functions and their real and imaginary parts are

$$\epsilon_1(\omega) = 1 - \frac{\omega_p^2}{\omega^2 + \gamma^2} \dots\dots\dots (1.21)$$

$$\epsilon_2(\omega) = \frac{\omega_p^2 \gamma}{\omega(\omega^2 + \gamma^2)} \dots\dots\dots (1.22)$$

The importance of plasma frequency is that all radiations with frequencies lower than the plasma frequency are reflected and the radiations that are transmitted through metals are those with a frequency higher than  $\omega_p$ . The position of  $\omega_p$  in metals is in ultra violet region and it is responsible for metallic lustre.

Only those metals which possess negative values for  $\epsilon_1(\omega)$  and small positive values for  $\epsilon_2(\omega)$  in the wavelength are employed for plasmonic application. In the case of SERS, the wavelength of interest is visible and infra red and the value of  $Re(\epsilon)$  of the metal is  $-20 \leq \epsilon_1(\omega) \leq -1$ . In the case of metal thin films, longitudinal surface plasma oscillations propagate at a metal-dielectric interface and these quantised propagating oscillations are termed as surface plasmons. The frequency of surface plasmon at which they propagate is related to plasma frequency as

$$\omega_{spp} = \frac{\omega_p}{\sqrt{2}} \dots \dots \dots (1.23)$$

The strong interaction of surface plasmon modes with external transverse radiation result in the confinement of these modes to the metal surface and these are described as surface plasmon polaritons (SPP). These are again classified into propagating SPP and localized SPP<sup>19-22</sup>. The propagating SPP is widely useful in surface plasmon resonance (SPR) and total internal reflection fluorescent (TIRF) microscopy. The schematic diagram of confinement of localized surface plasmons and propagating surface plasmon polariton is given in figure 1.2.

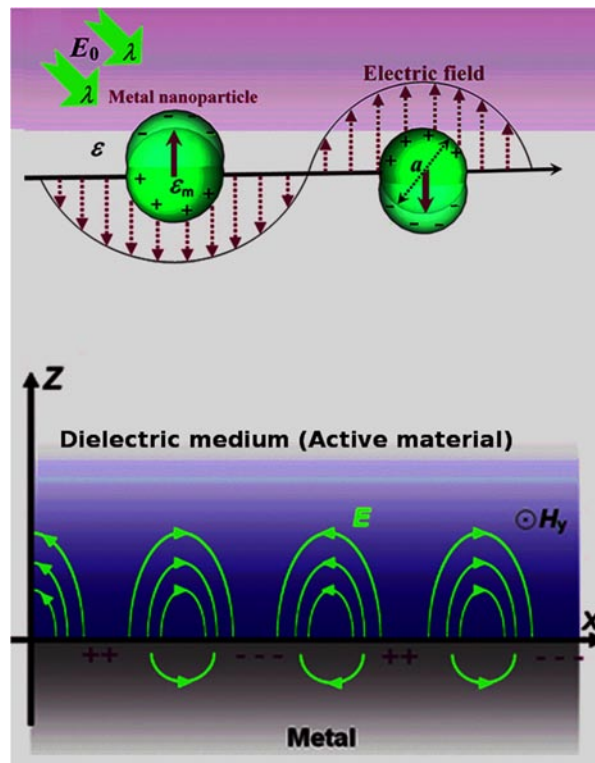


**Figure 1.2:** Schematic diagram of (a) confinement of localized surface plasmons (b) propagating surface plasmon polariton

When the dimension of the metal nanostructure is less than or comparable to the wavelength of incident radiation, surface plasmons are localized in metal nanostructures and is described as localized surface plasmons<sup>23</sup>. During a process of localized surface plasmon resonance, these surface plasmons induce a very large electric field around the nanoparticle as compared to that of the incident light. The generation of localized surface plasmon and the localized surface plasmon resonance can be explained as follows. In metal nanoparticles, the conduction electrons move almost freely through the lattice of ionic

cores. On irradiation, the electromagnetic field of the light forces the conduction electrons to move towards the surface of metal nanoparticle. As a consequence of confinement, electric dipoles are created by the accumulation of positive charges on the opposite side. The electric field generated by the electric dipole is opposite to that of incident light and act as a restoring force on the electrons to return to the equilibrium position. Thus the generated electric dipoles oscillate as a linear oscillator with a natural frequency of conduction electron oscillation, known as plasma frequency. Like resonance in oscillators, these dipoles oscillate with maximum amplitude when radiation of frequency equal to plasma frequency is incident upon it and this situation is known as localized surface plasmon resonance. Since the way in which the charges get accumulated in different morphologies and sizes is different, the resonance condition is strongly determined by nanoparticle size, shape and the environment.

### ***Field enhancement in metallic nanostructure***

During LSPR, the amplitude of oscillation will be maximum and partial light extinction happens within the metal nanostructures. As a consequence, the magnitude of electric field induced by the electric dipoles is enhanced, which is opposite in direction of the incident field. It is possible to solve analytically for enhanced electric field around metal nanoparticle whose size is comparable with that of incident radiation. In this case, field generated is uniform around the nanoparticle and by solving Maxwell equation enhanced electric field on a spherical nanoparticle of radius  $a$ , irradiated by  $z$  - polarized light of wavelength  $\lambda$  is

$$E_{out} = E_0 \hat{z} - \alpha E_0 \left[ \frac{\hat{z}}{r^3} - \frac{3z}{r^5} (x\hat{x} + y\hat{y} + z\hat{z}) \right] \dots\dots\dots (1.24)$$

Where  $\alpha$  is metallic polarisability and can be expressed  $\alpha = ga^3$ , where  $a$  is radius of sphere and  $g$  is defined as

$$g = \frac{\epsilon_{in} - \epsilon_{out}}{\epsilon_{in} + 2\epsilon_{out}} \dots\dots\dots (1.25)$$

where  $\epsilon_{in}$  and  $\epsilon_{out}$  represent dielectric function of metal and external environment respectively. When  $\epsilon_{in} = -2\epsilon_{out}$ , denominator of the equation 1.25 approaches to zero and this is the condition for occurrence of the maximum enhancement. According to Mie theory, the condition  $\epsilon_{in} = -2\epsilon_{out}$  occurs during localized surface plasmon resonance. The extinction spectrum for an arbitrary shaped metal nanostructure is given by Mie theory as

$$E(\lambda) = \frac{24\pi^2 Na^3 \epsilon_{out}^{3/2}}{\lambda \ln(10)} \left[ \frac{\epsilon_r(\lambda)}{(\epsilon_r(\lambda) + \chi \epsilon_{out})^2 + \epsilon_i(\lambda)^2} \right] \dots\dots\dots (1.26)$$

where  $\epsilon_r$  and  $\epsilon_i$  are the real and imaginary components of the metal dielectric function respectively and  $\epsilon_{out}$  is the dielectric constant of the external environment. Here  $\chi$  is the shape factor that accounts for metal nanostructures with various geometries and  $\chi = 2$  represents case for spherical shape.  $\epsilon_r$  is a function of wavelength and hence the position of LSPR is determined by the situation at which  $\epsilon_r = \chi \epsilon_{out}$ . As size increases and when the  $E$  inside nanoparticle is not uniform, multipolar terms should also be considered.

**Finite-difference time-domain (FDTD)**

The field enhancement in metals can be understood by solving Maxwell's equations subjected to the appropriate boundary. One such useful method is numerical method and is further classified into two groups. The first group is known as partial differential equation solvers and example are finite-difference time-domain (FDTD) techniques<sup>24</sup> and finite-element methods (FEM). The second classification is a semi-analytical method and examples are the discrete dipole approximation (DDA) and its derivatives or the multiple multipole (MMP) method.

Due to the rapid growth of power of desktop personal computers, nowadays electromagnetic modelling is easily available and anyone can run a fairly advanced simulation on a desktop and one can utilise the commercial software with full facilities or use freely available codes that can edit easily according to user's need. Commercial softwares include software based on advanced mathematical tools, such as finite-element methods (FEM) or finite-difference time-domain (FDTD) methods. Still, super computers are essential to run a full 3D simulation. So it is a difficult task to solve EM problem using these simulations. To carry out the simulation with acceptable accuracy and manageable computing time, the parameters such as solver parameters, algorithms, mesh precision, bounding box, and other boundary conditions should be optimised.

Finite-difference is a simple and intuitive numerical method of solving partial differential equations. In this method, the time-dependent Maxwell's equations are solved using a finite-difference approach, under a prescribed exciting field or radiation in the case of field enhancement in metal nanostructures. This exciting field can be an oscillating field with a fixed frequency  $\omega$ , and the accuracy of simulation increases when the

exciting field is a single short pulse. The simplicity of the FDTD scheme is one of the main advantages over the other numerical methods. However, as soon as FDTD method is extended to elaborate meshes (non-cubic, varying dimensions, etc.), which is a requirement for many SERS and plasmonics applications, this simplicity will be lost.

The basic steps involved in FDTD method is described in detail in the report by John B. Schneider<sup>24</sup>. FDTD method utilizes finite-difference approximations method to Ampere's and Faraday's laws of Maxwell equations which contain spatial and temporal derivatives. In FDTD method, derivative of a function is given by central differences and is given by the equation,

$$\left. \frac{df(x)}{dx} \right|_{x=x_0} \approx \frac{f(x_0 + \frac{\delta}{2}) - f(x_0 - \frac{\delta}{2})}{\delta} \dots\dots\dots (1.27)$$

Equation 1.27 is with second order accuracy and the error in approximation reduces to a minimum as the value of  $\delta$  approaches zero.

Based on the second order central differences, Kane Yee proposed the first FDTD algorithm and is termed as Yee algorithm. The steps involved in the Yee algorithm are as follows:

- 1) Replace all the derivatives in Ampere's and Faraday's laws with finite-differences. Discretize space and time so that the electric and magnetic fields are staggered in both space and time.
- 2) Solve the resulting difference equations to obtain "update equations" that express the (unknown) future fields in terms of (known) past fields.
- 3) Evaluate the magnetic fields one time-step into the future so they are now known (effectively they become past fields).

- 4) Evaluate the electric fields one time step into the future so they are now known (effectively they become past fields).
- 5) Repeat the previous two steps until the fields have been obtained over the desired duration.

with the above algorithm, the update equation for electric field and magnetic field are derived as

$$H_y^{q+\frac{1}{2}}\left[m+\frac{1}{2}\right] = H_y^{q-\frac{1}{2}}\left[m+\frac{1}{2}\right] + \frac{\Delta t}{\mu\Delta x}\left(E_z^q[m+1] - E_z^q[m]\right) \dots (1.28)$$

$$E_y^{q+\frac{1}{2}}[m] = E_y^q[m] + \frac{\Delta t}{\epsilon\Delta x}\left(H_x^{q+\frac{1}{2}}\left[m+\frac{1}{2}\right] - H_x^{q-\frac{1}{2}}\left[m+\frac{1}{2}\right]\right) \dots (1.29)$$

For getting update equations, electric and magnetic fields are positioned on a Yee cell and is schematically represented in figure 1.3

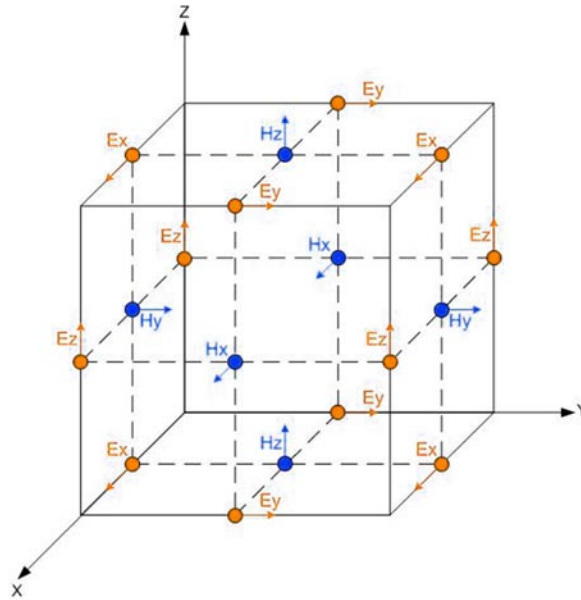


**Figure 1.3:** Schematic of Yee cell used in FDTD simulation

### 1.2.2.b Chemical enhancement mechanism (CE)

The chemical enhancement can be categorised as SERS of physisorbed molecules, SERS of chemically bonded molecules without charge-transfer (CT) resonance, SERS of chemically bonded molecules with CT resonance and surface enhanced resonance Raman scattering (SERRS). The resonance Raman scattering occurs when the sample is irradiated with an energy which matches with one of electronic transition in the molecule and as a result of resonance Raman scattering, Raman intensities of certain bands are selectively enhanced by several orders. The fundamental task to interpret the observed Raman spectrum from a chemically bonded molecules without resonance excitation is to identify the nature of bonding and characterize metal-molecule surface complexes. The steps involved in interpreting the spectra of above case are<sup>12,25</sup>.

- 1) Carry out Raman measurements of reference molecule with several excitation lines to exclude the contribution from resonance Raman effect. Select the laser line which does not produce resonance Raman effect for further experiments.
- 2) Using the same laser line as in 1, record the Raman spectra of the synthesized salt that correspond to the possible surface complex. Also, measure its UV-visible absorption spectrum and the excitation spectrum.
- 3) Record the SERS spectra of the samples with the same laser line as in 1.
- 4) Compute the Raman intensities theoretically for the reference molecule and the complex.

- 5) Apply the constraints of the surface selection rules to computed spectra for direct comparison with the observed SERS.

Interpretation and assignment of vibrational spectra of the metal-molecule surface complex can be carried out using the cost-effective technique of density functional theory (DFT)<sup>8</sup> which is based on quantum chemical calculations. Chemical enhancement mechanism provides not only the change in the relative intensities of the spectra but also the variation in the vibrational modes of a molecule as compared with the normal Raman spectra. The mechanism is either due to charge-transfer states involving transitions from the Fermi level of the metal to an unoccupied orbital of the molecule (or vice versa) or due to the formation of a surface complex involving the metal and the analyte, leading to a change in the properties of the molecule. Even though the order of enhancement factor corresponding to chemical enhancement is 1-2, the mechanism is necessary to account for the total enhancement in experimentally observed spectra. In practice, it is proven to be very difficult to study the chemical enhancement mechanism. Since the observed SERS spectra contain the information about the adsorbate and its environment, it is extremely important to understand the chemical mechanism for both as a fundamental study and for its relevance to analytical applications. Usually in CE enhancement, charge-transfer mechanism occurs through photon driven charge-transfer processes between the states near the Fermi level of metal and molecular orbitals of adsorbates<sup>8</sup>. As shown in figure 1.4, the photon incident upon system creates an electron-hole pair in the metal and the electron is excited as a "hot electron" and tunnel into lowest unoccupied molecular orbital (LUMO) of the adsorbate, thus generating a charge-transfer excited

state. Finally, the electron is de-excited to the highest occupied molecular orbital (HOMO) level.

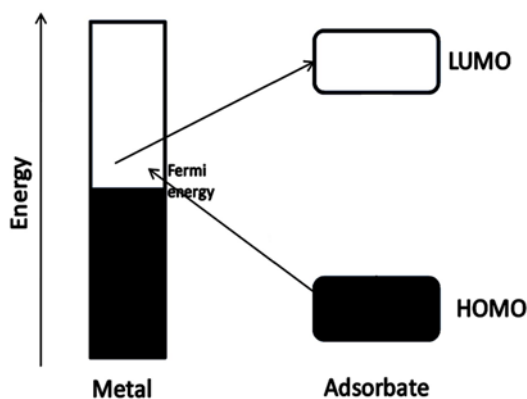


**Figure 1.4:** Charge-transfer mechanism between metal and adsorbate

The process involved in EM and CE enhancement is summarised in figure 1.5.

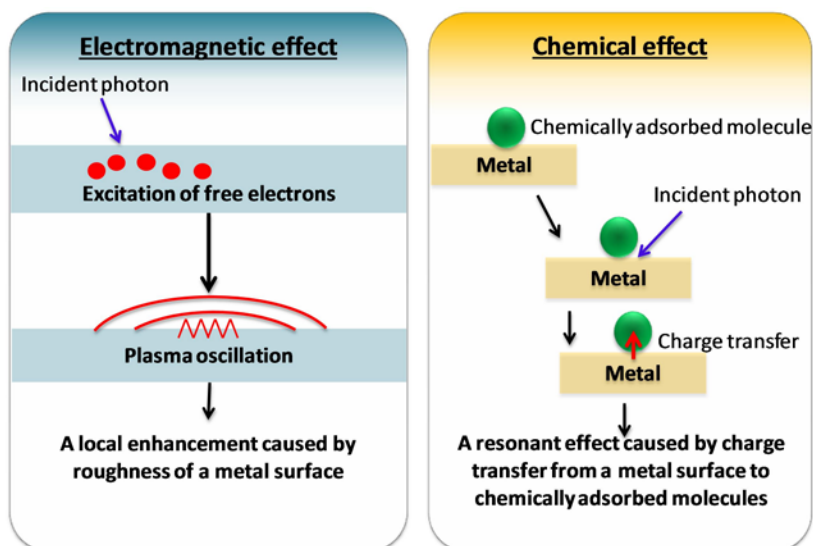


**Figure 1.5:** Schematic representation of EM and CE enhancement

### **1.2.3 Factors influencing EM enhancement**

#### ***Size effect***

The field enhancement depends on particle size and it does matter for a dimension range  $\sim 30\text{--}100$  nm. LSPR is red shifts as the size increases<sup>23</sup>. As the size of nanoparticles increases, irradiation loss increases and thus localized surface plasmons are damped strongly. As a result, the resonance peaks are broadened and correspondingly enhancement factor decreases dramatically. For particle size beyond 100 nm, resonance and enhancement effects disappear. Another consequence is the appearance of multipolar resonance peak such as quadrupole resonance which does not couple to light efficiently and hence no field enhancement. Hence size induced resonances increase the complexity of optical phenomena in metallic nanostructures.

#### ***Shape effect***

The resonance, the field enhancement and the spatial distribution are strongly affected by particle's shape. In certain shapes such as triangle, cube etc. electric field is concentrated at their sharp ends. This is named as lightning rod effect<sup>13</sup>. Shapes like nanocubes, nanocages, etc., produce more complicated effects during resonance. The field enhancement depends not only on shape but also on the orientation with respect to the field. The local field intensity enhancement factor at the vertices increased by two orders when the direction of electric field is changed. For nanorods, the electron oscillations are different along the rod axis and perpendicular to the rod

axis; they are described as longitudinal plasmons and transverse plasmons respectively. As the aspect ratio of nanorods increases, the position of longitudinal plasmons shifts towards longer wavelengths and the corresponding intensity increases. By using nanorods with different aspect ratios, SERS activity can be properly tuned.

### ***Interacting objects and gaps***

The existence of coupled plasmon resonances between two or more closely spaced nanoparticles is another important effect in SERS. As the two nanostructures approach each other, the field produced by induced dipole reinforce or weaken in a certain region of space between the nanostructures. The coupling causes plasmon resonance to concentrate in the middle of nanostructures and is called coupled plasmon resonances<sup>13</sup>. The coupling red shifts the resonance peaks and also enhances SERS effect. When the nanoparticles approach each other, they will be under the influence of not only the applied field but also the field due to other dipoles. Hence the intensity increases due to an increase in the field.

The field enhancement in metal nanoparticle, and "hot spots" in the junction between nanostructures, nanocube and triangle are schematically shown in figure 1.6.

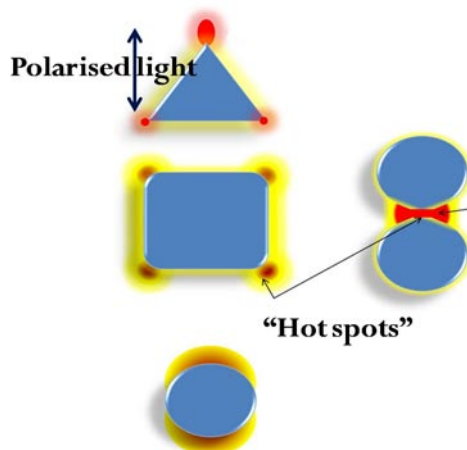


**Figure 1.6:** Field enhancement in metal nanostructures (red colour represent region of enhanced electric field)

These large enhancements due to coupled plasmon resonances at the gaps between nanostructures are termed as "hot spots". They play an important role in SERS as they provide enough enhancements to detect single molecules. The large enhancement factor is associated with strong spatial localization of the resonance at the "hot spots". Thus our main aim will be to create maximum "hot spots" so as to create maximum enhancement but the molecule must be adsorbed to that "hot spots" for obtaining the maximum enhancement. The average enhancement for the total substrate may not be increased since the presence of "hot spots" is not uniform.

#### ***Analyte-metal distance dependence of SERS***

The analyte-metal distance dependence of SERS intensity is important both mechanistically and practically<sup>26-28</sup>. The EM enhancement theory explains that the direct contact between the adsorbate and metal surface is not a requirement for SERS effect, but the adsorbate should be within a certain sensing volume. In

certain practical applications involving detection of immobilised biomolecule, the direct contact between adsorbate and metal is not at all possible because in this case the metal surface is modified with a capture for specificity and biocompatibility. According to the electromagnetic theory, the SERS effect is proportional to the fourth power of electric field. Hence the SERS enhancement factor varies as  $r^{-12}$ , where  $r$  is the distance between adsorbate and metal surface. Excitation wavelength also affects SERS enhancement factor. According to  $E^4$  enhancement, EM enhancement is maximum when LSPR position coincides with laser excitation wavelength. Later experiments proved that enhancement is maximum when LSPR position is at half the difference between excitation wavelength and Raman scattering wavelength<sup>29,30</sup>. Thus maximum enhancement is obtained when both the incident and scattered field are enhanced which is in accordance with EM prediction.

#### **1.2.4 Factors influencing the SERS enhancement**

The resultant SERS spectra depend on various parameters that listed below:

- The characteristics such as wavelength, angle of incidence, polarisation of excitation laser, etc.
- The nature, shape, size of SERS substrate and the orientation of the substrate with the excitation source.
- The intrinsic Raman scattering cross section of analyte.
- Adsorption properties of analyte on the substrate especially the nature of bonding and surface coverage.

### **1.3 Advancement of SERS substrates**

The basic requirement of a SERS substrate is that it should be any metal nanostructure platform that can support surface plasmon resonance and thereby enhance the Raman signals of an adsorbate as compared to its normal Raman spectra. According to the morphological appearance, SERS substrate can be broadly classified into two categories.

- 1) Random morphology SERS substrate: Roughened electrodes, metal nanocolloids, metal-island film on a planar substrate etc., are mainly included in this category
- 2) Ordered or periodic SERS substrates: Planar substrate with regular arrays of metallic nanostructures usually fabricated by nanolithography and related techniques.

Due to the inhomogeneous textures, it is very difficult to reproduce SERS enhancement in random morphology SERS substrates. Redox cycle reactions in the electrochemical cell are utilised to generate SERS substrates with roughened electrodes<sup>31</sup>. The technique is so popular that by adjusting the electrode potential, charge-transfer phenomenon between adsorbate and the metallic surface can be understood easily<sup>32,33</sup>. But the enhancement effect is very small. Metallic islands fabricated by vacuum deposition techniques on various substrates are another group among random morphology SERS substrate. Glass, quartz, silicon wafer or poly(dimethylsiloxane) (PDMS) can be used as a substrate for depositing metallic islands<sup>34-38</sup>. One advantage of this technique is that it is possible to prepare high purity SERS substrates and the technique is relatively easy. The technique can be electron beam evaporation or thermal evaporation or sputtering.

The nanocolloids of silver and gold are also common substrates and the advantages are easiness in preparation and very large enhancement factor. Chemical reduction method is a common method for synthesis of metal nanocolloids<sup>30,39</sup>. The stability of nanocolloids is a consequence of columbic or steric repulsions among particles. In order to avoid excessive aggregation and precipitation, stabilising agents are added to the colloids. The most commonly used metal colloids are citrate reduced colloid in which sodium citrate acts as both reducing and stabilising agents<sup>30,40</sup>.

The optical properties of nanocolloids can be easily tuned by varying stabilising agents. One effective alternative to citrate is borohydride<sup>41</sup>. But the stability is comparatively low. The evidence of single molecule SERS is first reported using aggregated silver colloid based SERS substrate with "hot spots"<sup>2</sup>. Even though the enhancement factor is very large, its stability and reproducibility are limited; hence alternative methods are developed for the fabrication of ordered planar substrate. Ordered nanorods and nanowires of silver are fabricated by template assisted synthesis<sup>42,43</sup>. Anisotropic structures of nanotriangles are fabricated by nanosphere lithography<sup>44</sup>. Nanosphere lithography and electron beam lithography<sup>45</sup> are the two conventional lithographic technique for designing periodic arrays of metal nanostructures with various shapes and thus with different enhancement factor.

Nanosphere lithography (NSL) is an inexpensive method to produce arrays of nanostructures with controlled shape and size. NSL basically involves self assembly of nanosphere such as polystyrene on a planar substrate. The self organised 2D colloidal spheres act as a deposition mask. Spin coating, drop casting etc. are usually employed

for deposition of nanospheres. After metal film evaporation, nanospheres are etched which result in arrays of metal nanostructures in the interstitial sites.

Electron beam lithography (EBL) is another approach to produce highly uniform and reproducible SERS substrate. The technique is based on the principle that after exposure of electrons, sensitive resists (e-resists) change their chemical properties. Using an EBL system, resist patterns are designed in serial manner and they behave as a drawing pen. Even though it provides low throughput, it doesn't require a mask unlike photolithography. A digital image is directly patterned on a desired substrate by controlling the electron beam position via a computer.

Nanotransfer printing (nTP)<sup>46,47</sup> is a method with high throughput to generate periodic SERS substrate. The pattern in a stamp fabricated via EBL is transferred to a desired substrate using some interfacial chemistry. In nTP, a realising layer is formed prior to metal film deposition to avoid the adhesion of metallic film on stamp<sup>48,49</sup>. The technique is more economic than SERS substrate prepared via EBL because in nTP the stamp can be reused which reduce the cost. A resolution of approximately 100 nm is reported for nTP<sup>50</sup>. One disadvantage is difficulty in transferring the metal film onto the desired substrate. Nanoimprinting technique is another promising technique for the fabrication of periodic SERS substrate with reproducible enhancement factor. Nanoimprint lithography offers flexibility in patterning which is simple and low cost. The technique involves transfer of patterns from a mold fabricated via electron beam lithography, termed as master, to polymers with the application of temperature and pressure so that the masters can be reused.

## 1.4 Interpretation of SERS spectra

There are three basic components involved in SERS: a Raman active molecule known as analyte molecule, SERS active substrate and an electromagnetic radiation. The interpretation of SERS data is complicated because of the existence of the following challenges:

- 1) Determination of the nature of adsorption of Raman active molecules with the SERS substrate: the molecule can be either physisorbed or chemisorbed to the metal surface which in turn determines the strength of bonding. The chemisorption may introduce a shift in the Raman peaks but physisorption does not bring any change in Raman spectra of molecules.
- 2) Interaction of electromagnetic radiation with a metal nanostructure can induce substrate excitations such as electron-hole pairs, surface plasmons or surface phonons. In particular, absorption of light by nanostructures can create enhanced local electric fields at the metallic surface location of adsorbed species and this field strongly affects the Raman activity of adsorbed molecule, termed as electromagnetic enhancement mechanism of SERS.
- 3) The incident field can interact with the Raman active adsorbed molecule resulting in photo-dissociation, photoreactions or simply photo-desorption and this will produce its own fingerprint on the resulting spectra.
- 4) Since scattering, absorption and the local field enhancement at the metal nanostructure is determined by the shape and size

of metal nanostructure, this will ultimately influence the SERS intensity. Also, the excitation of surface plasmons is getting affected by the dielectric constant of the medium.

- 5) If the excitation source for SERS induces new excitations in the molecule–nanostructure complex, such as charge-transfer transitions from the Fermi to LUMO level of the molecule or from HOMO to Fermi level, the process ends up in resonance Raman scattering and hence the final intensity will not resemble the original Raman spectrum of the parent molecule.
- 6) Finally, the presence of impurities may introduce their own fingerprint in the spectra and will strongly affect the SERS signal and further complicate the interpretation of the observed SERS spectra.

## **1.5 Enhancement factor**

The performance of a SERS substrate is evaluated by the enhancement factor (EF), which is defined with reference to the non-SERS properties of the same molecule in the same environment. Since it is difficult to account for all the parameters, EF is defined in such a way that the estimated EF should be independent of as many parameters as possible, which enables a direct comparison of the merits of different SERS substrates. Therefore, depending on applications and nature of SERS substrates, enhancement factor is defined in different ways, of which analytical enhancement factor and SERS substrate enhancement factor have received more acceptance<sup>8,51</sup>. The analytical enhancement factor (*AEF*) is the simplest and most intuitive approach. The Raman signal  $I_{RS}$  is measured for a given concentration ( $C_{RS}$ ) and under identical

experimental conditions and reparation conditions at a different concentration ( $C_{SERS}$ ) would give a SERS signal  $I_{SERS}$ . Then analytical enhancement factor is given by

$$AEF = \frac{I_{SERS} C_{RS}}{I_{RS} C_{SERS}} \dots\dots\dots (1.27)$$

The definition assumes that analyte molecule is spread over SERS substrate and Raman intensity linearly depends on laser power and analyte concentration. One of the major drawbacks of the definition is that since SERS is a surface sensitive technique, a molecule which is adsorbed to substrate is effectively contributing to SERS signal. Therefore the definition for SERS substrate enhancement factor (SSEF) includes the only number of adsorbed molecule to SERS substrate and is the best estimate of average EF for a given SERS substrate.

SSEF has been extensively used in SERS experiments and it is defined as

$$SSEF = \frac{I_{SERS} N_{vol}}{I_{RS} N_{surf}} \dots\dots\dots (1.28)$$

Here  $N_{vol}$  is the number of analyte molecules in scattering volume  $V$  and is given by  $N_{vol} = C_{RS}V$  and  $N_{surf}$  is the number of molecules participated in SERS.

## 1.6 Applications of SERS

SERS can be used as an excellent analytical tool in a myriad of cases and combinations since Raman spectra provide a chemical fingerprint information about a molecule. Compared to other techniques such as nuclear magnetic resonance and fluorescence spectroscopy, the

'spectroscopic fingerprint' based on SERS technique can be used in many more specific problems. With the advantage of Raman spectroscopy and high sensitivity, SERS has been exploited in a variety of applications in the fields spanning from scientific to industrial areas<sup>13,52</sup>. Development of new types of miniaturized Raman spectrometers and advancement of various qualified SERS substrates popularized SERS applications. Since its discovery in 1974, it is realized as a high sensitive analytical tool and irreplaceable tool in detecting molecules. SERS overcomes the inherent inefficiency such as long collection times and high detection limits of normal Raman spectroscopy. It is a popular technique in forensic science, the pharmaceutical industry, nanotechnology, art, semiconductors, bioscience, etc. Single cell or single molecule detection ability of SERS is useful for label-free detection applications<sup>13,53</sup>. In near-infra red (NIR) region, there is no probability of photo-decomposition. Hence in this region silver and gold nanoclusters based SERS can be used for *in vivo* applications.

### **1.6.1 Applications of SERS in biosensing**

SERS has been used in biological research both in fundamental and applied research to examine the structure, conformation and charge-transfer of bio molecules<sup>52,54,55</sup>. The complex structure of different photosystem II (PSII) pigment–protein complexes<sup>56</sup> and orientation of proteins<sup>57</sup> have been investigated by SERS. Real time monitoring of the structure, kinetics of electron-transfer and fluctuations in the configuration of cytochrome C on a monolayer of a modified electrode has been conducted using a time resolved two color laser Raman system<sup>58,59</sup>. “Smart” SERS substrate concept was developed after the detection of a dye labelled biotin at concentration levels as low as

$10^{-7}$  mol L<sup>-1</sup> and also after detection of DNA. Vo-Dinh *et al.*<sup>60</sup> reported the detection of DNA, which lead the way to DNA detection by SERS. The same group could detect HIV gene<sup>61</sup> and cancer markers<sup>62,63</sup>. The immobilized metal nanoparticle as SERS substrate can also be utilised to detect and identify various organisms such as bacteria, pathogens and multiple bacteria species<sup>64-66</sup>. SERS is also demonstrated as a promising technique for biomedical diagnostics such as detection of glucose in blood<sup>67</sup>. Real time detection of glucose in bovine plasma by SERS has been reported with the help of alkanethiol modified SERS substrate<sup>68</sup>.

### 1.6.2 Applications of SERS in electrochemical systems

The electrochemical applications of SERS<sup>53</sup> include the characterization of metal complexes with aromatic ligands and corrosion inhibitors. In the case of organic molecules, Faradaic reactions and adsorption geometry can be analysed. Study of several electrocatalytic processes, such as the oxidation of methanol and ethanol<sup>69,70</sup> and hydrogenation of benzene<sup>71</sup> on Pt, Rh and Pd surfaces can be conducted on the basis of transition metal based SERS substrates.

### 1.6.3 Applications of SERS in environmental analysis

Pesticides, herbicides, pharmaceutical chemicals in water and in saliva, banned food dyes, aromatic chemicals in regular aqueous solutions and in sea water, derivatives of chlorophenol and amino acids, explosives, nicotine, organic pollutants present in the humic fraction of soil, Technetium-99, endocrine disrupting chemicals and dissolved methane have been detected by SERS technique<sup>54,72-74</sup>. SERS-enabled optical fiber sensors are chemically stable and are not susceptible to environmental changes and hence they are ideal for remote sensing,

especially in a hostile environment. In the first report on SERS-enabled optical fiber sensors<sup>72</sup>, optical fiber was employed as only light delivering and collecting tool. Hence the progress has been moved towards the development of integration of the SERS substrate directly on one of the end faces of single-mode fibers, multi-mode fibers and optical fiber bundles. The use of photonic crystal fibers for SERS has also been reported. Photonic fibers offer the integration of microfluids and photonics<sup>75-77</sup>.

Detection of the single haemoglobin molecule, glucose and cancer gene are some of the examples of ultrafast detection capability of SERS technique. Recently biochips are introduced for label-free detection of pathogens and their toxins. The advantages of SERS over fluorescence spectroscopy is that its applications are not limited by the use of labelling agents and photo bleaching and hence it is possible to provide detailed chemical information about molecules even in a complex environment.

#### **1.6.4 Applications of SERS in bioimaging**

SERS has been realised as a method for the study of living cells, both in intracellular and extracellular measurements<sup>78</sup>. It is possible to identify biomolecules or intracellular components in single cells independently by SERS measurements. Eliasson *et al.*<sup>79</sup> demonstrated this measurements using gold-incorporated lymphocyte living cell. SERS allows not only the ultrasensitive detection but also helps to study various processes involved in a living cell. Breuzard *et al.*<sup>80</sup> studied the adsorption of mitoxantrone on the plasma membrane of sensitive (HCT-116 S) or BCRP/MXR-type resistant (HCT-116 R) cells by

SERS. Based on SERS technique Kneipp *et al.*<sup>81</sup> reported *in-vivo* detection of indocyanine green (ICG) on gold nanoparticles. The experiment delivers information about local molecular structure in its biological environment which is important for the study of cellular processes. Recently SERS has been successfully applied to distinguish cancerous cells from normal cells. Lee *et al.*<sup>82</sup> used Au/Ag core-shell nanoparticles conjugated with monoclonal antibodies and a highly sensitive cellular image of living normal HEK293 cells and HEK293 cells expressing PLC $\gamma$ 1 is obtained by SERS. The tumour development in the cell is characterized by abnormal expression of PLC $\gamma$ 1 protein.

## 1.7 Raman instrumentation

The progress in the field of instrumentation has dramatically advanced Raman spectroscopic technique for research and industrial applications. Sir C.V. Raman utilized sunlight as the excitation source and naked eye as photodetector for the measurement of Raman signal from a number of highly concentrated substances (mostly pure organic solvents). However, this setup was inadequate for many applications, which involve diluted solutions or solids. Discovery of laser together with highly sensitive and efficient detection system bring about the scope of Raman spectroscopy in the majority of applications. Modern implementations have lasers that possess characteristics such as large intensity and monochromaticity as the excitation source. A modern Raman spectrometer mainly consists of four components and is schematically shown in figure 1.7.

- 1) laser source,
- 2) sample-illumination system,

- 3) holographic optics,
- 4) suitable spectrometer with a detector.

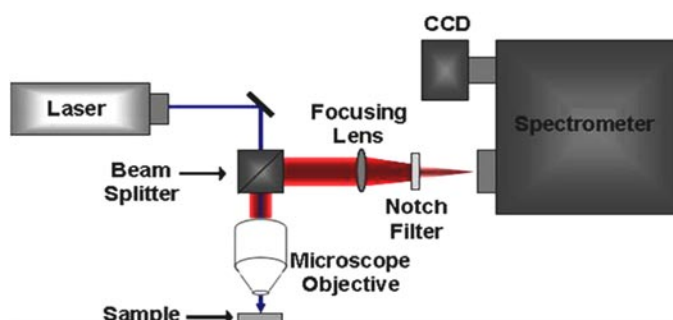


**Figure 1.7:** Schematic of a microRaman spectrometer

In traditional Raman experiments, the sample is irradiated with monochromatic light and the scattered light is observed at right angles to the incident radiation. However, in modern confocal Raman microscopes, the scattered signals are recollected by a microscope objective in  $180^\circ$  geometry.

### 1.7.1 Laser source

An extremely intense source of radiation is essential for increasing the intensity of very weak Raman scattered radiation. In a traditional spectrometer, the sample tube is surrounded by a collection of few mercury lamps. However, in modern Raman spectrometers, laser sources have become the standard irradiation system. The choice of the excitation wavelength depends on nature of the sample and hence very crucial for many Raman spectroscopic applications. The Raman scattering efficiency varies with fourth power of frequency of excitation and hence UV and visible lasers produce more intense Raman signal than

lasers with near-infrared (NIR) and IR wavelengths. Hence during early stages, short wavelength Argon and Krypton ion lasers were widely used. These lasers can generate Raman signals that are up to three times more intense than those produced with the corresponding He-Ne laser. But for Raman imaging experiments excitation with IR wavelengths are used. Moreover, the probability of resonance Raman scattering is high with the UV excitation if the wavelength of laser coincides with the electronic absorption of a molecule. The resonance Raman scattering process enhances the Raman intensity by a factor of  $10^2$  to  $10^4$ . At the same time, excitation with the UV or visible photons produces high fluorescence background which can drown the Raman signal invisible and hence limits its biomedical applications. However, the deep UV ( $< 250$  nm) is a fluorescence free region and also provide very high detection sensitivities and low-background noise. To reduce the fluorescence emission and photodecomposition due to shorter wavelength while keeping a reasonable Raman sensitivity, He-Ne source has been extensively practiced.

In biological samples, absorption of UV and visible wavelength results in photodamage and hence NIR (650 to 1400 nm) or IR excitation (1400 to 3000 nm) is the best choice. Both are much used for biomedical samples. Water absorption band in the IR region decreases the scattering efficiency and causes heating of the sample. Therefore excitation wavelength between 650 and 850 nm, where biochemical molecules possess very low absorption, is the best choice for cell and tissue imaging. Initially Many gas lasers like He-Ne (632.8 nm) and Ar-Kr (676.4 nm) were employed. Later NIR diode and solid state lasers (671, 785, 830 nm, etc.) have been preferred as excitation sources due to their small size, cost effectiveness and ease of operation compared to

most of the gas lasers. During focusing the laser to the sample, the laser power is mostly limited to 10 to 50 mW in order to avoid photodamage of the sample. In SERS, near infrared (NIR) laser sources such as diode lasers and Nd:YAG laser are advantageous due to the suitability for the excitation of localized surface plasmons on gold nanoparticles.

### **1.7.2 Sample-illumination system**

The type of sample illumination system to be used depends on the intensity and nature of radiation source. A confocal microscope is used to focus the laser into the sample through one of the auxiliary parts which helps to reduce the influence of fluorescence and other stray light background signals. It also offers advantages such as minimal sample requirements, high throughput, good collection efficiency and ability to collect signals from micron size samples with good lateral resolution. In Raman imaging instrumentation, this confocal microscope facilitates high resolution in the axial direction. In addition, a motorized microscope stage and motorized objectives are attached to scan in the spatial direction. Combined with transmission or reflection imaging, it is possible to precisely target the laser into the sample. Depending on the application and excitation wavelength, the objectives, that are well corrected for chromatic aberrations, are chosen. A sample holder, which is a simple capillary tube, is used for liquid samples. Usually, water is selected as solvent since water produces very weak Raman signal.

### **1.7.3 Filters**

Different types of holographic filters or wavelength selectors are used throughout the path of the laser. A narrow band-pass filter is placed in between source and sample and which is used to isolate the

single exciting line from plasma lines of the laser. Another holographic notch filter is placed in the collection path of scattered laser for efficient and narrow bandwidth rejection of Rayleigh line. Notch filter transmits less than 0.5% of the backscattered laser line and more than 90% of the remaining Raman scattered frequencies to the detector.

#### **1.7.4 Charge coupled devices**

In modern Raman systems, charge coupled devices (CCDs) are commonly used as detectors. The CCD is a chip which consists of a 2D array of silicon photosites known as pixels. Each photosite includes two conductive electrodes separated by thin silica dielectric layer. The photosite is also surrounded by a non-conductive barrier. The charges build up due to the interaction of photons on the chip are stored in the capacitor located below the electrodes. Once the Raman scattered photons signals are collected, the acquired spectra are generated using control electronics and computer. CCD can simultaneously collect the entire spectrum and also possess excellent sensitivity as compared with photodiode array detectors.

### **1.8 Advancements in surface enhanced Raman scattering**

Due to the extreme sensitivity of SERS, the discovery of SERS brought large progress in the field of surface science both in fundamental and applied research. It not only offers a stimulus for the study of enhanced optical scattering from the surfaces and interfaces, but also opened up various fields that include surface enhanced second-harmonic generation (SE-SHG)<sup>83,84</sup>, surface enhanced fluorescence (SEF)<sup>20,21</sup>, surface enhanced infrared spectroscopy (SEIRS)<sup>85,86</sup> and surface enhanced sum frequency generation (SE-SFG)<sup>87,88</sup>. Even though

it is realized as an ultrasensitive and in situ diagnostic probe that can be applicable to biological, electrochemical, catalytic and other ambient interfaces. SERS is not developed as a powerful technique as expected, because of three obstacles which blocked its practice and theory. First, the huge enhancement is not shown by transition metals, which have widened applications in industry. Second, the fabrication of an appropriate SERS-active substrate is still a challenge. The last is the vague knowledge about the total enhancement mechanisms.

### **1.8.1 Extension of SERS to transition metals**

The surface plasmon resonance of transition metals not in the visible region. Hence transition metals generally do not exhibit SERS mechanism. Various attempts have been developed to produce SERS active transition metals which include depositing SERS active metals onto the non-SERS active substrates such as semiconductors and depositing non-SERS active materials over SERS active substrates. Here SERS effect is induced due to long range electromagnetic effect by metals<sup>41,89-91</sup>. The strong electromagnetic field induced on SERS active substrates is damped significantly and its range is 3-10 atomic layers. Weaver *et al.*<sup>90</sup> developed a pinhole free transitional metal over the SERS active Au surface by electrochemical atomic layer epitaxy using constant current deposition at a low current density. This technique is highly promising and the adsorption of phthalic acid on anatase TiO<sub>2</sub> and anthrax biomarker on the Al<sub>2</sub>O<sub>3</sub> over layer were successfully investigated by SERS using substrates fabricated via above strategy<sup>92</sup>. Tian *et al.* showed small SERS effect in transition metals fabricated with proper methods of preparation<sup>93</sup>. SERS effect from the Pt, Fe, Zn, Ni, Co, Ru and Pd was achieved<sup>32,94</sup>, that were generated by

electrochemical oxidation-reduction cycle (ORC) and current controlled ORC. SERS enhancement factor varies from one to four orders of magnitude depending on the nature of the metals and the surface morphology.

### **1.8.2 Fabrication of versatile SERS active substrates**

To enhance the applicability of SERS technique, qualified SERS active substrates should possess large enhancement factor, good reproducibility in enhancement factor from one sample to another and SERS signal stability over a period of time. In addition, fabrication procedure should be simple and easy to be applied in parallel to many substrates<sup>95</sup>. Template structure involved in the substrate should be chemically inert, mechanically stable and should not produce any additional peaks in the Raman spectrum. Progress in nanotechnology shows its power to fabricate new SERS active substrates consisting of ordered and reproducible nanostructures. In principle, nanofabrication techniques offer a solution to two problems; one is the creation of well-defined structures to give extraordinary enhancement factors and the other is the opportunity to create reproducible structures in large numbers that will give rise to reproducible Raman signals. The well known substrates with metallic nanostructures include roughened metal electrodes, metal island like films, metal nanocolloids, silver coated nanospheres, silver coated titanium dioxide and silica nanoparticles, metal coated alumina nanoparticles, lithographic and grafting structures, silver membranes and silver coated cellulose<sup>12</sup>. Another important progress in SERS substrate is the development of anisotropic metal nanostructures that include synthesis of core-shell particles, triangular prisms, nanorices, nanocrescents<sup>96</sup>, rods, nanobars, dumbbells and

nanocubes<sup>97</sup> and even more obscure shapes have been illustrated. Each of these nanostructures may offer the ability to tune the plasmon band into the interested spectral regions (i.e, near IR).

### **1.8.3 Single molecule SERS**

Etchegoin and Le Ru<sup>98</sup> proposed a bianalyte approach for single molecule detection, in which two molecular species with approximately equal bonding affinity is simultaneously adsorbed within a "hot spot". Then, there has a probability of finding the two constituent probe molecule in the mixture is given by Poisson distribution. The occupancy of a single molecule in each "hot spots" can be proven by the detection of only one type of molecule in a statistically significant set of measurements. This bianalyte approach was refined by Van Duyne<sup>99</sup> using normal and deuterated Rhodamine 6G (R6G) dye molecules (to ensure virtually identical Raman cross sections in the molecular mixture) to show that the SERS spectra measured from a multiplicity of "hot spots" junctions were due to a single R6G molecule.

### **1.8.4 Tip enhanced SERS**

One of the milestone developments in SERS is tip enhanced SERS (TERS), in which a metallic AFM/STM tip is scanned over the surface of the sample so that the "hot spots" are formed between a tip and the surface<sup>100-102</sup>. TERS surmount diffraction limited detection limit of optical spectroscopic techniques through coupling scanning probe microscopy and Raman spectroscopy. TERS make use of the coupled plasmon resonance generated between a flat metallic surface and a tip as shown in figure 1.8. Nowadays, TERS technique has grown into the controllable tip-sample gap and the "hot spot" volume. The sensitivity

of this can be improved by employing ultra sharp tips or high aspect ratio nanoparticles which profoundly modify "hot spot" properties.

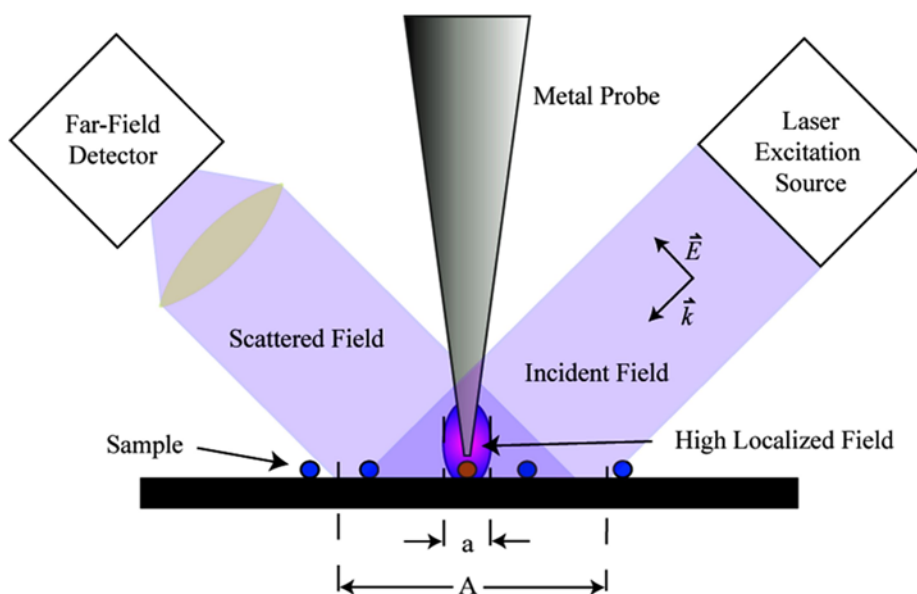


**Figure 1.8:** Tip enhanced SERS

### 1.9 SERS probes

Even though, SERS technique can be used with any Raman active analytes, good SERS probes must possess two major characteristics. The characteristic of a good SERS probe depends on intrinsic Raman scattering cross section and on metal-probe interactions. The intensity of normal Raman spectra also depends on the incident laser wavelength. For example, intense Raman spectra are observed for dyes with electronic energies close to the exciting laser energy. This is termed as resonance Raman scattering (RRS). Usually intensities of RRS are  $\approx 10^6$  larger than that of normal (off-resonance) Raman intensities. Hence

usually good SERS probes are good Raman scatterer like dyes. When SERS measurement is carried out under resonance Raman condition, it is referred as surface enhanced resonance Raman scattering (SERRS). Not all molecules with good Raman scattering cross section are good SERS probes, but the molecule should efficiently interact with metal surface. Some molecules such as thiols have strong affinity towards silver or gold surface and covalent bonds are formed with the metal surface. While molecules such as dyes interact with metal surface through physisorption. Electrostatic interaction is another common mechanism in which probes with opposite charge is adsorbed onto the charged metal substrate and hence in such cases it is not possible to consider the probe and substrate as independent. In biological application, surface functionalization of SERS substrate is carried out to specifically bind to one type of analyte. For example, metal substrate functionalised with antigens are used for specific detection of antibodies. Rhodamine 6G and benzene thiol are used as SERS probes throughout this thesis work.

Rhodamine 6G (R6G) has strong absorption in the green ( $\lambda_{\text{abs}}$  -535 nm) region and produces fluorescence in the blue region. R6G molecules carry a positive charge in solution and can easily adsorb negative charged metallic nanocolloids. The physisorption is by non-covalent bonding and it is easily reversible. R6G is a relatively large molecule which consists of 64 atoms including 4 conjugated ring structures with the very large intrinsic Raman scattering cross section. Using visible excitation wavelength, R6G can induce resonance Raman scattering which further improve SERS scattering cross section. The differential scattering cross section,  $d\sigma/d\Omega$  amounts to  $\sim 10^{-27} \text{ cm}^2 \cdot \text{sr}^{-1}$ .

But a serious drawback is that the collected photons include both inelastic scattered photons and photons emitted through fluorescence process. Even very weak fluorescence overwhelm the Raman signals and hence excitation wavelength far from absorption wavelength is chosen to avoid the fluorescence.

Benzene thiol (BT) forms a chemical bond with gold or silver substrate and possesses very large differential scattering cross sections  $d\sigma/d\Omega \sim 10^{-29} \text{cm}^2/\text{sr}$ . BT molecule has very small number of Raman active modes and has no absorption above 300 nm which avoids the fluorescent background of Raman spectra. BT forms a monolayer over the substrate which makes the molecules as a good analyte to test the uniformity of SERS substrate. It is also possible to calculate the enhancement factor accurately using BT than physisorbed R6G molecule.

## References

- [1] M. Fleischmann, P.J. Hendra, and A.J. McQuillan, *Chem. Phys. Lett.* **26**, 163 (1974).
- [2] K. Kneipp, Y. Wang, H. Kneipp, L.T. Perelman, I. Itzkan, R.R. Dasari, and M.S. Feld, *Phys. Rev. Lett.* **78**, 1667 (1997).
- [3] A. Smekal, *Naturwissenschaften* **11**, 873 (1923).
- [4] C. V. Raman and K.S. Krishnan, *Nature* **121**, 501 (1928).
- [5] J.R. Ferraro, K. Nakamoto, and C.W. Brown, *Introductory Raman Spectroscopy*, 2nd ed. (Academic Press, Boston, 2003).
- [6] H.W. Schroetter and H.W. Kloeckner, *Raman Spectroscopy of Gases and Liquids* (Springer, Verlag, Berlin,, 1979).

- [7] B. Schrader and D.S. Moore, *Pure Appl. Chem.* **69**, 1451 (1997).
- [8] E. Le Ru and P. Etchegoin, *Principles of Surface-Enhanced Raman Spectroscopy and Related Plasmonic Effects* (Elsevier, Oxford, UK, 2009).
- [9] D.L. Jeanmaire and R.P. Van Duyne, *J. Electroanal. Chem. Interfacial Electrochem.* **84**, 1 (1977).
- [10] J.A. Creighton, C.G. Blatchford, and M.G. Albrecht, *J. Chem. Soc. Faraday Trans.* **75**, 790 (1979).
- [11] M.L. Brongersma and P.G. Kik, editors, *Surface Plasmon Nanophotonics* (Springer Netherlands, Dordrecht, 2007).
- [12] R. Aroca, *Surface-Enhanced Vibrational Spectroscopy* (John Wiley & Sons, Ltd, Chichester, UK, 2006).
- [13] S. Schlücker, *Angew. Chem. Int. Ed.* **53**, 4756 (2014).
- [14] M. Moskovits, *J. Raman Spectrosc.* **36**, 485 (2005).
- [15] H. Xu, J. Aizpurua, M. Käll, and P. Apell, *Phys. Rev. E* **62**, 4318 (2000).
- [16] P.L. Stiles, J.A. Dieringer, N.C. Shah, and R.P. Van Duyne, *Annu. Rev. Anal. Chem.* **1**, 601 (2008).
- [17] A. Otto, “Classical” and “Chemical” Origins, in *Light Scattering in Solids IV*, Eds. M. Cardona and G. Güntherodt, *Topics in Applied Physics* (Springer-Verlag, Berlin, 1984).
- [18] W.L. Barnes, A. Dereux, and T.W. Ebbesen, *Nature* **424**, 824 (2003).
- [19] J.M. Brockman, B.P. Nelson, and R.M. Corn, *Annu. Rev. Phys. Chem.* **51**, 41 (2000).
- [20] W. Knoll, *Annu. Rev. Phys. Chem.* **49**, 569 (1998).

- [21] K.L. Kelly, E. Coronado, L.L. Zhao, and G.C. Schatz, *J. Phys. Chem. B* **107**, 668 (2003).
- [22] A.J. Haes, C.L. Haynes, A.D. McFarland, G.C. Schatz, R.P. Van Duyne, and S. Zou, *MRS Bull.* **30**, 368 (2011).
- [23] M.A. Garcia, *J. Phys. D. Appl. Phys.* **44**, 283001 (2011).
- [24] J.B. Schneider, *Understanding the Finite-Difference Time-Domain Method* (2012).
- [25] G. Sun, *Surface-Enhanced Raman Spectroscopy Investigation of Surfaces and Interfaces in Thin Films on Metals*, Ruhr University Bochum, China, 2007 ( Ph. D. Thesis).
- [26] L.A. Dick, A.J. Haes, and R.P. Van Duyne, *J. Phys. Chem. B* **104**, 11752 (2000).
- [27] J.A. Dieringer, A.D. Mcfarland, N.C. Shah, D.A. Stuart, A. V Whitney, C.R. Yonzon, M.A. Young, X. Zhang, and R.P. Van Duyne, *Faraday Discuss.* **132**, 9 (2006).
- [28] B.J. Kennedy, S. Spaeth, M. Dickey, and K.T. Carron, *J. Phys. Chem. B* **103**, 3640 (1999).
- [29] A.D. McFarland, M.A. Young, J.A. Dieringer, and R.P. Van Duyne, *J. Phys. Chem. B* **109**, 11279 (2005).
- [30] P.C. Lee and D. Meisel, *J. Phys. Chem.* **86**, 3391 (1982).
- [31] M. Fleischmann, *Chem. Phys. Lett.* **26**, 2 (1974).
- [32] W.B. Cai, B. Ren, X.Q. Li, C.X. She, F.M. Liu, X.W. Cai, and Z.Q. Tian, *Surf. Sci.* **406**, 9 (1998).
- [33] Y. Xie, D.Y. Wu, G.K. Liu, Z.F. Huang, B. Ren, J.W. Yan, Z.L. Yang, and Z.Q. Tian, *J. Electroanal. Chem.* **554-555**, 417 (2003).

- [34] R.P. Van Duyne, J.C. Hulteen, and D. a. Treichel, *J. Chem. Phys.* **99**, 2101 (1993).
- [35] K.S. Giesfeldt, R.M. Connatser, M.A. De Jesús, N. V. Lavrik, P. Dutta, and M.J. Sepaniak, *Appl. Spectrosc.* **57**, 1346 (2003).
- [36] K.S. Giesfeldt, R.M. Connatser, M.A. De Jesús, P. Dutta, and M.J. Sepaniak, *J. Raman Spectrosc.* **36**, 1134 (2005).
- [37] P. Freunsch, R.P. Van Duyne, and S. Schneider, *Chem. Phys. Lett.* **281**, 372 (1997).
- [38] L.A. Dick, A.D. McFarland, C.L. Haynes, and R.P. Van Duyne, *J. Phys. Chem. B* **106**, 853 (2002).
- [39] U. Nickel, K. Mansyreff, and S. Schneider, *J. Raman Spectrosc.* **35**, 101 (2004).
- [40] Y. Wang, D. Li, P. Li, W. Wang, W. Ren, S. Dong, and E. Wang, *J. Phys. Chem. C* **111**, 16833 (2007).
- [41] S. Zou and M.J. Weaver, *Anal. Chem.* **70**, 2387 (1998).
- [42] H. Chik and J.M. Xu, *Mater. Sci. Eng. R Reports* **43**, 103 (2004).
- [43] S.J. Joo Y, *Bull Korean Chem Soc* **16**, 808 (1995).
- [44] C.L. Haynes and R.P. Van Duyne, *J. Phys. Chem. B* **105**, 5599 (2001).
- [45] W. Yue, Z. Wang, Y. Yang, L. Chen, A. Syed, K. Wong, and X. Wang, *J. Micromech. Microeng.* **22**, 125007 (2012).
- [46] D. Bhandari, *Surface-Enhanced Raman Scattering : Substrate Development and Applications in Analytical Detection*, University of Tennessee - Knoxville, 2011 (Ph. D. Thesis).
- [47] N.A.A. Hatab, J.M. Oran, and M.J. Sepaniak, *ACS Nano* **2**, 377 (2008).

- [48] Y.-L. Loo, R.L. Willett, K.W. Baldwin, and J.A. Rogers, *J. Am. Chem. Soc.* **124**, 7654 (2002).
- [49] Y.-L. Loo, R.L. Willett, K.W. Baldwin, and J.A. Rogers, *Appl. Phys. Lett.* **81**, 562 (2002).
- [50] E. Menard and J.A. Rogers, *Springer Handbook of Nanotechnology*, 2nd edn. (Springer, Berlin 2007).
- [51] E.C. Le Ru, E. Blackie, M. Meyer, and P.G. Etchegoin, *J. Phys. Chem. C* **111**, 13794 (2007).
- [52] K. Kneipp, Katrin, Moskovits, Martin, editor, *Surface-Enhanced Raman Scattering: Physics and Applications* (Springer, Verlag, Berlin,, Harald, 2006).
- [53] M. Fan, G.F.S. Andrade, and A.G. Brolo, *Anal. Chim. Acta* **693**, 7 (2011).
- [54] G.A. Baker and Æ.D.S. Moore, *Anal Bioanal Chem* **382**, 1751 (2005).
- [55] V.M.S. V.P. Drachev, *Surface-Enhanced Raman Scattering: Physics and Applications (Topics in Applied Physics) 103* (Springer, Verlag, Berlin,, Heidelberg, 2006).
- [56] R. Picorel, G. Chumanov, T.M. Cotton, G. Montoya, S. Toon, and M. Seibert, *J. Phys. Chem.* **98**, 6017 (1994).
- [57] A. Kaminska, O. Inya-Agha, R.J. Forster, and T.E. Keyes, *Phys. Chem. Chem. Phys.* **10**, 4172 (2008).
- [58] P. Corio, G.F.. Andrade, I.C.. Diógenes, I.. Moreira, F.. Nart, and M.L.. Temperini, *J. Electroanal. Chem.* **520**, 40 (2002).
- [59] J.-J. Feng, D.H. Murgida, U. Kuhlmann, T. Utesch, M.A. Mroginski, P. Hildebrandt, and I.M. Weidinger, *J. Phys. Chem. B* **112**, 15202 (2008).

- [60] T. Vo-Dinh, *TrAC Trends Anal. Chem.* **17**, 557 (1998).
- [61] N.R. Isola, D.L. Stokes, and T. Vo-Dinh, *Anal. Chem.* **70**, 1352 (1998).
- [62] T. Vo-Dinh, L.R. Allain, and D.L. Stokes, *J. Raman Spectrosc.* **33**, 511 (2002).
- [63] M. Culha, D. Stokes, L.R. Allain, and T. Vo-Dinh, *Anal. Chem.* **75**, 6196 (2003).
- [64] M. Kahraman, A.I. Zamaleeva, R.F. Fakhrullin, and M. Culha, *Anal. Bioanal. Chem.* **395**, 2559 (2009).
- [65] B. Yan, A. Thubagere, W.R. Premasiri, L.D. Ziegler, L. Dal Negro, and B.M. Reinhard, *ACS Nano* **3**, 1190 (2009).
- [66] E. Temur, I.H. Boyaci, U. Tamer, H. Unsal, and N. Aydogan, *Anal. Bioanal. Chem.* **397**, 1595 (2010).
- [67] K.E. Shafer-Peltier, C.L. Haynes, M.R. Glucksberg, and R.P. Van Duyne, *J. Am. Chem. Soc.* **125**, 588 (2003).
- [68] O. Lyandres, N.C. Shah, C.R. Yonzon, J.T. Walsh, M.R. Glucksberg, and R.P. Van Duyne, *Anal. Chem.* **77**, 6134 (2005).
- [69] M.J. Weaver, *Top. Catal.* **8**, 65 (1999).
- [70] M.J. Weaver, *J. Raman Spectrosc.* **33**, 309 (2002).
- [71] J.-L. Yao, B. Ren, G.-K. Liu, D.-Y. Wu, R.-A. Gu, and Z.-Q. Tian, *J. Raman Spectrosc.* **34**, 221 (2003).
- [72] T. Vo-dinh, *Trends Anal. Chem.* **17**, 557 (1998).
- [73] R. Dijkstra, F. Ariese, C. Gooijer, and U. Brinkman, *TrAC Trends Anal. Chem.* **24**, 304 (2005).
- [74] R.A. Álvarez-Puebla and L.M. Liz-Marzán, *Energy Environ. Sci.* **3**, 1011 (2010).

- [75] H. Yan, J. Liu, C. Yang, G. Jin, C. Gu, and L. Hou, *Opt. Express* **16**, 8300 (2008).
- [76] Y. Han, S. Tan, M.K.K. Oo, D. Pristinski, S. Sukhishvili, and H. Du, *Adv. Mater.* **22**, 2647 (2010).
- [77] Y. Xuan, S. Chao, W. Damon, and C.G. Rebecca Newhouse, Bin Chen, Jin Z. Zhang, *J. Opt. Soc. Am. A* **27**, 977 (2010).
- [78] M.K. Hossain and Y. Ozaki, *Curr. Sci.* **97**, 192 (2009).
- [79] S.A. Maier and H.A. Atwater, *J. Appl. Phys.* **98**, 011101 (2005).
- [80] G. Breuzard, J.-F. Angiboust, P. Jeannesson, M. Manfait, and J.-M. Millot, *Biochem. Biophys. Res. Commun.* **320**, 615 (2004).
- [81] J. Kneipp, H. Kneipp, W.L. Rice, and K. Kneipp, *Anal. Chem.* **77**, 2381 (2005).
- [82] S. Lee, S. Kim, J. Choo, S.Y. Shin, Y.H. Lee, H.Y. Choi, S. Ha, K. Kang, and C.H. Oh, *Anal. Chem.* **79**, 916 (2007).
- [83] C.K. Chen, A.R.B. de Castro, and Y.R. Shen, *Phys. Rev. Lett.* **46**, 145 (1981).
- [84] K. Li, M.I. Stockman, and D.J. Bergman, *Phys. Rev. B* **72**, 153401 (2005).
- [85] A. Hartstein, J.R. Kirtley, and J.C. Tsang, *Phys. Rev. Lett.* **45**, 201 (1980).
- [86] Z. Zhang and T. Imae, *J. Colloid Interface Sci.* **233**, 99 (2001).
- [87] M. Bonn, H. Ueba, and M. Wolf, *J. Phys. Condens. Matter* **17**, S201 (2005).
- [88] A. V Balakin, V.A. Bushuev, B.I. Mantsyzov, I.A. Ozheredov, E. V Petrov, A.P. Shkurinov, P. Masselin, and G. Mouret, *Phys. Rev. E. Stat. Nonlin. Soft Matter Phys.* **63**, 046609 (2001).
- [89] Y. Zhang, X. Gao, and M.J. Weaver, *J. Phys. Chem.* **97**, 8656 (1993).

- [90] M.J. Weaver, S. Zou, and H.Y.H. Chan, *Anal. Chem.* **72**, 38 A (2000).
- [91] M.F. Mrozek, H. Luo, and M.J. Weaver, *Langmuir* **16**, 8463 (2000).
- [92] X. Zhang, J. Zhao, A. V Whitney, J.W. Elam, and R.P. Van Duyne, *J. Am. Chem. Soc.* **128**, 10304 (2006).
- [93] Z.-Q. Tian, B. Ren, and D.-Y. Wu, *J. Phys. Chem. B* **106**, 9463 (2002).
- [94] L.W.H. Leung and M.J. Weaver, *J. Am. Chem. Soc.* **109**, 5113 (1987).
- [95] G. Sauer, U. Nickel, and S. Schneider, *J. Raman Spectrosc.* **31**, 359 (2000).
- [96] G.L. Liu, Y. Lu, J. Kim, J.C. Doll, and L.P. Lee, *Adv. Mater.* **17**, 2683 (2005).
- [97] B.J. Wiley, Y. Chen, J.M. McLellan, Y. Xiong, Z.-Y. Li, D. Ginger, and Y. Xia, *Nano Lett.* **7**, 1032 (2007).
- [98] P.G. Etchegoin, E.C. Le Ru, and A. Fainstein, *Phys. Chem. Chem. Phys.* **13**, 4500 (2011).
- [99] S.L. Kleinman, E. Ringe, N. Valley, K.L. Wustholz, E. Phillips, K. a Scheidt, G.C. Schatz, and R.P. Van Duyne, *J. Am. Chem. Soc.* **133**, 4115 (2011).
- [100] M.J. Natan, *Faraday Discuss.* **132**, 321 (2006).
- [101] B. Pettinger, B. Ren, G. Picardi, R. Schuster, and G. Ertl, *Phys. Rev. Lett.* **92**, 096101 (2004).
- [102] J.A. Dieringer, A.D. McFarland, N.C. Shah, D.A. Stuart, A. V. Whitney, C.R. Yonzon, M.A. Young, X. Zhang, and R.P. Van Duyne, *Faraday Discuss.* **132**, 9 (2006).



## Development of colloidal SERS substrates using silver nanocubes

In this chapter, development of colloidal SERS active substrates with excellent sensitivity and high reproducibility using silver nanocubes synthesized via the solvothermal method is discussed. Finite-difference time-domain simulation is carried out in detail to visualize dipole generation in nanocube during localized surface plasmon resonance and to locate the respective "hot spots" in silver nanocube responsible for the huge Raman enhancement. The prediction is verified by SERS analysis of the synthesized nanocubes using Rhodamine 6G molecule. An excellent sensitivity with a detection limit of  $10^{-17}$  M and a very high enhancement factor of  $1.2 \times 10^8$  confirms "hot spots" in the nanocube. SERS activity is also carried out for crystal violet and for the food adulterant sudan I molecules.

The paper titled "Development of High-Sensitive, Reproducible Colloidal Surface-Enhanced Raman Spectroscopy Active Substrate Using Silver Nanocubes for Potential Biosensing Applications, **Kudilatt Hasna**, Kiran Lakshmi, Madambi Kunjukuttan Ezhuthachan Jayaraj, Kumaran Rajeev Kumar and Murukeshan Vadakke Matham, *Journal of Nanophotonics*, 2016, 10 (2), 026020" has been published based on the results presented in this chapter.

## 2.1 Introduction

SERS is one of the few truly nanoscale effects and is strongly linked to unique properties of metal nanostructures<sup>1</sup>. The dominant contribution to enhanced Raman signal of SERS up to 12 orders of magnitude is an account to localized surface plasmon resonance (LSPR) property of metallic nanostructures. These localized surface plasmons are coherent oscillations of free electrons in resonance<sup>1,2</sup> with incident light at a certain frequency and which is in the visible range for coinage metal nanoparticles such as Ag, Au and Cu<sup>3</sup>. A near-field enhancement occurs in the vicinity of metal nanoparticle during resonances and its magnitude extremely depends on the geometry and size of the metal nanoparticles. The electromagnetic field in gap region of a pair of strongly coupled nanoparticles and in sharp corners of nanocubes or triangles can be drastically amplified large enough for single molecule detection<sup>2,4</sup>. Although the “hot spot” phenomenon has been extensively investigated both from the theoretical and experimental point of view, it remains a mysterious and feebly understood topic. Lack of large scale SERS active substrates with high density of “hot spots” yielding huge enhancement is the main obstruction to the development of SERS technique for practical applications. Substantiate explorations have been being made to achieve rough metal surface<sup>5</sup>, metal nanocolloids<sup>6</sup> and well-ordered patterned structures<sup>7-9</sup> as SERS active substrates that have been fabricated by various methods and techniques<sup>10</sup>.

Though various SERS active substrates using sophisticated techniques are developed, researchers are still focused on colloidal SERS substrate, especially on silver or gold nanocolloids. Because, its

synthesis follow easy steps and it is easy to generate large enhancement factor by tuning their aggregation and shape. Metal nanocolloids hold a significant role in the development of SERS field because single molecule SERS detection was first reported in aggregated silver nanocolloids<sup>2</sup>. Typically metal nanocolloids are produced by reduction of metal salts in solution. The colloidal particles are stabilized in solution by coulombic or steric repulsions among particles and it is achieved by adding a stabilizing agent to the mixture that will prevent colloidal particles from excessive aggregation and precipitation. In some reactions, same compound act as both reducing and stabilizing agent. The size and shape of metal nanoparticles can be changed by using appropriate reducing and stabilizing agents.

## **2.2 Literature review on colloidal SERS substrates**

In order to possess specific surface plasmon property, metal nanoparticles with a dimension between 10 and 100 nm are desired. LSPR enhances the Raman signal of the molecules on or near the metal surface<sup>11</sup>. Therefore synthesis of metal nanoparticles with different surface plasmon wavelengths and electric field enhancement is important in the field of SERS research. Various methods have been developed for the preparation of metal nanoparticles with different sizes, shapes and compositions. Wet chemistry methods such as chemical reduction, laser ablation and photoreduction offer inexpensive and simple approaches for metal nanocolloid generation.

### ***Chemical reduction***

In chemical reduction method, metal salts are reacted with variety of reducing agents and capping agents. The first report on the synthesis of

metal nanocolloidal solution was in 1979 by Creighton<sup>12</sup> using ice-cold sodium borohydride ( $\text{NaBH}_4$ ) solution for the reduction of silver nitrate ( $\text{AgNO}_3$ ) and potassium tetrachloroaurate(III)  $\text{K}[\text{AuCl}_4]$  to synthesize silver and gold nanocolloids respectively. In the preliminary work itself, it is seen that SERS signal intensity is strongly depends on excitation wavelength<sup>12</sup>. Another common method for silver nanoparticle preparation is the reduction of  $\text{AgNO}_3$  by sodium citrate under boiling<sup>13,14</sup>. The commonly used reducing agents are sodium citrate<sup>19</sup>, sodium borohydride<sup>15</sup>, hydrazine<sup>16</sup> and hydroxylamine hydrochloride<sup>17,18</sup>. The size, shape, size distribution and aggregation of nanoparticles are controlled by the reaction temperature, reaction time, the type of metal salts, reducing agents and capping agents.

Solution based synthesis of metal nanoparticles mainly involves three stages: nucleation (reduction of metal ions to zerovalent atoms), seeding (evolution from nuclei to seeds) and growth (evolution from seeds to nanocrystals). Shape controlled synthesis is possible by controlling thermodynamics and kinetics of each stage. Successful modifications such as selective etching, modifying the surface free energy, etc., are employed to control population and structure of seed which enables the synthesis of metal nanostructures with different morphologies.

### ***Laser ablation and photoreduction***

Laser ablation and photoreduction are other common methods for the synthesis of 'chemically pure' metal nanoparticles without any residual ions or by-products. Ag, Au, Cu and Pt nanoparticles are synthesized via laser ablation method both in aqueous solution and in

organic solvents. These nanocolloidal solutions have been successfully demonstrated for SERS and SERRS spectral studies of several absorbates<sup>19,20</sup>. The method involves a pulsed laser (1064 nm, 532 nm, 355 nm from a Nd:YAG laser) to ablate metal plates or foils placed in distilled water or sodium chloride (NaCl) solution<sup>21,22</sup>. Laser pulse energy, nature of the solvent, time of ablation and laser wavelength control the properties of formed metal nanocolloids<sup>21</sup>.

In photoreduction method, radiation such as gamma or UV is commonly used to reduce the metal salt<sup>23,24</sup>. Ciou *et al.*<sup>25</sup> prepared silver nanoprisms by photoirradiation (using sodium lamp) of silver nitrate in trisodium citrate and sodium bromohydrate.

### ***Silver nanocolloids as SERS active substrates***

Coinage metals like gold, silver and copper exhibit LSPR absorption in the visible range. Among them, the highest efficiency of plasmon absorption is exhibited by silver. The most efficient mechanism, by which radiation interacts with matter is the localized surface plasmon resonance in metal nanostructures. Another advantage of silver is that its plasmon resonance can be tuned to any wavelength in the visible region. Colloidal SERS substrates are formed by dispersing metal particles in liquid and these particles are indefinitely dispersed in the solution. The complexity of colloidal SERS substrate preparation depends on the type of target molecule, equipment used for analysis, etc. Following are the common methods that are employed for the preparation of silver nanocolloids: Lee and Meisel method<sup>14</sup>, Leopold and Lendl method<sup>18</sup>, Creighton method<sup>12</sup>, etc.

Even though the unstable colloidal solution is not suitable for SERS measurement, controlled aggregation favours the performance of SERS substrate with the formation of "hot spots". Various routes for aggregation of metal nanocolloids include the addition of a passive electrolyte such as potassium nitrate and an active electrolyte such as potassium chloride. Polymers or long-chain ions such as poly(L-lysine)<sup>26</sup>, DNA<sup>27</sup>, etc., are also been used as aggregation agents which generate shell with nanogaps which again act as "hot spots" and produce enhancement factor of the order  $10^8$  to  $10^9$ . These types of aggregation systems provide an adaptable platform for SERS substrate that is able to generate high electromagnetic effect and offer detection of a single molecule. Hence with proper knowledge of colloids, metal nanocolloids with very strong control on size and shape can be synthesized which open a new door for fabrication of competitive SERS substrate based on nanocolloids.

Since the report on colloidal gold and silver suspensions by Creighton *et al.*<sup>12</sup>, many reports dealing with tight control of size, shape, aggregation and surface properties of silver and gold nanocolloids have been published. Large number of synthetic protocols are currently available for the controlled preparation of colloidal nanostructures with various shapes such as spheres<sup>32</sup>, rods<sup>28</sup>, cubes<sup>29</sup>, octahedra<sup>30</sup> and various other geometries<sup>31,32</sup> within a wide size range. Moreover, the potential of colloidal metal nanoparticles with anisotropic morphology to localize electromagnetic fields at certain points known as "hot spots" support the synthesis of triangular plates<sup>33</sup>, nanostars<sup>34</sup>, etc., to perform as an efficient SERS substrate.

### 2.3 Synthesis of silver nanocubes by solvothermal method

In the present work, silver nanostructures were grown by solvothermal method. The solvothermal process is a potential method for synthesis of nanoparticles with different morphologies in economic and simple way. Solvothermal process involves high pressure and its reactions are mainly characterized by nature of precursors, temperature and reaction time<sup>35,36</sup>.

Uniform sized silver nanocubes were synthesized via solvothermal method following the previous reports<sup>37</sup>. 20 ml ethylene glycol (EG) solution of NaCl with different concentration (0, 0.1, 0.5, 10 & 20 mM) and 0.8 g of polyvinylpyrrolidone (PVP) was stirred for 1 hr. The mixed solution was added dropwise into 20 ml to a magnetically stirred EG solution of AgNO<sub>3</sub> (0.1 & 0.15 M) for 1 hr. Afterwards, the solution was transferred into a 100 ml teflon-lined autoclave and was kept at 160 °C for different reaction times (2, 4, 6 and 12 hrs) in an electric oven. Sodium chloride is added into the precursor solution that act as nucleation seed for the growth of nanocubes. Finally, the products were centrifuged with acetone and then with de-ionized water at 8000 rpm for 30 min. The supernatants were removed and this process was repeated three times in order to purify silver nanocolloids. Finally, samples were preserved in de-ionized water.

The chemical reaction for the formation of silver atoms is given below:



Silver atoms are formed by reducing  $\text{AgNO}_3$  precursor with EG with the mechanism given by the above equations<sup>38</sup>. These silver atoms accumulate and form nanoparticles when its concentration reaches a critical value. Due to the relatively high reaction temperature, Brownian motion and mobility of surface atoms increase which enhances the probability of collision, adhesion and coalescence. However, PVP is added to the reaction to serve primarily as a stabilizer against aggregation, but it can also serve as a reductant and even play a role in controlling shape. The reduction does not occur without PVP, and well-defined silver nanostructures have not been produced by this system with other polymers<sup>39</sup>. With the addition of NaCl into  $\text{AgNO}_3$  solution, AgCl colloids are generated which act as a nucleation seed for the growth of silver nanowires and the diameter of nanowires is determined by the size of initial AgCl nucleation seeds. With the increase of NaCl concentration, large quantities of AgCl colloids are generated. Since reaction time is longer, AgCl is decomposed into silver and chloride ion. This generates a situation at which concentration of silver ions is large and initial seeds with various morphology such as single crystal, single-twinned and multi-twinned silver are generated and these seeds nucleate rapidly and grow into silver nanocubes, bipyramids and nanowires respectively. The progression of growth of silver nanostructures is schematically represented in figure 2.1.

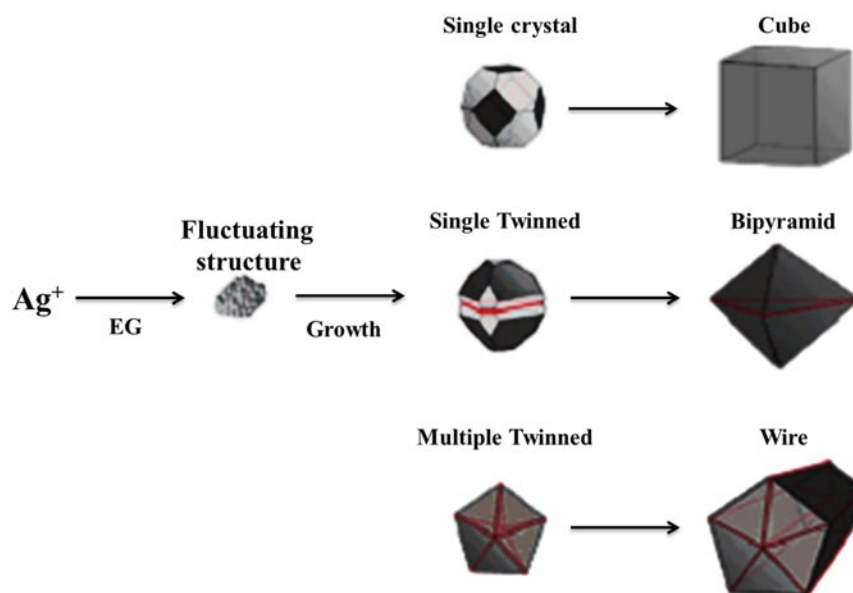


**Figure 2.1:** Illustration of path leading to the formation of well-defined silver nanostructures

## 2.4 Characterization of silver nanocubes

### 2.4.1 Morphological characterization

Morphological studies of the synthesized nanocolloids were carried out using Zeiss Ultra 55 FESEM (field emission scanning electron microscope). FESEM images of silver nanostructures synthesized at 180 °C for 2 hrs using NaCl concentration of 0.1mM and 10 mM are shown in figure 2.2(a) and 2.2(b) respectively. Morphology of the samples synthesized using 20 mM NaCl for 2 hrs and 12 hrs is shown in figure 2.2(c) and 2.2(d).

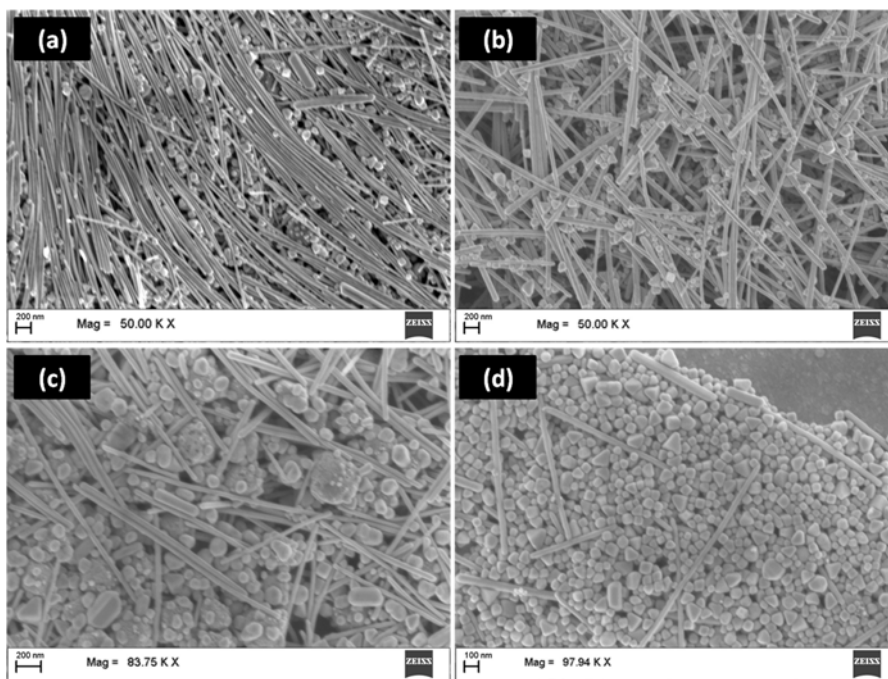
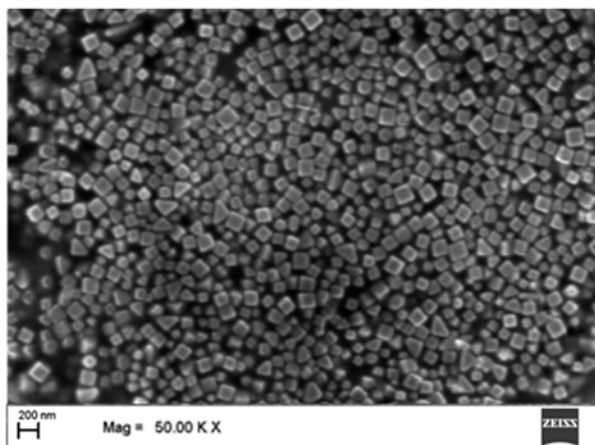


**Figure 2.2:** FESEM images of silver nanostructures synthesized (a) for 0.1 M  $\text{AgNO}_3$  and 0.5 mM NaCl at 160 °C for 2 hrs (b) for 0.1 M  $\text{AgNO}_3$  and 10 mM NaCl at 160 °C for 2 hrs (c) for 0.1 M  $\text{AgNO}_3$  and 20 mM NaCl at 160 °C for 2 hrs (d) for 0.1 M  $\text{AgNO}_3$  and 20 mM NaCl at 160 °C for 12 hrs

From the figure 2.2, it is clear that a large number of silver nanowires are formed for a lower concentration of NaCl. When the concentration increases, other structures such as silver nanocubes, bipyramids, etc., are formed in addition to silver nanowires. When reaction time increases to 12 hrs, number of silver nanowires are decreased and some bipyramidal structures along with large number of truncated silver nanocubes are formed. Since the number of silver ions also plays an important role in controlling the final morphology of synthesized silver nanostructures,

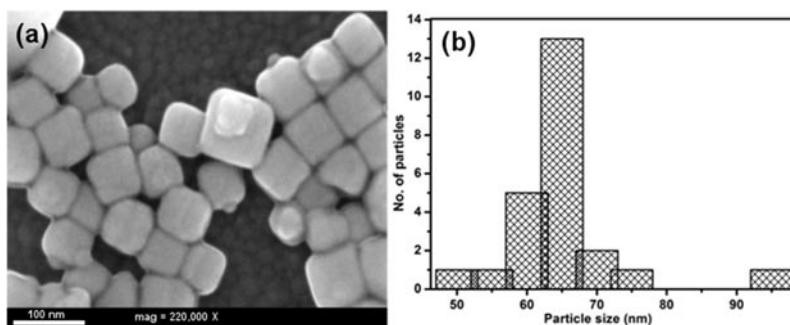
the samples are prepared for  $\text{AgNO}_3$  concentration of 0.15 M for the growth of silver nanocubes only.

Figure 2.3 shows FESEM image of the sample prepared for an  $\text{AgNO}_3$  concentration of 0.15 M and NaCl concentration of 20 mM at  $180^\circ\text{C}$  for 12 hrs. It is observed that, with the increase of silver nitrate concentration, sample with silver nanocubes (Ag NCs) only is formed.



**Figure 2.3:** FESEM image of silver nanocubes synthesized at  $160^\circ\text{C}$  for 12 hrs via solvothermal reaction

Figure 2.4(a) and 2.4(b) show magnified FESEM image of synthesized silver nanocube and the corresponding size distribution of the nanocubes. It is observed that the nanocubes are grown nearly with homogeneous size with an average size of 65 nm.



**Figure 2.4:** (a) magnified FESEM image of silver nanocubes (b) particle size distribution of the nanocubes

### 2.4.2 Optical characterization

Surface plasmon resonance (SPR) study was carried out by measuring ultraviolet–visible (UV–Vis) absorption spectra of silver nanocolloids acquired with Jasco V 570 UV-Vis-NIR spectrophotometer. Localized surface plasmons are coherent dipole oscillations of conduction electrons in metal nanostructures in resonance with incident light of wavelength comparable with the size of the metal nanostructure. The natural frequency of oscillations is known as plasmon frequency and when an electromagnetic radiation of frequency matches with plasmon frequency incident upon metal nanostructures, plasmon oscillates with maximum amplitude and is known as localized surface plasmon resonance (LSPR). At LSPR, light is absorbed by the metal nanostructures. Hence an absorbance peak is obtained in UV-Vis absorption spectrum corresponds to LSPR.

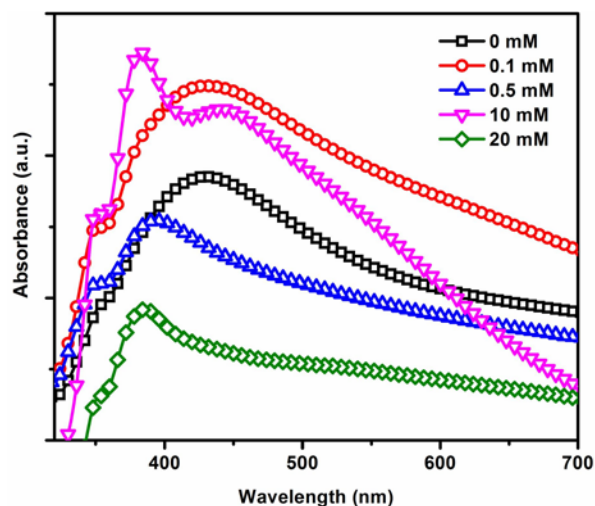


**Figure 2.5:** UV-Vis absorption spectra of silver nanostructures synthesized at different NaCl concentration at 160 °C for 2 hrs

Figure 2.5 shows UV-Vis absorption spectra of metal nanostructures synthesized for different NaCl concentrations at 160 °C for 2 hrs. It is observed that number and position of LSPR peaks vary with NaCl concentration. For an NaCl concentration of 0.1 mM, two peaks at 350 and 427 nm are observed which are attributed to transverse and longitudinal plasmons present in silver nanowires. For higher concentrations of NaCl, position and number of LSPR vary due to the formation of a mixture of nanowires and other irregular structures which are in accordance with FESEM results.

The variations in UV-Vis absorption spectra of silver nanostructures synthesized using 20 mM NaCl, at 160 °C for various reaction time are given in figure 2.6. From figure 2.6, it is clear that LSPR peaks change with reaction time which is in accordance with FESEM images. The

broadening in LSPR peaks in all the spectra is due to the inhomogeneous size distribution of the synthesized structures (section 1.2.3).

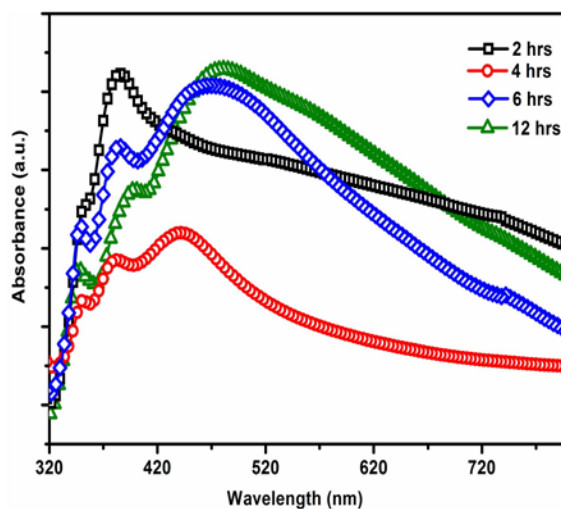


**Figure 2.6:** UV-Vis absorption spectra of silver nanostructures synthesized using 20 mM NaCl, at 160 °C for various reaction time

The UV-Vis absorption spectrum of silver nanocubes is given in figure 2.7(a). The spectrum shows more than one resonance peak, because a cube has several distinct symmetries for dipole resonance. The main dipole resonance peak is at 465 nm and two smaller resonance peaks are observed at 350 and 389 nm as shoulders.

Scattering cross section for a 65 nm silver nanocube was calculated via Mie theory using Lumerical FDTD (finite-difference time-domain method) simulation software and is given in figure 2.7(b). Mie scattering in 3D set up was used for calculating scattering cross section of silver nanocube. Perfectly matched layers (PML) were employed as boundary

along x and y directions. The computational domain consists of a square of grid points with a resolution of  $x = y = z = 3$  nm. Grids of smaller dimensions indicate that the simulation results are converged. The simulation time was set at 200 fs so that the fields decay completely before the termination of simulation.

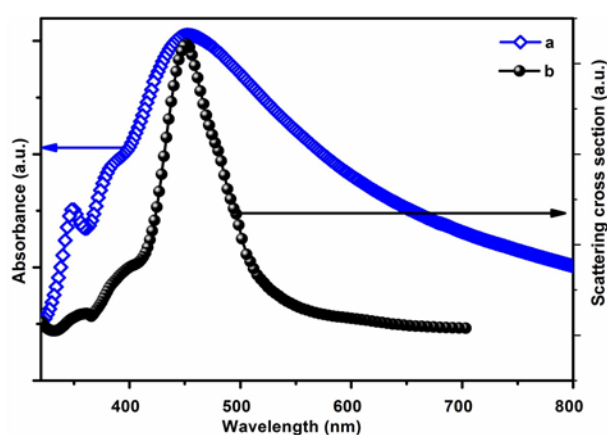


**Figure 2.7:** (a) UV-Vis absorption spectrum of silver nanocubes (b) calculated scattering cross section for silver nanocube

Figure 2.7 clearly confirms that the experimental spectrum matches with predicted spectrum. Mainly two different ways of charge accumulation are possible in Ag NC, one along edges and other across diagonal of cubes. The diagonals can be body diagonals or face diagonals. The two possible dipole generation in silver nanocubes are schematically represented in figure 2.8. The variation in position of LSPR in accordance with morphology can be explained on the basis of Mie theory. According to Mie theory, the extinction spectrum for an arbitrary shape is given by<sup>40</sup>

$$E(\lambda) = \frac{24\pi^2 N a^3 \varepsilon_{out}^{\frac{3}{2}}}{\lambda \ln(10)} \left[ \frac{\varepsilon_i(\lambda)}{\varepsilon_r(\lambda) + \chi \varepsilon_{out}^2(\lambda) + \varepsilon_i^2(\lambda)} \right] \dots\dots\dots 2.1$$

where  $\varepsilon_r$  and  $\varepsilon_i$  are real and imaginary components of metal dielectric function respectively and  $\varepsilon_{out}$  is the dielectric constant of external environment. Here  $\chi$  is the shape factor that accounts for metal nanostructures with various geometries and  $\chi = 2$  represents case for spherical shape.  $\varepsilon_r$  is a function of wavelength and hence the position of LSPR is determined by the situation at which  $\varepsilon_r = -\chi\varepsilon_{out}$ . In fact, the position of surface plasmon is determined by the magnitude of restoring force offered by the positive ion core in metal nanostructures. In the case of charge accumulated across diagonals, the charge separation will be large. Hence surface plasmon resonance corresponding to dipoles created on diagonally opposite corners is red shifted with that corresponding to the edges.

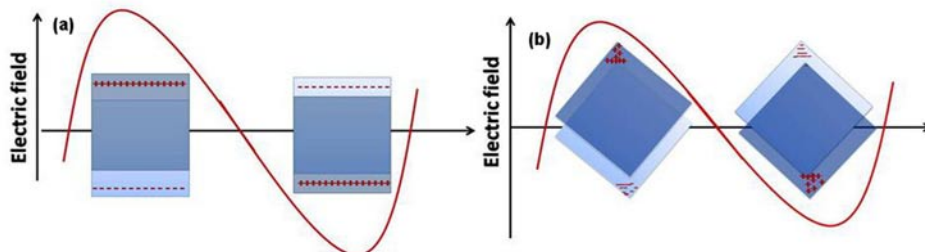


**Figure 2.8:** Schematic representation of the generation of dipoles (a) at the edges and (b) at the corners of cubic structure.

### 2.4.3 Electric field enhancement studies in silver nanocubes

Finite-difference time-domain method (FDTD) is one of the analytical methods for solving Maxwell's equations<sup>41,42</sup>. The 2D FDTD method (Lumerical Solutions Ltd.) was carried out to calculate the

electric field distribution and to locate "hot spots" in nanocube. Perfectly matched layers (PML) were employed as boundary along x and y directions. The computational domain consists of a square of grid points with a resolution of  $x = y = 0.5$  nm. Grids of smaller dimensions indicate that the simulation results are converged. A total field scattering field plane wave source with wavelength corresponding LSPR of nanocubes with propagation along y axis is used for simulation.

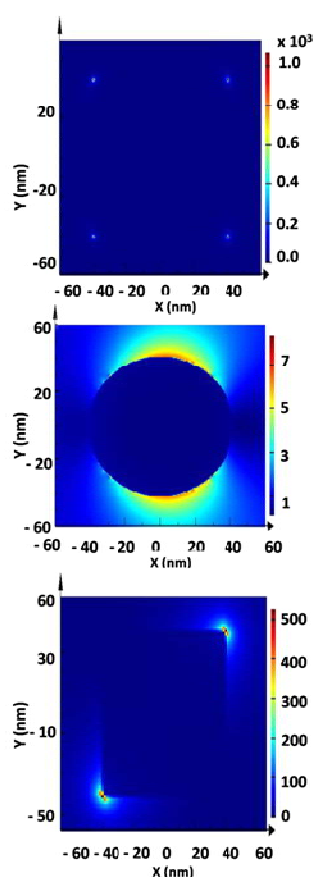


**Figure 2.9:** Electric field intensity distribution (a) at the corners of silver nanocube of size 65nm (b) surrounding spherical silver nanoparticles of size 65nm (c) at cross-diagonal corners of nanocube of size 65nm

The excitation wavelength is selected in accordance with the theory that maximum electric field enhancement is induced only on excitation with a wavelength corresponding to localized surface plasmon resonance<sup>7</sup>. Figure 2.9(a) visualises the "hot spots" appearing at the corners of nanocube and figure 2.9(b) shows field enhancement around spherical silver nanoparticles. Figures 2.9(a) and 2.9(b) confirm the huge enhancement in the electric field at sharp corners of nanocube as compared with a spherical shape. It is also observed that electric field enhancement occurs across the diagonal of the cube (figure 2.9(c)). These results clearly support the predicted dipole generation in silver nanocube. Hence the three peaks are assigned as follows: the peak at 350 nm arises from one edge of the cube being positively charged while the opposite side is negatively charged. The LSPR peaks observed at 389 and 465 nm are assigned to dipoles generated across the face and body diagonals of the cube respectively.

#### **2.4.4 SERS characterization of silver nanocubes**

Raman measurements were performed on a Horiba Jobin Yvon LabRAM HR microRaman spectrometer with 514.5 nm of Ar ion laser and 632.8 nm of HeNe laser as excitation lines. The probed area was 1  $\mu\text{m}$  in diameter and the incident power was 9 mW. All the spectra were obtained at room temperature with an integration time of 5 s. Rhodamine 6G (R6G) molecule was used as the reporter probe for SERS measurement. Silver nanocube based SERS substrate was fabricated by dropping the solution on to a cleaned silicon substrate and then allowed to dry naturally. Loading probe molecules onto Ag nanocubes was accomplished by dropping 30  $\mu\text{L}$  of R6G solutions onto the as-prepared substrate and dried naturally.

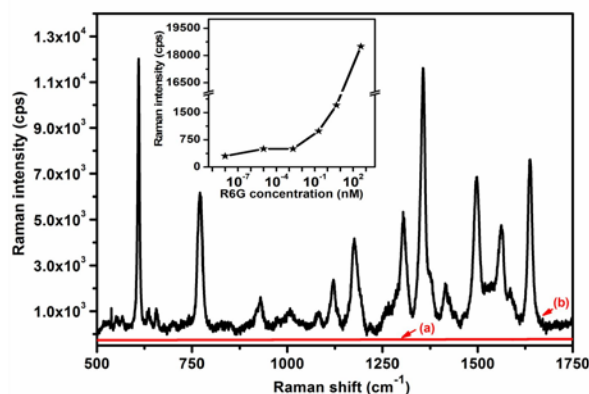


**Figure 2.10:** Normal Raman spectrum of R6G molecule (curve a) and SERS spectrum of  $4.5 \times 10^{-7}$  M R6G with using silver nanocube as SERS active substrate (curve b). Inset shows intensity variation of prominent peak,  $611 \text{ cm}^{-1}$  of R6G as a function of concentration.

FDTD analysis provides the information that the synthesized nanocubes generate "hot spots" at the corners. But the field enhancement does not have a large dependence on edge length, since "hot spots" are generated at the corners and field intensity is mainly affected by the variation in angles between edges. Even though the size distribution is not homogenous in nature, the prepared silver nanocubes are excellent candidates for SERS active substrates with good uniformity.

So as to demonstrate competency in SERS activity of the synthesized nanocube colloids, SERS spectra were recorded with Rhodamine 6G (R6G) as test molecule with concentration varying from high to the detection limit. SERS studies of R6G were conducted under surface enhanced resonance Raman conditions on excitation with Ar ion laser of wavelength 514.5 nm which is near the peak absorption wavelength of R6G ( $\sim 532$  nm) and is shown in figure 2.10. Figures 2.10 shows

representative Raman measurement of R6G molecule in methanol with a concentration of  $4.5 \times 10^{-7}$  M on a bare glass substrate and on silver nanocube based SERS substrate respectively. Figure 2.10 clearly demonstrates the capability of silver nanocube as SERS active substrate. The measured spectral characteristics of R6G on nanocube surfaces include 611, 773, 1011, 1184, 1311, 1363, 1568, and 1650  $\text{cm}^{-1}$ . The 611, 773, and 1184  $\text{cm}^{-1}$  modes are associated with C–C–C ring in-plane bending, out-of-plane bending and C–C stretching vibrations respectively, and the 1363, 1572, and 1649  $\text{cm}^{-1}$  modes are associated with aromatic C–C stretching vibrations and 1011  $\text{cm}^{-1}$  is associated with the phenyl ring and  $\text{COOC}_2\text{H}_5$  side group<sup>43,44</sup>.

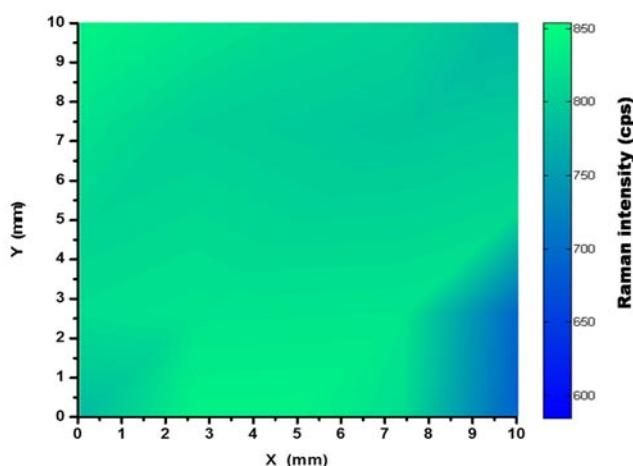


**Figure 2.11:** Variation in Raman intensity of R6G over Ag NC based SERS substrate

The detection limit of our Ag NC based SERS active substrate is determined by repeating the Raman experiment under the same conditions with lower concentrations of R6G. The corresponding

intensity variation of the prominent peak,  $611\text{cm}^{-1}$  of R6G as a function of concentration is shown inset of figure 2.10. The prominent peaks of R6G are clearly observed even at a concentration of  $10^{-17}$  M and thus detection limit is found to be  $10^{-17}$  M. The reproducibility and uniformity of nanocube based SERS substrates are confirmed by repeated SERS measurements on different positions and on different sets of samples. The 2D colour mapping in figure 2.11 shows that different points in the substrate provide SERS signal with almost the same intensity.

In order to isolate electromagnetic enhancement in Ag NC, SERS studies were performed under non-resonant condition with an excitation wavelength of 632.8 nm. Figure 2.12(a) and 2.12(b) show Raman measurement of R6G molecule in methanol with a concentration of  $9 \times 10^{-6}$  M on Ag NC based SERS substrate under non resonant (632.8 nm) and resonant excitation (514.5 nm) respectively. From the figure 2.12 it is clear that Raman intensity is almost comparable with each other which confirm the high sensitivity of silver nanocube based SERS substrate. The detection limit using 632.8 nm excitation is found to be 5 nM.

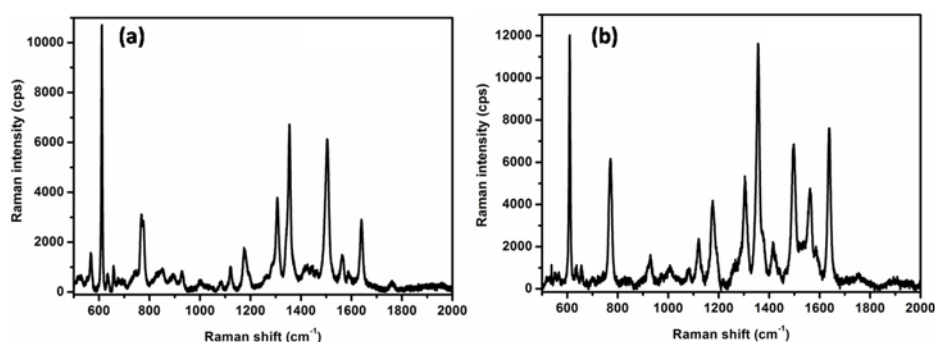


**Figure 2.12:** SERS spectra of  $9 \times 10^{-6}$  M R6G under (a) non-resonant (b) resonant excitation

The competence of the fabricated colloid based SERS substrate can be shown by demonstrating its capability of detecting multi analyte molecule. SERS analysis were again carried out using crystal violet and food adulterant Sudan I as probe molecule. The SERS spectra of  $6 \times 10^{-6}$  M crystal violet and  $3 \times 10^{-6}$  M Sudan I are given in figure 2.13. All the peaks match with the characteristic peaks of crystal violet<sup>46</sup> and Sudan I<sup>46</sup>. The peaks at 802, 912, 1172 and 1372  $\text{cm}^{-1}$  in the spectrum matches with characteristic peaks of crystal violet.

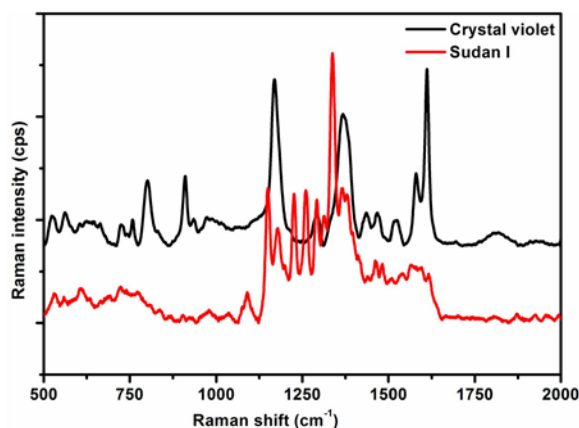


**Figure 2.13:** SERS spectra of  $6 \times 10^{-6}$  M crystal violet and  $3 \times 10^{-6}$  M Sudan I

The average enhancement factor of the SERS substrates is roughly calculated using the well-known equation<sup>40</sup>. Enhancement factor,  $EF = \frac{I_{SERS}/N_{SERS}}{I_{RS}/N_{RS}}$ , where  $I_{SERS}$  and  $I_{RS}$  represent the intensity of the same band of R6G (here,  $611 \text{ cm}^{-1}$ ) of SERS spectrum and normal Raman spectrum, and  $N_{SERS}$  and  $N_{RS}$  represent the corresponding number of molecules in the detection volume. Intensity of SERS spectrum of  $10^{-17}$  M R6G molecule,  $I_{SERS} = 300$  counts (figure 2.10).

Normal Raman spectrum of R6G molecules under same measurement condition (accumulation time was 10 s) was carried out and is given in figure 2.14. It is found that  $I_{RS} = 1500$  counts.

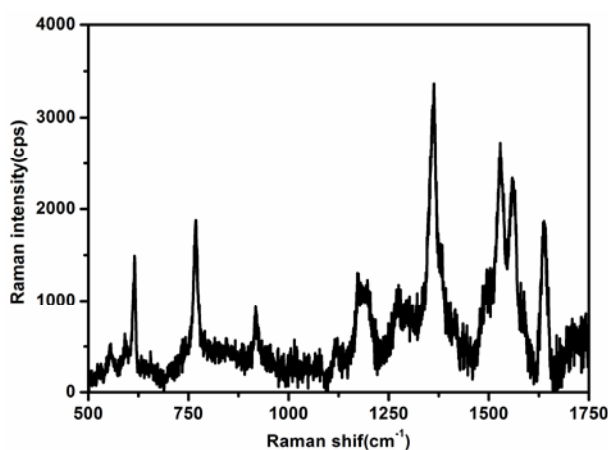


**Figure 2.14:** Normal Raman spectrum of Rhodamine 6G molecule

$N_{RS}$  is estimated using the equation,  $N_{RS} = \rho N A V / (M.W)$ , where  $\rho$  is density of R6G and its value is 1.26 g/mL and  $M.W$ , molecular weight = 479.02 g/mol.  $V$  is the collection volume and is equal to laser spot area multiplied with collection depth. Based on our instrument, laser spot size is  $1\mu\text{m}$  and depth of focus is also  $1\mu\text{m}$ . Hence  $N_{RS}$  is estimated to be  $1.24 \times 10^9$ .  $N_{SERS}$  in focused area is roughly estimated to be 1 or 2. Finally, EF is estimated to be  $1.2 \times 10^8$ . The earlier reports on SERS activity of sharp silver nanocubes show that a maximum enhancement factor of  $2.96 \times 10^5$  can be achieved<sup>45</sup>. The economically synthesized, reproducible SERS substrate with large enhancement factor is expected to be a significant contribution in the field of qualified SERS substrates.

## 2.5 Conclusion

Uniform silver nanocubes are synthesized via solvothermal method by reducing silver nitrate with ethylene glycol. The concentration of NaCl, AgNO<sub>3</sub> and reaction time are optimized for the synthesis of silver nanocubes. The LSPR in silver nanocubes are studied in detail by UV-Vis absorption spectra and Mie scattering simulation. The field enhancement is investigated by FDTD method and it is observed that the "hot spots" are located at the corners of nanocube. SERS activity of the Ag nanocubes synthesized is successfully investigated and found very competent with high reproducibility and detection limit of 10<sup>-17</sup> M. SERS activity for crystal violet and for food adulterant Sudan I molecule are also tested and which demonstrates the multi-analyte detection capability of the SERS substrate. Based on these result it can be proposed that Ag nanocubes are promising SERS substrates for the detection of trace amount of chemical analytes.

## References

- [1] M.A. Garcia, J. Phys. D. Appl. Phys. **44**, 283001 (2011).
- [2] (a) K. Kneipp, Y. Wang, H. Kneipp, L.T. Perelman, I. Itzkan, R.R. Dasari, and M.S. Feld, Phys. Rev. Lett. **78**, 1667 (1997).  
b) S. Nie, S. R. Emory. Science. **275**, 1102 (1997).  
c) A. Otto, I. Mrozek, H. Grabhorn and W. Akemann, J. Phys.: Condens, Matter, **4**, 1143 (1992).
- [3] M.L. Brongersma and P.G. Kik, editors, *Surface Plasmon Nanophotonics*(Springer Netherlands, Dordrecht, 2007).
- [4] Y. Lu, G.L. Liu, and L.P. Lee, Nano Lett. **5**, 5 (2005).
- [5] K.-H. Yang, Y.-C. Liu, and C.-C. Yu, J. Mater. Chem. **18**, 4849 (2008).
- [6] H. Liang, H. Yang, W. Wang, J. Li, and H. Xu, J. Am. Chem. Soc. **131**, 6068 (2009).

- [7] Y.-R. Zhang, Y.-Z. Xu, Y. Xia, W. Huang, F.-A. Liu, Y.-C. Yang, and Z.-L. Li, *J. Colloid Interface Sci.* **359**, 536 (2011).
- [8] L. Gunnarsson, E.J. Bjerneld, H. Xu, S. Petronis, B. Kasemo, and M. Käll, *Appl. Phys. Lett.* **78**, 802 (2001).
- [9] B. Cui, L. Clime, K. Li, and T. Veres, *Nanotechnology* **19**, 145302 (2008).
- [10] M.J. Banholzer, J.E. Millstone, L. Qin, and C.A. Mirkin, *Chem. Soc. Rev.* **37**, 885 (2008).
- [11] S. Schlücker, editor, *Surface Enhanced Raman Spectroscopy* (Wiley-VCH Verlag GmbH & Co. KGaA, Weinheim, Germany, 2010).
- [12] J.A. Creighton, C.G. Blatchford, and M.G. Albrecht, *J. Chem. Soc. Faraday Trans. 2* **75**, 790 (1979).
- [13] Y. Wang, D. Li, P. Li, W. Wang, W. Ren, S. Dong, and E. Wang, *J. Phys. Chem. C* **111**, 16833 (2007).
- [14] P.C. Lee and D. Meisel, *J. Phys. Chem.* **86**, 3391 (1982).
- [15] X. Dong, X. Ji, J. Jing, M. Li, J. Li, and W. Yang, *J. Phys. Chem. C* **114**, 2070 (2010).
- [16] U. Nickel, K. Mansyreff, and S. Schneider, *J. Raman Spectrosc.* **35**, 101 (2004).
- [17] M. V Cañamares, J. V Garcia-Ramos, J.D. Gómez-Varga, C. Domingo, and S. Sanchez-Cortes, *Langmuir* **21**, 8546 (2005).
- [18] N. Leopold and B. Lendl, *J. Phys. Chem. B* **107**, 5723 (2003).
- [19] H. Cui, P. Liu, and G.W. Yang, *Appl. Phys. Lett.* **89**, 153124 (2006).
- [20] M.S. Sibbald, G. Chumanov, and T.M. Cotton, *J. Phys. Chem.* **100**, 4672 (1996).

- [21] M. Procházka, P. Mojzeš, J. Štěpánek, B. Vlčková, and P.-Y. Turpin, *Anal. Chem.* **69**, 5103 (1997).
- [22] T.M.C. John Neddersen, George Chumanov, *Appl. Spectrosc.* **47**, 1959 (1993).
- [23] R. Sato-Berrú, R. Redón, A. Vázquez-Olmos, and J.M. Saniger, *J. Raman Spectrosc.* **40**, 376 (2009).
- [24] S. Tan, M. Erol, A. Attygalle, H. Du, and S. Sukhishvili, *Langmuir* **23**, 9836 (2007).
- [25] S. Ciou, Y. Cao, H. Huang, D. Su, and C. Huang, **113**, 9520 (2009).
- [26] C.H. Munro, W.E. Smith, and P.C. White, *Analyst* **118**, 731 (1993).
- [27] S. Basu, S. Jana, S. Pande, and T. Pal, *J. Colloid Interface Sci.* **321**, 288 (2008).
- [28] Y. Yang, L. Xiong, J. Shi, and M. Nogami, *Nanotechnology* **17**, 2670 (2006).
- [29] S.H. Im, Y.T. Lee, B. Wiley, and Y. Xia, *Angew. Chemie* **117**, 2192 (2005).
- [30] J. Zhang, Y. Gao, R.A. Alvarez-Puebla, J.M. Buriak, and H. Fenniri, *Adv. Mater.* **18**, 3233 (2006).
- [31] C.G. Khoury and T. Vo-dinh, *J. Phys. Chem. C* **112**, 18849 (2008).
- [32] W. Li, P.H.C. Camargo, X. Lu, and Y. Xia, *Nano Lett.* **9**, 485 (2009).
- [33] Y. Sun, B. Mayers, and Y. Xia, *Nano Lett.* **3**, 675 (2003).
- [34] A. Garcia-Leis, J.V. Garcia-Ramos, and S. Sanchez-Cortes, *J. Phys. Chem. C* **117**, 7791 (2013).
- [35] A.A. Chernov, *Annu. Rev. Mater. Sci.* **3**, 397 (1973).

- [36] R. Roy, J. Solid State Chem. **111**, 11 (1994).
- [37] W.C. Zhang, X.L. Wu, C.X. Kan, F.M. Pan, H.T. Chen, J. Zhu, and P.K. Chu, Appl. Phys. A **100**, 83 (2010).
- [38] B. Wiley, Y. Sun, B. Mayers, and Y. Xia, Chemistry **11**, 454 (2005).
- [39] B.J. Wiley, S.H. Im, Z.-Y. Li, J. McLellan, A. Siekkinen, and Y. Xia, J. Phys. Chem. B **110**, 15666 (2006).
- [40] P.L. Stiles, J.A. Dieringer, N.C. Shah, and R.P. Van Duyne, Annu. Rev. Anal. Chem. **1**, 601 (2008).
- [41] R.L. K. S. Kunz, *The Finite-difference Time-domain Method for Electromagnetics* (Boca Raton, Florida: CRC press, 1993).
- [42] S.C.H. A. Taflove, *Computational Electrodynamics: The Finite-Difference Time-domain Method* (Boston: London:ArtechHouse, 2000).
- [43] P. Hildebrandt and M. Stockburger, J. Phys. Chem. **88**, 5935 (1984).
- [44] A.M. Michaels, M. Nirmal, and L.E. Brus, J. Am.Chem. Soc. **121**, 9932 (1999).
- [45] J.M. McLellan, A. Siekkinen, J. Chen, and Y. Xia, Chem. Phys. Lett. **427**, 122 (2006).
- [46] H. Ahn, P. Thiyagarajan, L. Jia, S. Kim, J. Yoon, E.L. Thomas, and J. Jang, Nanoscale **5**, 1836 (2013).
- [47] W. Cheung, I.T. Shadi, Y. Xu, and R. Goodacre, J. Phys. Chem. C **114**, 7285 (2010).



## Development of patterned SERS substrates using pyramidal arrays and nanotriangular arrays

This chapter highlights fabrication of patterned SERS substrates using pyramidal arrays and nanotriangular arrays with uniformly distributed "hot spots" so that SERS substrates possess spatial reproducibility as well as sample to sample reproducibility. A new replication method is introduced for the fabrication of micrometer sized pyramidal arrays. The steps involved are fabrication of silicon master with inverted pyramidal structure via photolithography and replication of pyramidal arrays from the silicon master using a commercially available replication kit. To further increase density of "hot spots" and enhance SERS activity of patterned SERS substrates by an economic way, nanotriangular array based SERS substrate is fabricated. Arrays of triangular pits are fabricated by electron beam lithography and are replicated to PMMA by nanoimprinting technique. In addition to sample to sample reproducibility of SERS enhancement, the method also offers fabrication of an economic SERS substrate.

The paper entitled "Fabrication of cost-effective, highly reproducible large area arrays of nanotriangular pillars for surface enhanced Raman scattering substrate", **Kudilatt Hasna**, Aldrin Antony, Joaquim Puigdollers, Kumaran Rajeev Kumar, and Madambi Kunjukuttan Jayaraj, *Nano Research*, DOI 10.1007/s12274-016-1190-y has been published based on the results presented in this chapter.

### 3.1 Introduction

Electromagnetic SERS enhancement is sensitive to size, shape, spatial arrangement and dielectric environment of metal nanostructures<sup>1</sup>. Metal nanostructures with "hot spots" provide enhancement factor as high as  $10^{12}$ - $10^{15}$  and enable detection of even a single molecule<sup>2-4</sup>. Although very large enhancement factor with single molecule detection capability is reported in colloidal SERS substrate, reproducibility of the SERS signal is low in the colloidal substrate. In order to overcome the issue of colloidal SERS substrate in sample to sample reproducibility of SERS signal, patterned or periodic substrates are desirable. Lithography is a conventional technique to fabricate arrays of metal nanostructures with uniform and controlled morphology. It is reported that in addition to "hot spots" at small gaps<sup>5</sup>, anisotropic nanostructures such as triangles, cones, etc., with highly sharp surface features also show strong SERS effect due "lightening effect"<sup>6</sup>.

Lithography is classified into photolithography and electron beam lithography (EBL). The dimension of nanostructures fabricated by photolithography is limited by optical diffraction limits. But using electron beam lithography, it is possible to control size, shape and inter-particle distance of nanostructures with great accuracy<sup>7-9</sup>. Another advantage of EBL is that no physical mask is needed. SERS substrates with reproducible SERS enhancement have been fabricated by EBL. Gunnarsson *et al.*<sup>10</sup> fabricated triangular and circular silver nanostructures and evaluated the inter-particle coupling effect on SERS performance. It is reported that intensity of SERS signal decreases with increase in inter-particle distance<sup>10</sup>. It is suggested that enhancement is contributed by the edges of nanostructures. Similar experiments by Liu *et al.*<sup>11</sup>

shows that array of Au nanoposts can be employed as SERS substrates. Yu *et al.*<sup>12</sup> fabricated gold nanodiscs and nanoholes by EBL and their SERS activity was compared as a function of inter-particle separation and dimension of the nanostructures. It is also noted that nanostructures that are fabricated close to each other show the best performance and SERS activity of nanodisc increases with decrease in the dimension of nanodisc and decreases with decrease in the dimension of nanoholes. The best performance is observed for nanohole arrays of diameter 370 nm and a pitch of 500 nm and its enhancement factor is  $4 \times 10^5$ . Electron beam lithography is also employed to fabricate a hybrid multi-scale aperiodic nanostructure and enhancement factor of  $10^8$  is achieved<sup>13</sup>. This EBL based approach for fabrication of aperiodic nanostructure is also used for the creation of matrices of randomly distributed metal nanoparticles with several shapes and sizes. Such substrates with interconnected prolates/oblates structures are highly reproducible and presented a SERS enhancement factor of  $5 \times 10^8$ <sup>14</sup>. Theiss *et al.*<sup>15</sup> developed EBL based SERS substrate by angle deposition technique which produces an enhancement factor of  $10^9$ . The SERS substrate consists of dimers of metal nanoparticles separated by 1 nm and the technique employs a double mask procedure for the deposition. Metal nanostructures with controlled gaps were also fabricated using optical lithographic technique combined with atomic layer deposition<sup>16</sup>. Although the EBL approaches resulted in SERS substrate with reproducible enhancement, it faces difficulties such as time-consuming and high cost since EBL requires clean rooms and special nanofabrication tools.

Alternative fabrication methods such as soft lithography<sup>17</sup>, replica molding<sup>18</sup>, etc., have been used to fabricate quasi-3D plasmonic

nanostructures and thus SERS substrates with high throughput at low cost have been produced. Yu *et al.*<sup>12</sup> reported the fabrication of nanohole arrays with different diameters and an enhancement factor up to  $10^6$  has been obtained. The same group reported the fabrication of unique gold quasi-3D plasmonic nanostructures on poly(dimethylsiloxane) (PDMS) using electron beam lithography (EBL) and soft lithography<sup>19</sup>. But this method is not an easy process for large scale fabrication of SERS substrates.

Wang *et al.*<sup>18</sup> fabricated arrays of closely packed Ag pyramids using inverted pyramidal arrays on silicon. The pyramids provide plentiful "hot spots" and are distributed at sharp nanotip and at four edges of the pyramid. The substrate provides homogeneous "hot spots" with an average EF of  $2.84 \times 10^7$ . Polymer SERS substrates with pyramids and inverted pyramidal structures are fabricated by multistep, molding and replication technique, and enhancement factors of  $7.2 \times 10^4$  and  $1.6 \times 10^6$  are obtained respectively for pyramids and inverted pyramids<sup>20</sup>. Wu *et al.*<sup>17</sup> demonstrated a cost-effective and deterministic nanoimprint lithography (NIL) for patterning large area 3D cone arrays. A UV-curable imprint resist material is employed for duplicating patterns from a silicon master. Polymer cone structures with tip size less than 10 nm have been successfully duplicated from silicone cones and its SERS activity is compared with the silicon cones. An improvement in SERS sensitivity is observed for polymer cones imprinted onto a reflective metallic mirror surface. This 3D NIL technique again offers a cost-effective method for fabrication of SERS substrates for various sensor applications and explore a technique for future integration of such SERS substrates with optical elements as well as micro-electro-mechanical systems (MEMS) components.

Nanotransfer printing (nTP) is another high resolution printing technique to transfer thin metal film from a "stamp" to a "substrate" and it is enabled by some of the interfacial chemistry to control the transfer<sup>21</sup>. The stamp can be either rigid fabricated via EBL or an elastomeric stamp. This technique can fabricate complex patterns over very large area by a single step process and is additive in nature. Hatab *et al.*<sup>8</sup> successfully transferred periodic array of square, triangular and elliptical pillars on the stamp onto PDMS and these patterned substrate are demonstrated as a SERS active substrate. The gap between the nanostructures is controlled by physical manipulation of PDMS substrates. Barcelo *et al.*<sup>22</sup> fabricated a variety of patterned nanoparticle assemblies of Au and Ag and transferred to silicon, glass, and metal coated substrates.

In the present study, a replication method is introduced for fabrication of micron-sized pyramidal arrays and nanoimprinting technique is employed for fabrication of nanotriangular arrays.

## **3.2 Experimental details**

### **3.2.1 Fabrication of inverted pyramidal structures by photolithography**

The steps involved in the photolithographic process are schematically represented in figure 3.1(a). A photoresist with uniform thickness is spin coated over silicon wafer with desired orientation and is exposed to ultraviolet radiation through a photomask which contains patterns of desired dimensions and shapes. Then the photoresist is developed by reacting with corresponding solvents so that either the irradiated area (positive resist) or the unirradiated area (negative resist)

is washed away. Finally, etching is carried out to get desired depth for the structures. It is reported that silicon wafers are anisotropically etched with solutions such as potassium hydroxide (KOH) or tetramethyl ammonium hydroxide (TMAH) with  $\text{pH} > 12$ . Due to the different densities of Si atoms on (100), (110) and (111) planes, the OH etching rate of (111) plane is about 30 times slower than the etching rate of (100) and (110) planes<sup>23,24</sup>. Average etching rate for silicon with TMAH is estimated to be  $0.4 \mu\text{m}/\text{min}$ <sup>25</sup>. The etching mechanism in Si<100> wafer with TMAH is schematically represented in figure 3.1(b). During etching, (100) and (110) crystal planes are being etched while (111) planes act as an etch stop. It is due to the different binding energies of silicon in different planes. Hence the etching of silicon wafer with (100) orientation always ends with inverted square-based pyramidal structures.

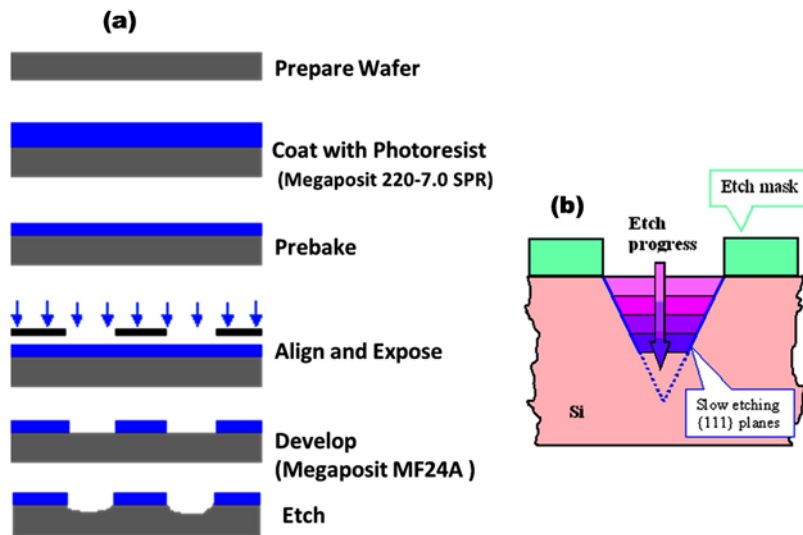


**Figure 3.1:** Schematic diagram showing (a) the steps involved in photolithography (b) chemical etching mechanism of silicon<100>

Here p-type Si<100> wafer was subsequently sonicated in acetone, isopropyl alcohol, and de-ionized water for 5 min to remove organic contaminants. Megaposit 220-7.0 SPR is used as photoresist and it is a positive photoresist so that the resist is removed in exposed areas when it reacts with developer Megaposit Developer MF24A. The mask was designed by photolithography to include squares with desired spacing between the squares. The sample was then etched in a 2.5% tetramethyl ammonium hydroxide (TMAH) solution at 80 °C for 8 min. More details can be seen in the report by Iduabo John Afa<sup>25</sup>.

### 3.2.2 Fabrication of pyramidal array based SERS substrate

Patterns in silicon master are transferred into a polymer substrate through simple replication technique and the steps involved is schematically given in figure 3.2.

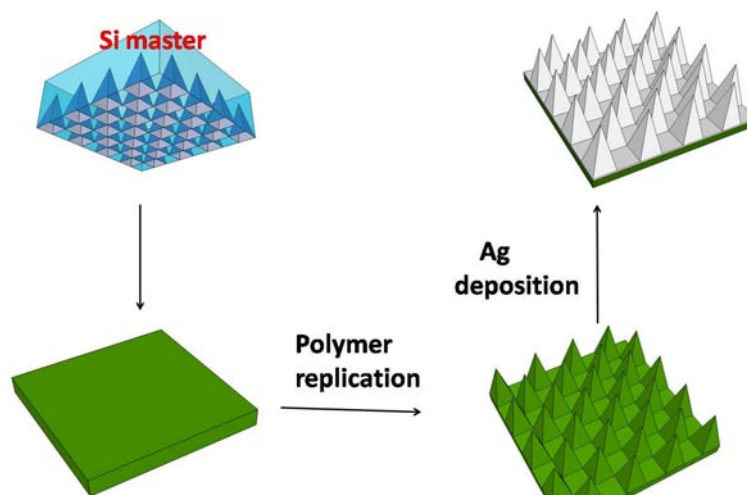


**Figure 3.2:** Schematic diagram showing the steps involved in replication method for fabrication of pyramidal arrays

In order to fabricate a substrate with pyramidal arrays, a stamp loaded with silicon master was pressed into two component silicone based molding material (President SEM Replication Kit, TED PELLA, INC.) and was allowed to polymerize for 5-7 min at room temperature. After polymerization, the mold was mechanically detached and this procedure led to the formation of a periodic array of pyramidal shaped structures. Over the pyramidal structure, silver film was deposited by thermal evaporation at a rate of  $1 \text{ \AA} / \text{sec}$  under a pressure of  $7.5 \times 10^{-6}$  mbar.

### **3.3 Results and discussion**

#### **3.3.1 Morphological characterization**

Atomic force microscopic (AFM) image of silicon master with inverted pyramidal structure is shown in figure 3.3(a) with a pyramidal base dimension of  $2.5 \text{ \mu m}$  and height of  $1.5 \text{ \mu m}$ . Figure 3.3(a) confirms the uniformity and sharpness of the master substrate. A daughter mold with pyramidal structure was fabricated from silicon master using the replication kit. As displayed in figure 3.3(b) surface morphology of replica is exactly the reverse image of the 3D features on the silicon master and thus in comparison, it is seen that 3D structures are faithfully reproduced by the given method. The technique is less time-consuming and follows no complicated steps. Finally, a thin continuous layer of silver with a thickness of  $70 \text{ nm}$  was thermally evaporated onto the polymer pyramid surfaces to generate the SERS substrate.

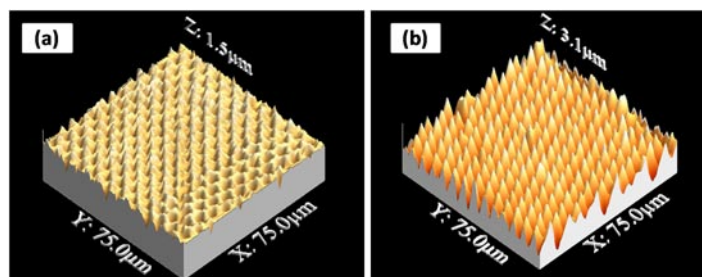


Figure 3.3: AFM images of (a) silicon master and (b) replica

### 3.3.2 SERS studies on pyramidal arrays

#### *Optimization of silver film thickness over the replica*

The silver film itself can produce SERS effect at lower thickness because of the formation of "hot spots" at this thickness range. Therefore, in order to obtain SERS from sharp tips of pyramids only, silver film of different thickness was deposited over a planar substrate and its SERS activity is compared. To test SERS activity, the substrates were dipped in  $10^{-3}$  M benzene thiol (BT) solution so that a monolayer of BT is formed over the substrate.

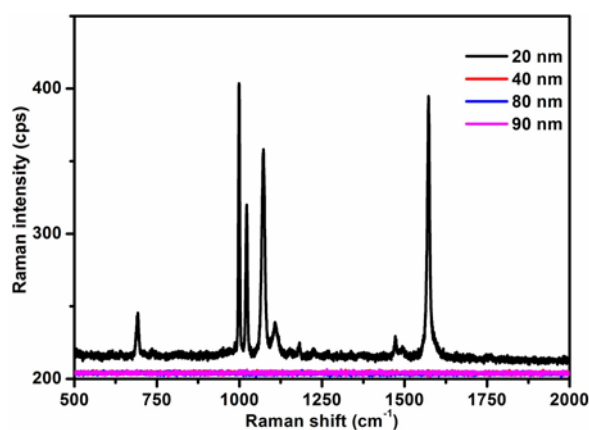
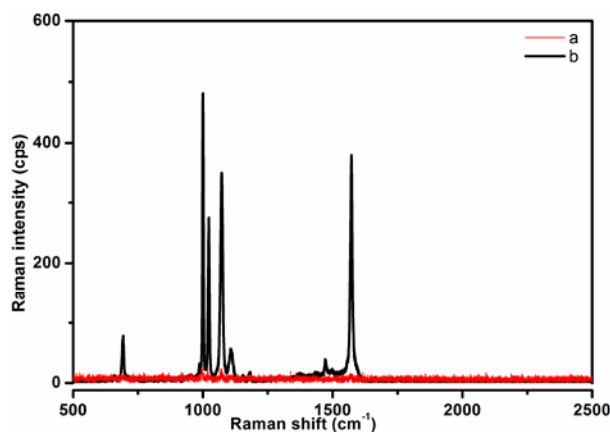


Figure 3.4: SERS activity of silver film with different thickness over planar substrate for an acquisition time of 1s

Figure 3.4 compares SERS activity of silver film on a planar substrate with thickness 20, 40, 80 and 90 nm. It is observed that film of thickness 20 nm enhanced Raman signal of BT while film with thickness between 40 to 90 nm doesn't produce any SERS signals which is the confirmation of growth of the continuous silver film over the planar substrate. Hence silver film of thickness around 60 nm is deposited over a planar substrate and patterned replica substrate and their SERS activity is compared (figure 3.5). From the figure, it is clear that planar substrate doesn't produce any signals and the pyramidal array based SERS substrate enhanced the Raman signals of BT. The feeble SERS activity of planar replica substrate is attributed to roughness present in the polymer material. From 3.5(b) it can be clearly seen that pyramidal structure based substrate exhibit excellent SERS as compared to the planar replica. The spectra of pyramidal based SERS substrate shows a characteristic peak of benzene thiol which is assigned according to the early reported studies<sup>26,27</sup>. The Ag-S bond formation is evident with the presence of a peak at  $1469\text{ cm}^{-1}$ . The peaks at  $1570$ ,  $1066$  and  $1017\text{ cm}^{-1}$  comes from the C–C stretching, in plane phenyl ring stretching and in-plane ring deformation, whereas peaks  $996$ ,  $684$  and  $413\text{ cm}^{-1}$  can be assigned to the C-H wagging mode, the C–H out of plane deformation and C–S stretching, respectively. The absence of peak at  $917\text{ cm}^{-1}$  associated with the S-H bond which is present in BT solution indicates that monolayer of benzenethiol was formed onto silver surface<sup>28</sup>.



**Figure 3.5:** SERS activity of (a) planar SERS substrate (b) pyramidal array based SERS substrate for an acquisition time of 1s

Here SERS enhancement in pyramidal structures can be explained on the basis of electromagnetic enhancement which is caused due to the strong concentration of the electromagnetic field around sharp nanotips which is well proved in various reports<sup>18,29</sup>. The reports also show that the electromagnetic enhancement in pyramidal structures is from the sharp tip and also from sharp edges of pyramids.

The characteristic of a good SERS substrate is not only to exhibit large enhancement factor but also gives good homogeneity and reproducibility in Raman enhancement. To evaluate the uniformity of SERS signal, spectra are collected from randomly selected pyramids. The corresponding SERS spectra are shown in figure 3.6. The results provide information that the Ag pyramidal arrays hold excellent homogeneity in SERS performance. Similarly, reproducibility of the signal from batch to batch is also tested by fabricating pyramidal substrates from the same silicon master template. It is estimated that the relative standard deviation is less than 7% across the SERS substrate and also for a different set of substrates. Hence, the spectra are reproducible over a large area and from sample-to-sample. It also

provides positive result that all the replicas provide same SERS activity and hence good reproducibility. Unlike other fabrication techniques, here the replication method is very simple and fast. So the fabrication technique is promising for replication of pattern from the master template.

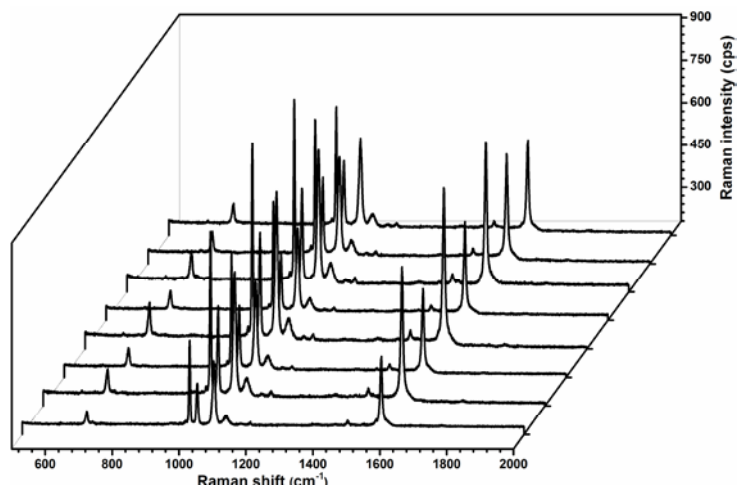


**Figure 3.6:** Spatial uniformity of SERS signal over the replica

The pyramidal array based SERS substrates provide

- point to point reproducibility of Raman enhancement
- the sample to sample reproducibility of Raman enhancement
- fabrication technique is simple and economic

But here the number of "hot spots" in detection volume during measurement is less because the size of pyramids is in the micrometer range. Hence triangular arrays with nanometer dimension are fabricated

by a nanoimprinting technique which results in increased number of "hot spots" in detection volume.

### 3.4 Fabrication of nanotriangular array based SERS substrate

The schematic of fabrication process of SERS substrate is illustrated in figure 3.7 which includes three major phases: (a) fabrication of the master mold with pits of triangular shape via electron beam lithography (b) duplication of a daughter mold with arrays of triangular pillars on polymethylmethacrylate (PMMA) sheet by nanoimprinting technique and (c) metal deposition on triangular pillars to generate the SERS substrate.

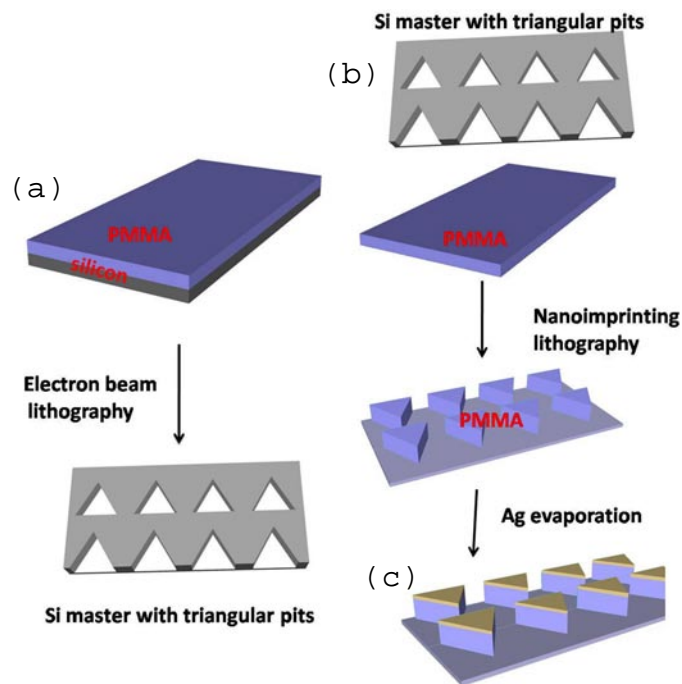


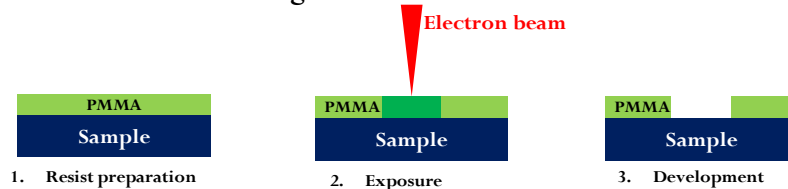
**Figure 3.7:** Schematic diagram of the nanoimprinting process for fabricating triangular arrays as ultrasensitive SERS substrates

### 3.4.1 Fabrication of silicon master substrates with nanotriangular pits via EBL

Electron beam lithography (EBL) allows the fabrication of periodic arrays of arbitrary shapes with desired dimension as well as tunable inter-particle distance in 100 nm size range down to 20 nm. EBL combine with angle evaporation technique offers the control of inter-particle distance down to 1–2 nm in disparately sized particles<sup>30,31</sup>. In the initial stages of nanolithographic based SERS substrates, electron beam lithography (EBL) is one of the most used methods in which 10–50 keV beam of electrons focused on to an electron beam resist (e-beam resist) coated on a solid support, generally PMMA covered SiO<sub>x</sub>/Si wafers. The electron resist can be positive or negative type.

Here also PMMA, a positive e-resist, is used for EBL and reactive ion etching (RIE) is employed for etching of pattern to get desired dimensions of nanostructures. Various steps involved in EBL are shown in figure 3.8.

#### Step I: Electron beam Etching



#### Step II: Reactive Ion Etching

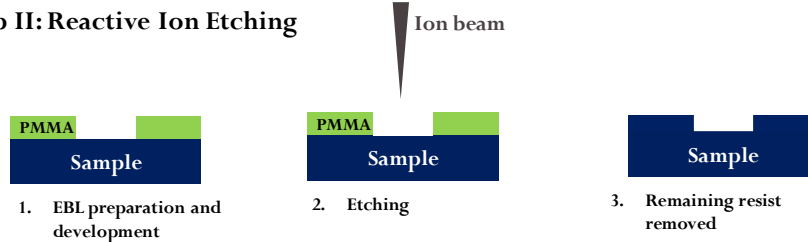


**Figure 3.8:** Schematic diagram showing the steps involved in electron beam lithography

Three silicon masters with triangular pits having edge length 200, 300 and 400 nm are fabricated by EBL and its dimensions are schematically represented in figure 3.9 and are designated as M1, M2 and M3. A square grid of nanotriangle pillar arrays with dimensions of  $50\ \mu\text{m} \times 50\ \mu\text{m}$ , nanotriangle edge lengths of 200 to 400 nm, and pitches of 250 nm were fabricated via EBL using a Raith Elphy Plus (SEM based system) equipped with software for correcting the proximity effect. Three hundred nm thick PMMA (polymethylmethacrylate, Good Fellow) used as an e-beam resist was spin-coated onto silicon. The PMMA resist was exposed to a 49 pA electron beam with dose in the range of  $305\ \mu\text{As}/\text{cm}^2$ . Following the electron beam exposure, the PMMA resist was developed in 1:3 methyl isobutyl ketone/isopropanol (MIBK/IPA) mixture for 30 s, then spray-rinsed with IPA for 30 s and blown dry with nitrogen.

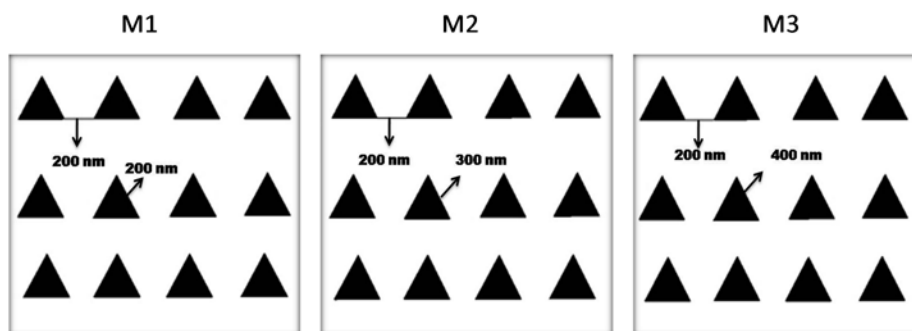


**Figure 3.9:** Design of silicon master 1 (M1), master 2 (M2) and master 3 (M3)

Reactive ion etching (RIE) was carried out on silicon substrate to get a depth of 250 nm. Fifty sccm of  $\text{SF}_6$  and 90 sccm of  $\text{C}_4\text{F}_8$  gases were used for etching and passivation cycles, respectively. RIE of silicon was performed using inductively coupled plasma (ICP). The ICP

power, pressure, and RIE time were adjusted at 300 W, 15 mT and 4 min respectively to achieve desired depth of 250 nm. Finally, PMMA resist were removed on reacting with acetone and isopropyl alcohol. The detailed fabrication steps are tabulated in the following tables.

**Table 3.1:** Step 1 - PMMA spin coating for master fabrication

Spin parameters for 300 nm PMMA on silicon		
PMMA 5% in anisole	Spin coating steps: 1	
RPM: 4500	Acceleration: 4500	Time: 1 min
Baking : 1 hr at 180° C		

**Table 3.2:** Step 2 - E-beam lithography parameters

Write field: 50 $\mu\text{m}$ x 50 $\mu\text{m}$		
dose		
Triangle 200 nm 305 $\mu\text{As}/\text{cm}^2$	Triangle 300 nm 440 $\mu\text{As}/\text{cm}^2$	Triangle 400 nm 442 $\mu\text{As}/\text{cm}^2$

**Table 3.3:** Step 3 - PMMA developing process

Step 1: 30" rinse with MIBK:IP (1:3)	Step 2: 30" rinse with IPA	Step 3: purge nitrogen	Step 4: 5' dry at 95 °C
---	-------------------------------	------------------------------	----------------------------

**Table 3.4:** Step 4 - Reactive ion etching (RIE) parameters

Etching 250 nm of depth	
Etching cycle: 90 sccm $\text{C}_4\text{F}_8$	Passivation cycle: 50 sccm $\text{SF}_6$
ICP power: 300 W	Pressure: 15 mT
RIE time: 4 min	

**Table 3.5:** Step 5 - PMMA removal process

First, react with 10' acetone	Then, with 10' isopropanol
-------------------------------	----------------------------

FESEM images of silicon masters M1, M2 and M3 are shown in figure 3.10(a), (b) and (c).

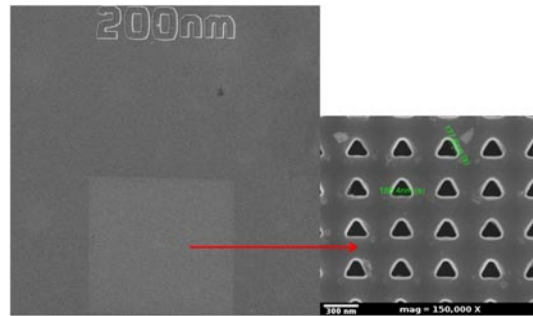


**Figure 3.10 a:** FESEM image of M1

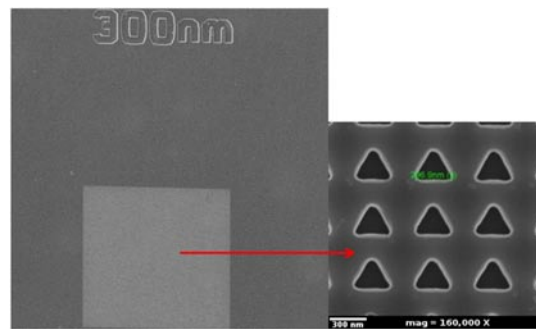


**Figure 3.10 b:** FESEM image of M2

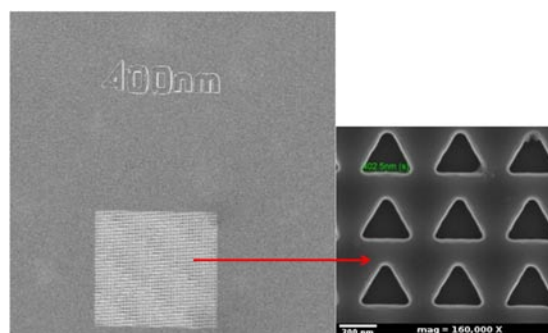


**Figure 3.10 c:** FESEM image of M3

A typical field emission scanning electron microscope (FESEM) image of silicon master M2 with an edge length of 200 nm is shown in figure 3.11 and the separation between triangle is 200nm. Fabrication of nanotriangles with sharp edges over a large area can be clearly observed in figure 3.11(b). The pits of nanotriangles are clearly visible in figure 3.11(c). The thickness of PMMA resist and reactive ion etching parameter played an important role for the successful fabrication of perfect triangular pits with sharpened features.

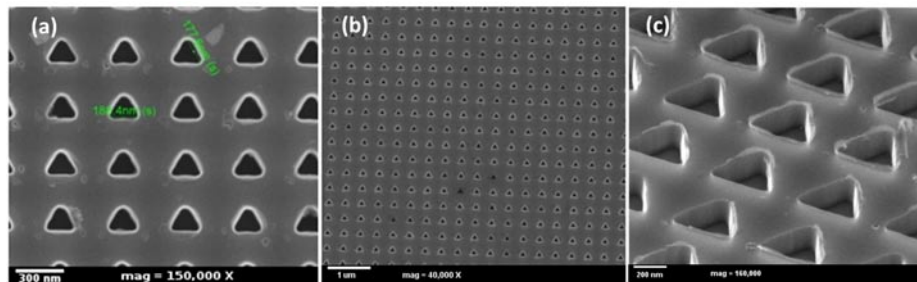


**Figure 3.11:** FESEM image of silicon master with triangular pits of edge length 200nm (a) top view (b) large area view (c) depth view

### 3.4.2 Fabrication of nanotriangular pillars via NIL

Replica with nanotriangular pillar arrays was fabricated using nanoimprint lithography (NIL) with a custom designed NIL machine. In NIL, silicon master that includes nanotriangular pits was pressed against PMMA substrate, which was previously heated above its glass transition temperature, at a given pressure for a specific time. After being cooled down, the master was removed from the substrate so that silicon master can be reused. The NIL parameters are tabulated in table 3.6.

**Table 3.6:** NIL parameters for nanotriangular pillar arrays

<b>Substrate:</b>	<b>PMMA Sheet - 125<math>\mu</math>m (Good Fellow)</b>		
<b>NIL steps parameters</b>			
Step 1	Pressure: 0 bar	Temperature: 80 °C	Time: 150 s
Step 2	Pressure: 0 bar	Temperature: 160 °C	Time: 60 s
Step 3	Pressure: 50 bar	Temperature: 160 °C	Time: 300 s
Step 4	Pressure: 50 bar	Temperature: 80 °C	Time: 150 s
Step 5	Pressure: 0 bar	Temperature: 50 °C	Time: 150 s

During both NIL steps, a chlorosilane coupling agent, (3-acryloxypropyl)methyldichlorosilane, was used to prime the substrate. This was followed by spin-coating of a UV-curable NIL resist, composed of a low viscosity UV-curable acrylated poly(dimethylsiloxane) material, a multifunctional acrylate cross-linker, and a free radical initiator.

Daughter mold with nanotriangular pillars on PMMA sheet by nano-imprinting technique were successfully fabricated from the master mold and their FESEM images are shown in figure 3.12(d)-3.12(f). From figure 3.12, it is seen that surface morphology of the daughter mold is exactly reverse of the master mold which indicates the success of our replication. Finally, a 60 nm thin layer of Ag was thermally evaporated onto the replica substrate to generate a SERS active substrate. During thermal vacuum evaporation, Ag may deposit only on the top surfaces of the pillars rather than down the entire pillar height because of shadow effects. This can cause it to form arrays of triangles with a thickness of 60 nm.

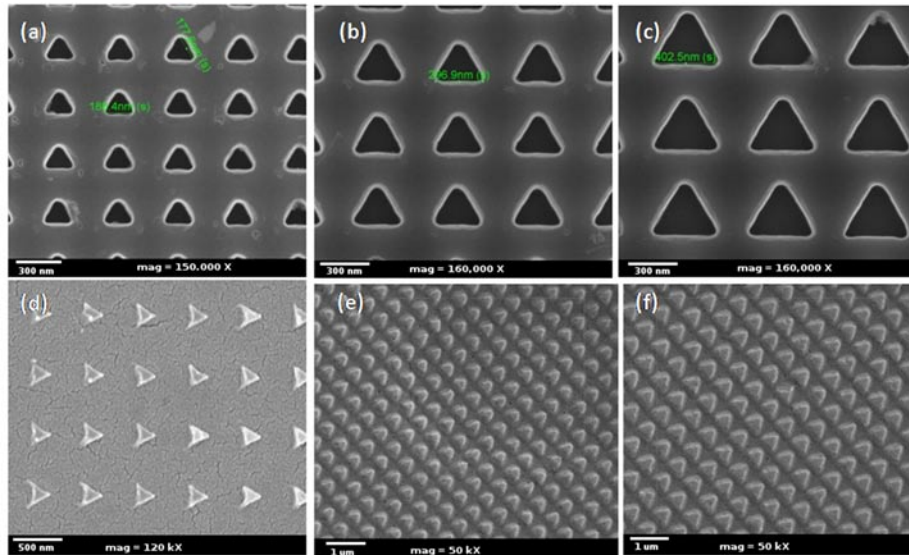


**Figure 3.12:** FESEM images of inverted nanotriangular pillars with edge lengths of (a) 200 nm, (b) 300 nm, and (c) 400 nm, fabricated via EBL. Nanotriangular pillar arrays with edge lengths of (d) 200 nm, (e) 300 nm, and (f) 400 nm fabricated via nanoimprinting. (d) has a higher magnification of 120,000X

### 3.5 Results and discussion

#### 3.5.1 FDTD simulation

3D FDTD (three dimensional finite-difference time-domain) simulations were carried out on silver nanotriangles using commercial software Lumerical FDTD solutions. Mie scattering was employed to study LSPR of silver nanotriangle. In order to study the effect of PMMA on LSPR position of silver nanotriangle, the simulation was carried out for the case of silver nanotriangles with and without PMMA. From figure 3.13, it is clearly observed that the presence of PMMA blue shifts the SPR position from 560 to 480 nm which is clearly attributed to the effect of variation in dielectric environment<sup>32</sup>.

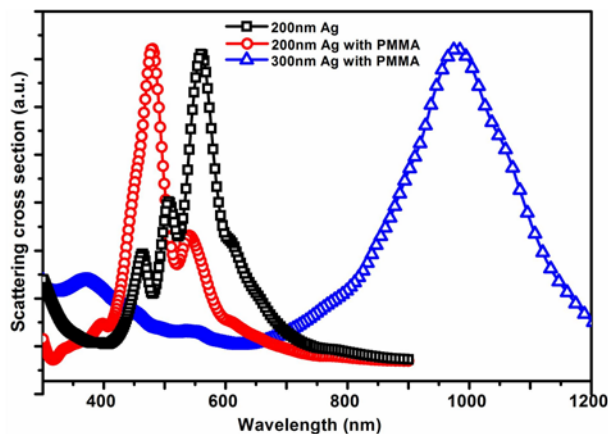


**Figure 3.13:** Scattering cross section of silver nanotriangles with and without PMMA, and edge lengths of 200 and 300 nm

It is also observed that as edge length of triangle varies from 200 to 300 nm, LSPR peaks shift from 560 to 980 nm (figure 3.13). The red shift can be attributed to increased charge separation of dipoles for large edge length.

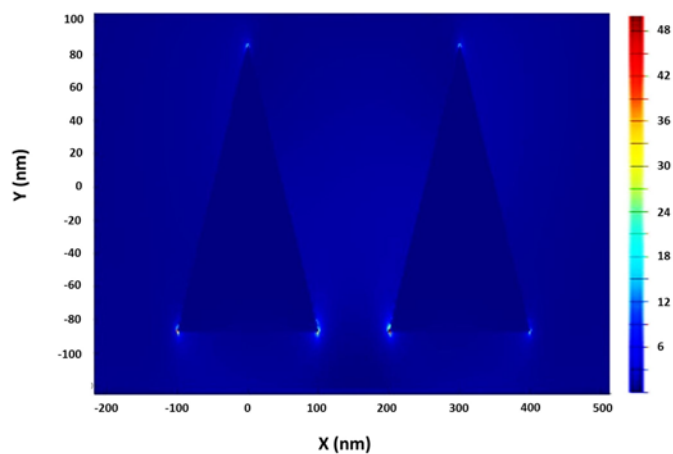


**Figure 3.14:** Electric field enhancement in silver nanotriangle array of edge length 200 nm

The electrical field enhancement in silver nanotriangle arrays was visualized by FDTD under 633 nm excitation source and corresponding field distribution is given in figure 3.14. As shown in the figure, "hot spots" will always distribute at the corners. The electric field was monitored at a wavelength equivalent to Raman excitation, ie. 633 nm and these "hot spots" are efficient contributors of Raman enhancement in SERS.

### 3.5.2 SERS characterization

In order to demonstrate silver nanotriangular arrays patterned by nanoimprint lithography as a promising SERS active substrate and to check the sensitivity and uniformity of the arrays, benzene thiol (BT) was used as analyte molecule. BT molecules are arranged as a monolayer over the substrate while dipping silver deposited PMMA substrates in  $10^{-3}$  M BT for 5 min. The SERS spectra were acquired by Horiba Jobin Yvon LabRAM HR microRaman spectrometer with a laser excitation wavelength of 632.8 nm, and a collection time of 1 s. SERS spectra of monolayer BT on silver nanotriangle arrays of edge length 200, 300 and 400 nm have been measured in an air environment and is shown in figure 3.15.

All the spectra show characteristic peak of benzene thiol which is assigned according to the earlier reports<sup>26,27</sup>. The absence of a peak at  $917\text{ cm}^{-1}$  associated with the S-H bond which is present in BT solution indicates that monolayer of benzenethiol is formed over silver nanotriangular array<sup>28</sup>. It is also observed that silver film on flat PMMA does not produce any SERS signal. Thus it is confirmed that the silver nanotriangles with sharp corners enhance Raman scattering cross section

of BT while the planar PMMA-silver substrate couldn't produce any detectable signal.

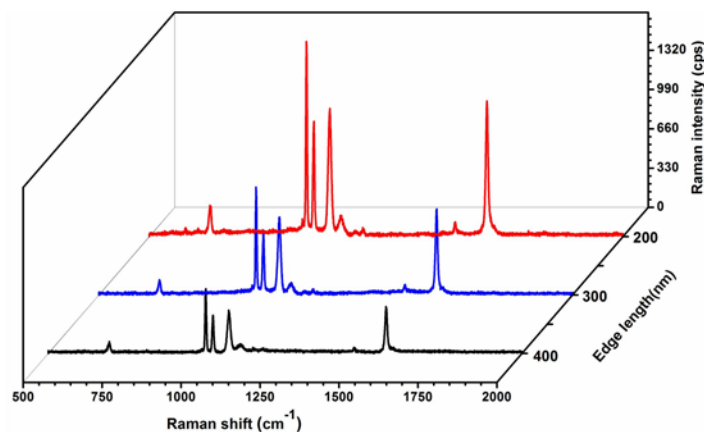


**Figure 3.15:** SERS spectra of  $10^{-3}$  M BT on nanotriangular pillar arrays of edge length 200 nm, 300 nm and 400 nm

As the edge length decreases from 400 to 200 nm, Raman intensity increases from 550 to 1600 counts. The variation in Raman enhancement with an edge length of the triangle is attributed to the variation in LSPR position and the corresponding shift from excitation wavelength 632.8 nm. It is already reported that maximum enhancement is observed when SPR approaches to excitation wavelength<sup>1</sup>. As compared with SPR positions of nanotriangles of edge length 300 and 400 nm, those with 200 nm are closer to 632.8 nm and hence produce stronger electric fields at their corners and higher Raman intensity.

#### ***Calculation of enhancement factor***

To assess enhancement ability of the nanotriangular arrays, the enhancement factor (EF) is calculated by comparing the Raman signal

intensities in SERS and in normal Raman spectrum. Normal Raman spectrum of liquid benzene thiol was collected over 5 s and SERS spectra of monolayer BT was collected for a collection time of 1 s. The powers used for the respective measurement were 7 mW and 0.549 mW with 632.8 nm as excitation wavelength. The spot size and depth of focus of 632.8 nm laser line for 100X objective are 1 and 1  $\mu\text{m}$  respectively.

The enhancement factor is defined as<sup>28</sup>

$$EF = (I_{\text{SERS}}/I_{\text{REF}}) \times (N_{\text{REF}}/N_{\text{SERS}}) \dots\dots\dots 4.1$$

For accurate comparison between the two measurements,  $I_{\text{SERS}}$  and  $I_{\text{REF}}$  were normalized with respect to incident laser power and acquisition time.  $I_{\text{SERS}}$  and  $I_{\text{REF}}$  before the correction were 1600 and 140 counts respectively. The number of molecules probed during SERS measurement is calculated from the information on the areal density of BT on monolayer formation and is  $3.3 \times 10^{14} \text{ cm}^{-2}$ . The actual number of SERS probed BT molecules are calculated by considering the area of nanotriangle and number of nanotriangles in detection area. From the FESEM images (figure 3.12), the number of nanotriangles in the detection volume will be 6. Finally,  $N_{\text{SERS}}$  is calculated as 330 molecules. Since only corners of triangle hold "hot spots", the number of BT molecules that contribute to SERS signal is even very small and will be about 20 molecules.

The number of molecules contributing to the neat Raman spectra,  $N_{\text{REF}}$  is estimated using the formula,

$$N_{REF} = \rho N_A V / (M.W) \dots\dots\dots 4.2$$

where  $\rho$  is the density of BT and its value is 1.073 g/mL and  $M.W = 110.18$  g/mol, molecular weight of BT.  $N_A$  is Avogadro number.  $V$  is the collection volume of the liquid BT and is equal to laser spot area multiplied with collection depth. Based on our instrument, laser spot size is 1  $\mu\text{m}$  and depth of focus is also 1  $\mu\text{m}$ . Hence  $N_{REF}$  is calculated to be  $1.46 \times 10^{10}$ .

It is clearly seen that even though a number of molecules sampled in SERS measurement are very small, SERS signal intensity is many orders higher than the normal Raman spectrum. The Raman peak at  $998 \text{ cm}^{-1}$  is used for computing the SERS enhancements because it is furthest removed from Ag-S bond ( $1469 \text{ cm}^{-1}$ ) corresponding to the vibration, where molecular polarizability and in turn Raman intensity is modified dramatically<sup>28</sup>. Thus it is possible to estimate enhancement factor more accurately. The average enhancement factor of our nanotriangular pillar array based SERS substrate of edge length 200 nm is calculated to be  $2.9 \times 10^{11}$  which is highest reported value for a patterned substrate. The enhancement factor corresponding to edge length of 300 and 400 nm are  $1.8 \times 10^{11}$  and  $1.1 \times 10^{11}$  respectively. Even though selecting the most appropriate peak is very important for estimating average enhancement factor with good accuracy, variation in EF with edge length is found to be relatively independent of the choice of Raman peak chosen for comparison. It is concluded that edge length variation has very little ability to affect SERS enhancement which is consistent with theoretical results from FDTD.

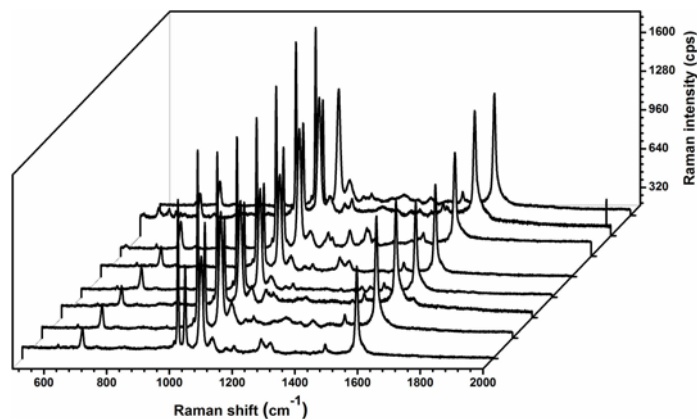


**Figure 3.16:** SERS spectra of  $10^{-3}$  M BT from randomly selected points

SERS substrate must possess not only large enhancement factor, but also spectra should be reproducible over a large area and from sample to sample. Thus uniformity and reproducibility of the Raman signal were tested and figure 3.16 provide Raman signals from randomly selected points on the substrate. It is estimated that the relative standard deviation is less than 5% across the SERS substrate and also for a different set of substrates. Hence, the spectra are reproducible over a large area and from sample-to-sample. This is because a large number of nanotriangle can be successfully replicated from a single silicon master onto PMMA sheets, which again provide the same enhancement factor for BT.

The SERS activity of physisorbed Rhodamine 6G molecule as analyte again confirms the excellent sensitivity of nanotriangular array based SERS substrate. Figure 3.17 shows SERS spectra of  $5 \times 10^{-7}$  M R6G molecules and all the peaks correspond to characteristic peaks of R6G molecule<sup>33</sup>.

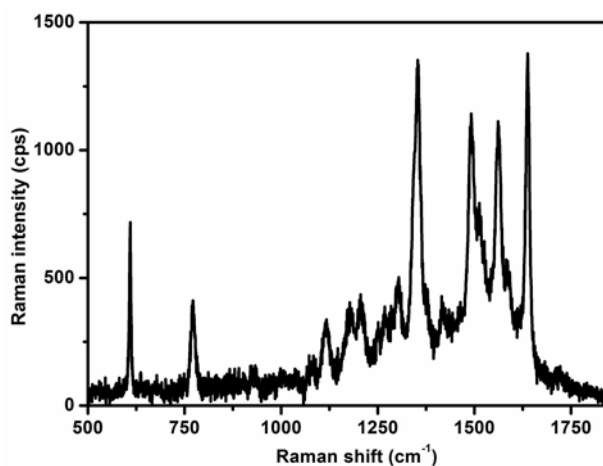


**Figure 3.17:** SERS spectra of  $5 \times 10^{-7}$  M R6G molecule

An estimation of enhancement factor described in previous reports based on patterned SERS active substrates fabricated via lithographic technique ranges from  $10^3$  to  $10^9$ . Quasi-3D gold nanostructures on poly(dimethylsiloxane) PDMS based SERS substrates fabricated using electron beam lithography generated an enhancement factor of  $6.4 \times 10^5$ <sup>19</sup>. Gold nanograting and gold nanodisc fabricated via EBL provide an enhancement factor of  $36.4 \times 10^4$  and  $3.8 \times 10^4$  respectively<sup>34</sup>. Qiuming Yu *et al.* fabricated gold nanohole and nanodisc arrays by electron beam lithography and reported an enhancement factor of  $1.3 \times 10^3$ <sup>12</sup>. Gold coated on silicon nanopillars give an enhancement factor  $1.2 \times 10^8$ <sup>28</sup>. Additionally, recent reports have revealed that an enhancement factor of order  $10^7$  -  $10^8$  is sufficient for single-molecule spectroscopy<sup>35,36</sup>. Thus our new SERS substrate fabricated via given fabrication method possess exceeding advantages of the single fabrication step for silicon master to produce multiple substrates with uniform array of nanotriangular pillars which unlock a method to reduce cost of SERS substrate and to

fabricate large area uniform reproducible SERS substrate with very large enhancement factor with single molecule detection capability.

### 3.7 Conclusion

Highly-reproducible large area arrays of inverted nanotriangles were successfully fabricated via electron beam lithography. To overcome the expense of EBL, nanoimprinting was employed to fabricate nano-triangular arrays. The edge lengths of the triangles varied from 200 to 400 nm and their heights were fixed at 250 nm. Highly effective SERS active substrates with cost advantages, large-area uniformity, reproducibility, and excellent sensitivity with enhancement factors of  $2.9 \times 10^{11}$  were produced from the nanotriangle pillar arrays. The enhancement factor demonstrated here is the highest reported for a patterned SERS substrate.

### References

- [1] M.A. Garcia, *J. Phys. D. Appl. Phys.* **44**, 283001 (2011).
- [2] J.P. Camden, J. a Dieringer, Y. Wang, D.J. Masiello, L.D. Marks, G.C. Schatz, and R.P. Van Duyne, *J. Am. Chem. Soc.* **130**, 12616 (2008).
- [3] W. Li, P.H.C. Camargo, X. Lu, and Y. Xia, *Nano Lett.* **9**, 485 (2009).
- [4] E.C. Le Ru, P.G. Etchegoin, and M. Meyer, *J. Chem. Phys.* **125**, 204701 (2006).
- [5] K.L. Wustholz, A.-I. Henry, J.M. McMahon, R.G. Freeman, N. Valley, M.E. Piotti, M.J. Natan, G.C. Schatz, and R.P. Van Duyne, *J. Am. Chem. Soc.* **132**, 10903 (2010).
- [6] T. Qiu, W. Zhang, and P.K. Chu, *Recent Pat. Nanotechnol.* **3**, 10 (2009).

- [7] M.A. De Jesús, K.S. Giesfeldt, J.M. Oran, N.A. Abu-Hatab, N. V Lavrik, and M.J. Sepaniak, *Appl. Spectrosc.* **59**, 1501 (2005).
- [8] N.A.A. Hatab, J.M. Oran, and M.J. Sepaniak, *ACS Nano* **2**, 377 (2008).
- [9] J.M. Oran, R.J. Hinde, N. Abu Hatab, S.T. Retterer, and M.J. Sepaniak, *J. Raman Spectrosc.* **39**, 1811 (2008).
- [10] L. Gunnarsson, E.J. Bjerneld, H. Xu, S. Petronis, and B. Kasemo, **802**, 4 (2011).
- [11] Y. Liu, Z. Zhang, Q. Zhao, and Y. Zhao, *Appl. Phys. Lett.* **93**, 173106 (2008).
- [12] Q. Yu, P. Guan, D. Qin, G. Golden, and P.M. Wallace, *Nano Lett.* **8**, 1923 (2008).
- [13] A. Gopinath, S. V Boriskina, W.R. Premasiri, L. Ziegler, B.M. Reinhard, and L. Dal Negro, *Nano Lett.* **9**, 3922 (2009).
- [14] S.M. Wells, S.D. Retterer, J.M. Oran, and M.J. Sepaniak, *ACS Nano* **3**, 3845 (2009).
- [15] J. Theiss, P. Pavaskar, P.M. Echternach, R.E. Muller, and S.B. Cronin, *Nano Lett.* **10**, 2749 (2010).
- [16] H. Im, K.C. Bantz, N.C. Lindquist, C.L. Haynes, and S.-H. Oh, *Nano Lett.* **10**, 2231 (2010).
- [17] W. Wu, M. Hu, F.S. Ou, Z. Li, and R.S. Williams, *Nanotechnology* **21**, 255502 (2010).
- [18] Y. Wang, N. Lu, W. Wang, L. Liu, L. Feng, Z. Zeng, H. Li, and W. Xu, *Nano Res.* **6**, 159 (2013).
- [19] Q. Yu, S. Braswell, B. Christin, J. Xu, P.M. Wallace, H. Gong, and D. Kaminsky, *Nanotechnology* **21**, 355301 (2010).

- [20] Z. Xu, H.-Y. Wu, S.U. Ali, J. Jiang, B.T. Cunningham, and G.L. Liu, *J. Nanophotonics* **5**, 053526 (2011).
- [21] Y.-L. Loo, R.L. Willett, K.W. Baldwin, and J.A. Rogers, *J. Am. Chem. Soc.* **124**, 7654 (2002).
- [22] S.J. Barcelo, A. Kim, W. Wu, and Z. Li, *ACS Nano* **6**, 6446 (2012).
- [23] R. Hull, *Properties of Crystalline Silicon* (INSPEC, the Institution of Electrical Engineers, London, 1999).
- [24] K. Sato, M. Shikida, Y. Matsushima, T. Yamashiro, K. Asaumi, Y. Iriye, and M. Yamamoto, *Sensors Actuators A Phys.* **64**, 87 (1998).
- [25] I.J. Afa, *Etching Techniques for Thinning Silicon Wafers for Ultra Thin High Efficiency IBC Solar Cells*, Universitat Politecnica de Catalunya (UPC), Barcelona, 2014 (M.Sc. Dissertation).
- [26] C.E. Taylor, J.E. Pemberton, G.G. Goodman, and M.H. Schoenfish, *Appl. Spectrosc.* **53**, 1212 (1999).
- [27] M.R. Gartia, Z. Xu, E. Behymer, H. Nguyen, J. a Britten, C. Larson, R. Miles, M. Bora, A.S.-P. Chang, T.C. Bond, and G.L. Liu, *Nanotechnology* **21**, 395701 (2010).
- [28] J.D. Caldwell, O. Glembocki, F.J. Bezares, N.D. Bassim, R.W. Rendell, M. Feygelson, M. Ukaegbu, R. Kasica, L. Shirey and C. Hosten, *ACS Nano* **5**, 4046 (2011).
- [29] N.C. Linn, C.-H. Sun, A. Arya, P. Jiang, and B. Jiang, *Nanotechnology* **20**, 225303 (2009).
- [30] C. Vieu, F. Carcenac, A. Pépin, Y. Chen, M. Mejias, A. Lebib, L. Manin-Ferlazzo, L. Couraud, and H. Launois, *Appl. Surf. Sci.* **164**, 111 (2000).
- [31] A.A. Tseng, C.D. Chen, and K.J. Ma, *IEEE Trans. Electron. Packag. Manuf.* **26**, 141 (2003).

- [32] P.L. Stiles, J.A. Dieringer, N.C. Shah, and R.P. Van Duyne, *Annu. Rev. Anal. Chem.* **1**, 601 (2008).
- [33] A.M. Michaels, M. Nirmal, and L.E. Brus, *J. Am. Chem. Soc.* **121**, 9932 (1999).
- [34] W. Yue, Z. Wang, Y. Yang, L. Chen, A. Syed, K. Wong, and X. Wang, *J. Micromech. Microeng.* **22**, 125007 (2012).
- [35] P.G. Etchegoin and E.C. Le Ru, *Phys. Chem. Chem. Phys.* **10**, 6079 (2008).
- [36] E.C. Le Ru, E. Blackie, M. Meyer, and P.G. Etchegoin, *J. Phys. Chem. C* **111**, 13794 (2007).

.....✂.....



## **Development of recyclable SERS substrates using TiO<sub>2</sub> nanorods decorated with Ag nanoparticles**

In the previous chapters, fabrication of SERS substrates using traditional metal nanostructures is discussed. This chapter describes the development of recyclable SERS substrate using TiO<sub>2</sub> nanorods decorated with silver nanoparticles. This helps to overcome single-use problem of traditional SERS substrates. Ag-TiO<sub>2</sub> based SERS substrate provides excellent sensitivity with an enhancement factor of about  $2 \times 10^8$  and with single molecule detection capability. The photocatalytic nature of TiO<sub>2</sub> facilitates fabrication of recyclable multifunctional sensor for rapid detection of food adulterants, pesticides, etc.

The paper titled "Development of highly sensitive recyclable surface enhanced Raman scattering substrates using TiO<sub>2</sub> nanorods decorated with Ag nanoparticles", **K. Hasna**, P. P. Subha, M. K. Jayaraj and K. Rajeev Kumar, has been communicated to the journal *Nanotechnology* based on the results presented in this chapter and it is under review.

## 4.1 Introduction

3D nanostructures are far superior to the conventional substrate due their potential to extend the arrangement of "hot spots" along the third dimension and thus enhance the density of "hot spots". They also supply increased surface area for adsorbing higher number of probe molecules. 3D self-assembly is one of the methods for producing 3D hierarchical SERS substrates. But poor control and reproducibility of this method demand the essentiality of another template method. Various reduction methods are emerged for decorating noble metal nanoparticles on to 3D nanoscaffold or nanorod structures. The examples include anodic aluminum oxide (AAO) tubes, TiO<sub>2</sub> and ZnO nanorods, carbon nanotubes, etc. decorated with Au or Ag nanoparticles (NPs)<sup>1-3</sup>. The array of vertically aligned nanowires or nanorods (e.g., TiO<sub>2</sub>, ZnO nanorod arrays) are unsuitable for SERS active applications because of limitation in massive amounts of loading of metal nanoparticles and thus formation of "hot spots" with high density. Also, propagation of excitation light into the decorated nanoparticles is limited owing to significant scattering and adsorption which effectively decreases enhancement factor and the detection limit. To overcome this deficiency, instead of vertically aligned structures, branch type substrates are designed that can expose the "hot spots" to excitation volume. The emerged substrate, branched scaffolds in ZnO nanorod arrays, is one of the examples<sup>4</sup>. The uniform spatial distribution of the branched scaffolds can efficiently supply the "hot spots" to SERS enhancement and thus improved sensitivity and reproducibility. Huang *et al.*<sup>5</sup> reported a unique SERS substrate based on silver nanoparticles decorated on the graft of Si nanoneedles which is supported onto surface of ZnO nanorod arrays

and the subsequent decoration of silver nanoparticles. A catalyst-assisted vapor-liquid-solid (VLS) growth mechanism was employed for the graft of silicon needles onto the ZnO nanorods. The decoration of silver nanoparticles was carried out using galvanic displacement reaction. An enhancement factor of  $8.7 \times 10^7$  and a detection limit of  $10^{-16}$  M is achieved for the designed SERS substrate.

Tang *et al.*<sup>6</sup> reported decoration of silver nanoparticle onto arrays of cone-shaped ZnO nanorods and 3D surface-enhanced Raman scattering substrate was fabricated for rapid detection of trace polychlorinated biphenyls<sup>6</sup>. Electrodeposition technique was employed for growth of cone-shaped ZnO on planar Si wafer. Physical ion-sputtering was employed for the uniform deposition of silver nanoparticles and during sputtering small silver nanoparticles were decorated onto side wall and large sized were grown at the top ends of the cone-shaped ZnO nanorods. It was proposed that due to sharp top ends of the cone-shaped ZnO nanorods three kinds of inter-particle nanoscaled gaps are generated and contributed to the high sensitivity of SERS substrates. Three types of "hot spots" are formed by 1) coupling between the small silver nanoparilces that are grown on the same ZnO nanorod 2) coupling between silver nanoparticles growing on the two adjacent ZnO nanorods and 3) interaction between the large Ag spheres on the top ends of two neighboring ZnO nanorods.

Li *et al.*<sup>7</sup> fabricated multifunctional recyclable SERS substrate of Au-coated TiO<sub>2</sub> nanotube arrays. The substrate exhibited high sensitivity, stable SERS effect as well as photocatalytic activity and also the report is highlighted with a novel method for the fabrication of recyclable SERS substrates that eliminate single use problem of

traditional SERS substrate. As compared to ZnO, TiO<sub>2</sub> is more stable and possess the additional property of photocatalytic activity and thus has been widely used for degradation of organic pollutants. Hence 3D SERS substrate based on TiO<sub>2</sub> is highly desirable so that a recyclable SERS substrate with excellent SERS enhancement can be developed.

## 4.2 Experimental details

### 4.2.1 Synthesis of TiO<sub>2</sub> nanorods

In a typical TiO<sub>2</sub> nanorod synthesis, fused silica substrates were ultrasonically cleaned sequentially in acetone, isopropyl alcohol (IPA) and de-ionized (DI) water. Before the hydrothermal experiment, a compact thin layer of TiO<sub>2</sub> was deposited onto the well-cleaned fused silica substrate by immersion in an alcoholic titanium tetra isopropoxide (TTIP) solution at room temperature. As obtained films were annealed at 800°C for 1 hr in air ambient. The thin layer of TiO<sub>2</sub> deposited on fused silica substrates which act as a seed layer was further used for growth of TiO<sub>2</sub> nanorods by the solvothermal process. The different volume of titanium tetra isopropoxide (TTIP), Ti{OCH(CH<sub>3</sub>)<sub>2</sub>}<sub>4</sub> (97%; Alfa Aesar) was added to a mixture of de-ionized water and concentrated hydrochloric acid (HCl, 36.5% by weight) taken in a volume ratio of 1:1. The mixture was stirred well at room temperature and transferred into a teflon lined autoclave. The solvothermal experiment was carried out at 180<sup>0</sup> C for 3 hrs. After synthesis, the fused silica substrate was taken out, rinsed extensively with de-ionized water and dried in ambient air. The TiO<sub>2</sub> substrates were synthesized for 0.4, 0.6 and 0.8 ml volume of TTIP and the samples are named as T1, T2 and T3, respectively.

#### 4.2.2 Deposition of silver nanoparticles on TiO<sub>2</sub> nanorods

The decoration procedure is schematically represented in figure 4.1. TiO<sub>2</sub> nanorods were decorated with silver nanoparticles (AgNP) by reducing  $[\text{Ag}(\text{NH}_3)_2]^+$  with glucose.  $[\text{Ag}(\text{NH}_3)_2]^+$  solution was prepared by dropwise addition of ammonium hydroxide to 0.1 M AgNO<sub>3</sub> solution until it became clear and colorless. Afterwards, as-prepared TiO<sub>2</sub> nanorod substrate was placed into this solution for 5 min and subsequently kept in de-ionized water for several seconds. Then the substrates were immersed into 0.1 M glucose solution for 5 min followed by dipping once again into the de-ionized water for 2 min to remove any glucose molecule.

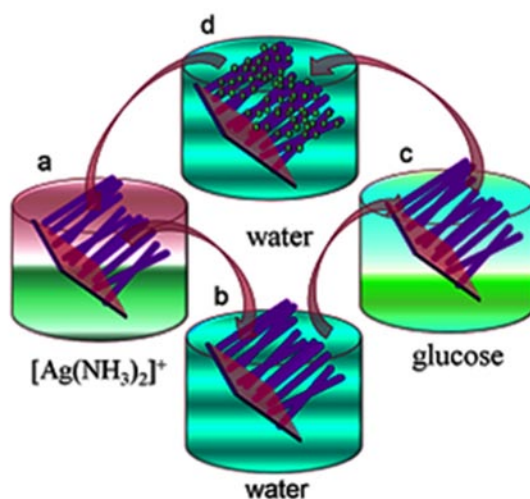


**Figure 4.1:** Schematic of Ag decoration on TiO<sub>2</sub> nanorods

This decorating procedure was performed many cycles to manage the density and the size of silver nanoparticles on the surface of the TiO<sub>2</sub> nanorods. The Ag-TiO<sub>2</sub> samples prepared by one, two, three, four, five, six and seven cycles are named as C1, C2, C3, C4, C5, C6 and C7 respectively.

### 4.3 Results and discussion

The morphology of the  $\text{TiO}_2$  nanorods was characterized using a field emission scanning electron microscope (Zeiss Ultra 55 field emission scanning electron microscope) and figure 4.2(a) and 4.2(b) show FESEM image of  $\text{TiO}_2$  nanorods synthesized using 0.6 ml of TTIP (sample T2). It is clear that the  $\text{TiO}_2$  nanorods are not grown vertically, but in an inclined direction with substrate surface which is favorable for increasing number of silver nanoparticles with "hot spots" in detection volume. The average diameter of nanorod is about 80 nm.

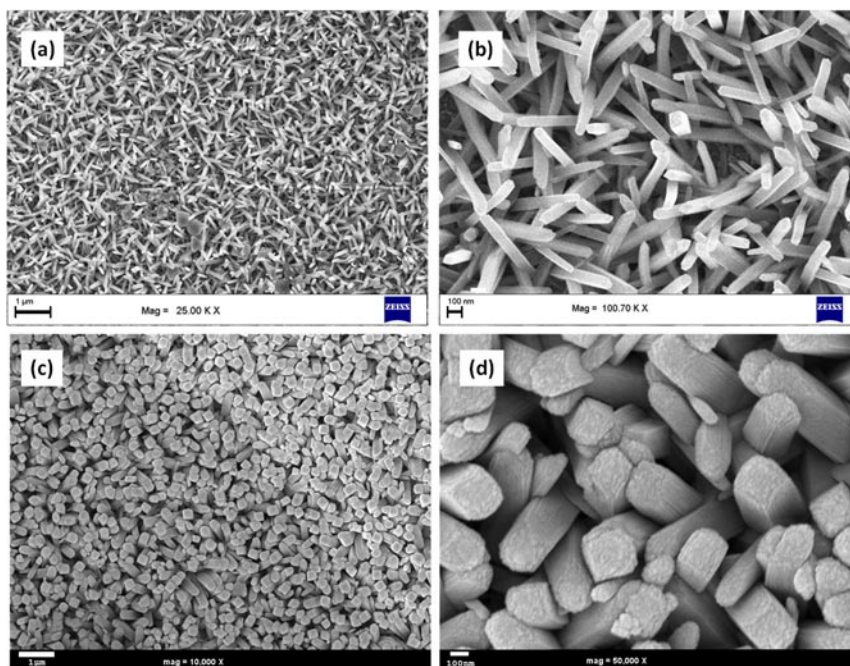


**Figure 4.2:** FESEM image of (a) sample T2 (b) magnified image of T2 (c) sample T3 (d) magnified image of T3

Morphology of seed layer used for growth of nanorods is shown in figure 4.3. From the SEM image, it is observed that nanoparticles of size about 20 nm are uniformly distributed over a quartz substrate. These nanoparticles in seed layer act as a nucleation site for the growth of TiO<sub>2</sub> nanorods. Since the nanorods are grown from a different point on the seed layer, the morphology of the sample resulted in a scaffold-like structure of TiO<sub>2</sub> nanorods. On further increasing TTIP volume to 0.8 ml, closely packed nanorods with a diameter of about 350 nm are grown (sample T3) and is shown in figure 4.2(c) and 4.2(d). These closely packed nanorod arrangement enables increased surface area for the deposition of silver nanoparticles and also promotes the formation of different types of "hot spots" on the surface of TiO<sub>2</sub> nanorods. In addition, since the seed layer consists of closely arranged nanoparticles over whole substrate (figure 4.3), the large-scale uniform arrangement of nanorods are formed on the fused silica substrate which offers point to point reproducibility of SERS signal.

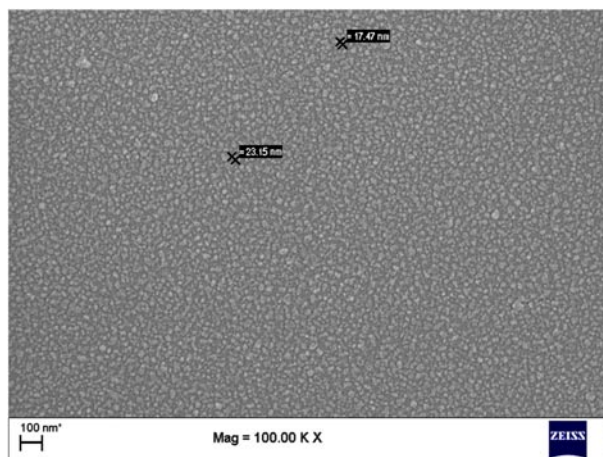


**Figure 4.3:** SEM image of seed layer used for growth of TiO<sub>2</sub> nanorods

The structural characterization of TiO<sub>2</sub> nanorods by X-ray diffraction technique (XRD, PANalytical X'pert PRO X-ray diffractometer) shows that TiO<sub>2</sub> nanorods are grown in rutile phase of tetragonal structure of TiO<sub>2</sub> (ICDD file no 03-065-1118) (figure 4.4).

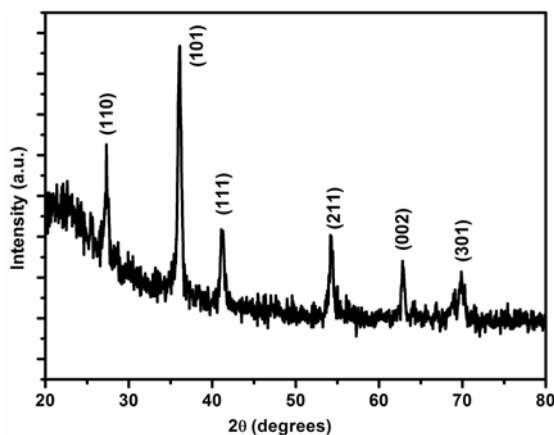


**Figure 4.4:** XRD pattern of TiO<sub>2</sub> nanorods grown by hydrothermal method

The electromagnetic enhancement in decorated silver nanoparticle was investigated by finite-difference time-domain (FDTD) method (Lumerical Solutions Ltd.). FDTD method enables to locate the field enhancement in silver nanoparticles decorated on nanorod. A plane polarized source of wavelength 514.5 nm was incident on TiO<sub>2</sub> nanorod of diameter 80 nm decorated with 12 nm sized silver nanoparticles. As seen in figure 4.5, field enhancement occurs in tiny gaps between the decorated nanoparticles. It is also observed that "hot spots" are not generated in between the nanoparticles that are decorated on the sidewall of vertically aligned nanorods. The FDTD results provide the information that number of decorated nanoparticles with tiny gaps on

nanorods should be increased to fabricate Ag-TiO<sub>2</sub> based SERS substrate with high sensitivity.

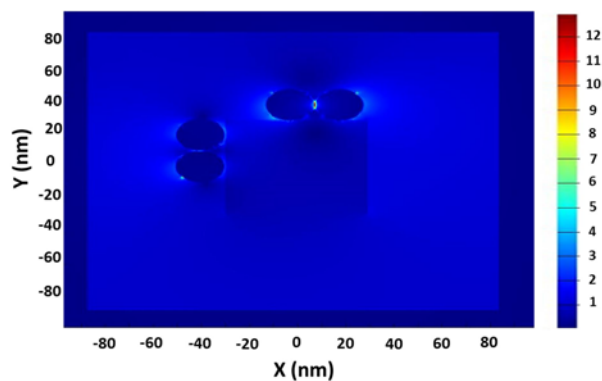


**Figure 4.5:** FDTD simulation of TiO<sub>2</sub> nanorod decorated with silver nanoparticles

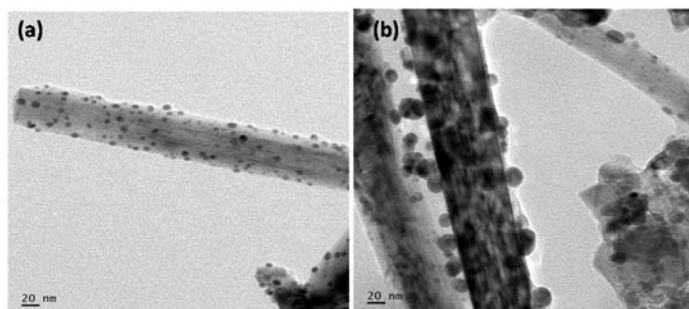


**Figure 4.6:** (a) TEM image of sample C1 (b) sample C2

Unlike high-cost vacuum based techniques used for fabrication of hybrid SERS substrate, a simple chemical reduction procedure was employed for the decoration of silver nanoparticle onto TiO<sub>2</sub> nanorods. The density of "hot spots" can be tuned by increasing cycles of decoration procedure. Detailed TEM (transmission electron microscope):

JEOL, JEM-2100) observations shown in figure 4.6(a) and 4.6(b) proves that with single decoration cycle, randomly distributed silver nanoparticle of uniform size of about 5 nm are formed and the size and density of silver nanoparticles increases with increase in decoration cycle to two. The corresponding size is estimated to be around 20 nm. From figure 4.6(b), it can be clearly seen that tiny gaps are formed between the Ag nanoparticles which provide a better opportunity for the formation of "hot spots" that enables SERS detection at extremely low molecular concentrations. High resolution TEM (HRTEM) image shown in figure 4.7 confirms (111) plane of face centered cubic structure of silver nanoparticles (ICDD No 01-087-0719).

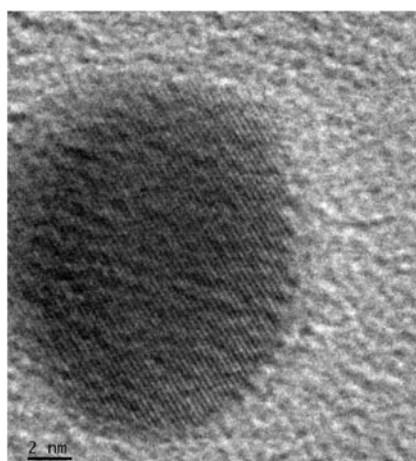


**Figure 4.7:** HRTEM image silver nanoparticle in sample C2

In order to optimize the number of decoration cycle for the development of SERS substrate with maximum enhancement, SERS activity of the as-prepared substrate (sample T2) was evaluated using Rhodamine 6G (R6G) molecule as a probe molecule. Raman measurements were performed on Horiba Jobin Yvon LabRAM HR

microRaman spectrometer with the 514.5 nm excitation line. SERS activity of Ag-TiO<sub>2</sub> substrate with different decoration cycle is given figure 4.8. All characteristics peaks of R6G can be clearly seen and is identified. The Raman peaks at 611, 771, and 1125 cm<sup>-1</sup> are associated with C–C–C ring in-plane, out-of-plane bending, and C–H in-plane bending vibrations, respectively, while the bands at 1189, 1360, 1508, and 1649 cm<sup>-1</sup> are assigned to symmetric modes of in-plane C–C stretching vibrations<sup>8,9</sup>. It is observed that SERS intensity is improved sharply from sample C1 to C6 and then decreases (inset of figure 4.8).

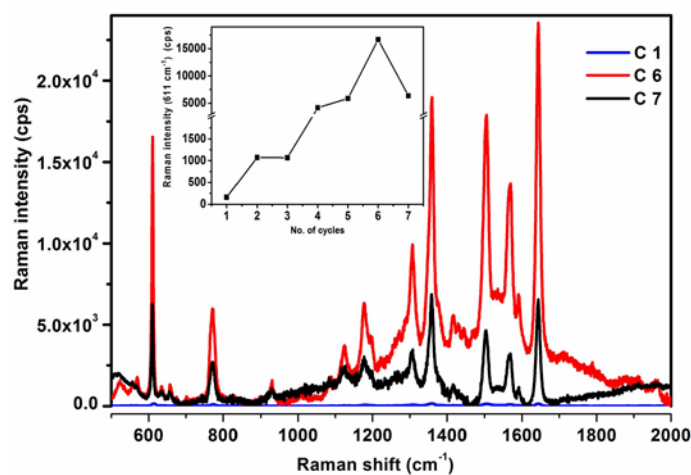


**Figure 4.8:** SERS spectra of  $10^{-5}$  M R6G molecule for sample C1, C6 and C7. Inset shows intensity variation of prominent peak, 611 cm<sup>-1</sup> of R6G for the samples C1, C2, C3, C4, C5, C6 and C7

The SERS intensity variations with different decorating cycle can be ascribed to the particular arrangement of nanoparticles over the prepared substrate which is verified through TEM analysis given in figure 4.6. For substrates with one cycle of decoration procedure,

nanoparticles are generated with large gaps which do not promote coupling between nanoparticles. As the number of cycles increases, nanoparticles become bigger and efficient gaps for generation of "hot spots" are created between the neighboring silver nanoparticles. The density of silver nanoparticles with "hot spots" is increased up to decoration cycle of six. For a decoration cycle of seven, the tiny gaps are combined to form bigger particles; it decreases the SERS activity of substrate. TEM image shows in figure 4.9 confirm the formation of bigger silver nanoparticles of size about 50 nm for the sample C7.

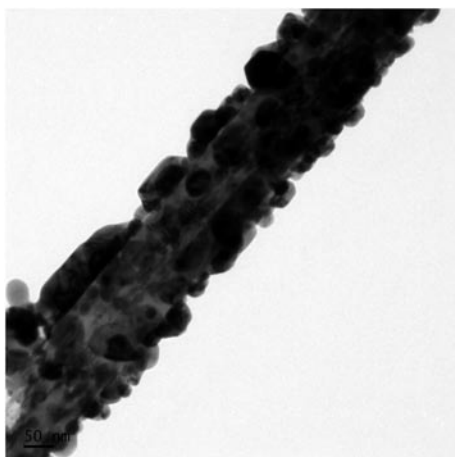


**Figure 4.9:** TEM image of sample C7

Dependence of TiO<sub>2</sub> nanorod density on SERS enhancement is also evaluated. Figure 4.10 compares SERS activity of TiO<sub>2</sub> nanorod samples T1, T2 and T3 with two Ag decoration cycles using  $5 \times 10^{-7}$  M R6G molecule as test molecule. The variation in Raman intensity of the peak at  $611 \text{ cm}^{-1}$  is shown inset of figure 4.10. As the TTIP volume increased from 0.4 ml to 0.8 ml, a huge enhancement in SERS activity is

observed which can be attributed to increased "hot spots" due to the formation of closely packed nanorods. But for TTIP volume of 1 ml, Ag-TiO<sub>2</sub> substrate exhibit no SERS activity at all due to the oxidation of silver nanoparticles at the surface of TiO<sub>2</sub> nanorod array. Hence it can be concluded that there is an optimum nanorod density for the development of efficient SERS substrate. It is found that substrate with a higher density of nanorods is decorated with an efficient number of "hot spots" by a lesser number of Ag decoration cycles as compared to that of lower density.

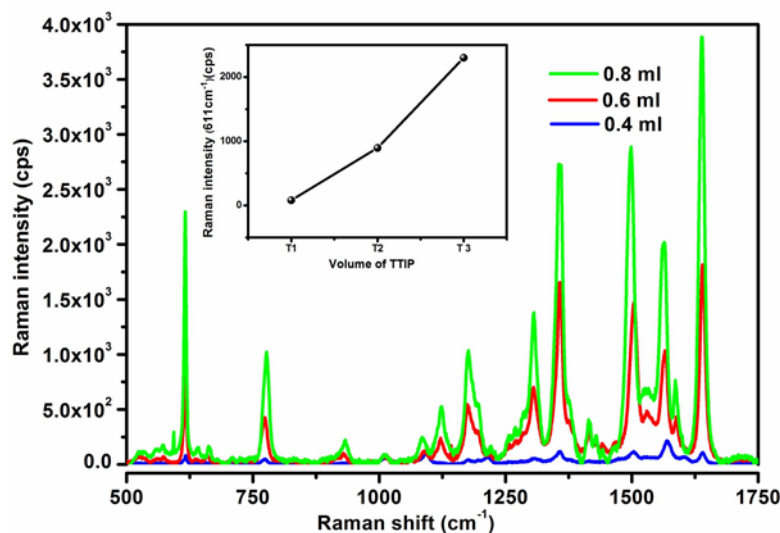


**Figure 4.10:** SERS spectra of  $5 \times 10^{-7}$  M R6G molecules using samples T1, T2 and T3. Inset shows intensity variation of prominent peak,  $611 \text{ cm}^{-1}$  of R6G as a function of TTIP volume

The increase in SERS activity with an increase in nanorod density can be explained on the basis of formation of different types of "hot spots". As the density of nanorods increased, the silver nanoparticles at

adjacent nanorods are coupled and "hot spots" are generated in between the nanorods also. Hence the excellent sensitivity of sample T3 can be attributed to the formation of "hot spots" between the nanorods in addition to that formed on individual nanorods.

Subsequently, the SERS substrate with an efficient number of "hot spots" was chosen to check the SERS signal sensitivity and the reproducibility using the same analyte molecule. SERS measurement was carried out for R6G concentration down to  $10^{-17}$  M. It is observed that detection limit of Ag-TiO<sub>2</sub> SERS substrate to R6G is as low as  $10^{-17}$  M. The corresponding spectrum is shown in figure 4.11. For SERS measurements, a 30  $\mu$ L drop of R6G at  $10^{-17}$  M concentration was spread over a 0.5 mm $\times$ 0.5 mm AgNPs decorated TiO<sub>2</sub> substrate. Assuming that the molecules are uniformly distributed over substrate, there are about 180 R6G molecules spread over the whole substrate for a concentration of  $10^{-17}$  M. Since silver nanoparticles are decorated on 3D TiO<sub>2</sub> nanorods of length around 500 nm and diameter 80 nm, the effective area of the SERS substrate will be larger than 0.5 mm $\times$ 0.5 mm. Therefore when the 180 molecules are adsorbed to a very large area, number of molecules in the detection volume will be one or two. It is also seen that SERS signal is observed at some specific point of the scanned surface. These observations indicate the detection of a single molecule, or a very few number of molecules if aggregation of R6G molecules occurred.

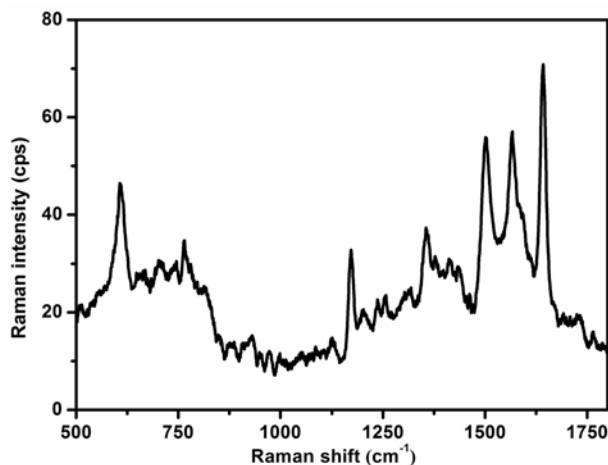


**Figure 4.11:** SERS spectrum of  $10^{-17}$  M R6G molecule

The EF can be calculated by  $EF = \frac{I_{SERS}/N_{SERS}}{I_{RS}/N_{RS}}$ . Here also  $I_{RS}$  represents the intensity of the same band of R6G (here,  $611\text{ cm}^{-1}$ ) and its value is 1500 counts (figure 2.14 in chapter 2).  $I_{SERS} = 30$  counts. Here SERS measurements are carried out for an accumulation time of 1 s.  $N_{SERS} = 1$  and  $N_{RS} = 1.24 \times 10^9$ . So, the EF is estimated to be  $2 \times 10^8$  (section 2.4.4).

The uniformity of as prepared substrate was also examined by collecting SERS signal of  $10^{-6}$  M R6G solution from randomly selected spots across the substrate. It is confirmed that SERS signals are highly reproducible over a large area under identical experimental conditions such as the laser power and the integration time, and is shown in figure 4.12.

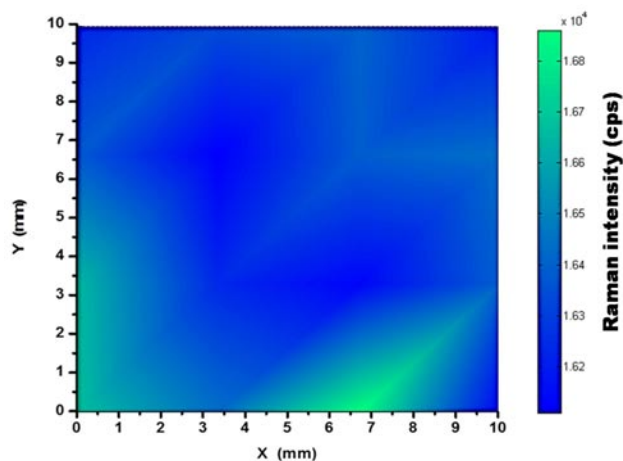


**Figure 4.12:** SERS spectra of  $10^{-6}$  M R6G from randomly selected spots across the substrate

The uniqueness of as prepared Ag-TiO<sub>2</sub> based SERS substrate over already reported TiO<sub>2</sub> nanorod array based SERS substrate<sup>7,10</sup> is the very large enhancement factor which is due to the formation of different types of efficient "hot spots" at the surface of TiO<sub>2</sub>. In the as-prepared substrate, the unaligned growth of nanorods enabled the formation of "hot spots" in between adjacent nanorods. Since the nanorods are grown inclined with the surface, "hot spots" generated on the side wall of nanorods can efficiently contribute to total SERS intensity. It is also believed that the improved detection sensitivity is not only due to very large SERS activity of this substrate but also the sorption effect of the as-prepared metal-semiconductor hybrid substrate. It should be mentioned that the particularly inclined growth of nanorod has increased surface area, which will lead to a better enrichment of "hot spots" and the analyte molecules.

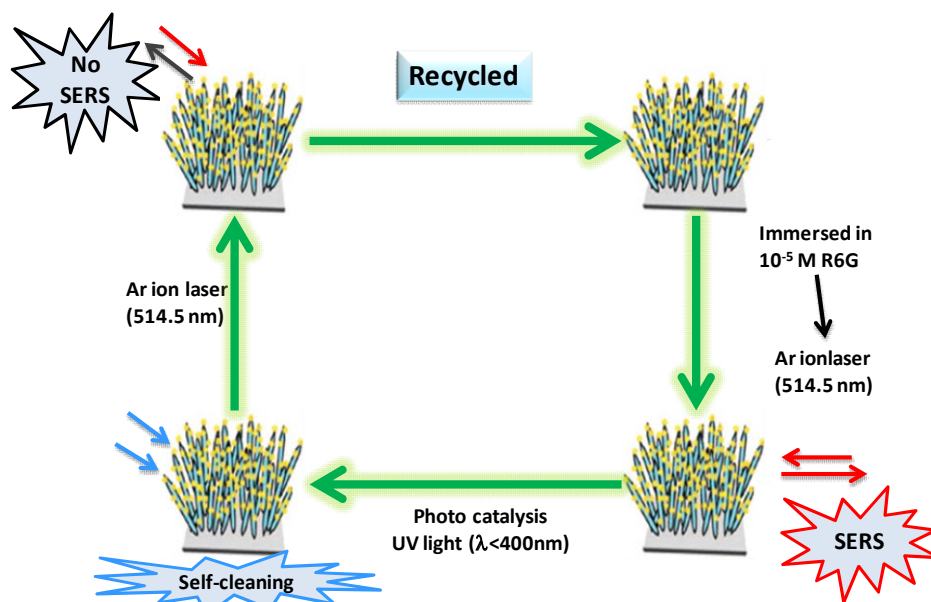


**Figure 4.13:** Schematic of recycling nature of Ag-TiO<sub>2</sub> based SERS substrate

The advantage of Ag-TiO<sub>2</sub> based SERS substrate over traditional SERS substrate is its recycling ability. It is well known that TiO<sub>2</sub> hold an excellent photocatalytic activity and out of different crystal phases of tetragonal TiO<sub>2</sub>, rutile phase of tetragonal crystal structure exhibits more photocatalytic activity<sup>11,12</sup>. The recycling of as fabricated Ag-TiO<sub>2</sub> based SERS substrate is schematically shown in figure 4.13. In order to demonstrate recycle capacity of Ag-TiO<sub>2</sub> substrate, the SERS substrate with  $1 \times 10^{-5}$  M R6G molecules was exposed to UV radiation (366 nm) for 6 hr and it was observed that the molecules are completely degraded. The SERS activity after photodegradation is given in figure 4.14. From the figure 4.14, it is clearly seen that the presence of any Raman peaks corresponding R6G confirms the complete degradation of R6G molecules.

During photocatalysis in  $\text{TiO}_2$ , electrons from the valence band of  $\text{TiO}_2$  are excited to the conduction band by absorbing UV, resulting in the formation of electron-hole pairs. The reaction of electrons in the conduction band with  $\text{O}_2$  produce superoxide radicals ( $\text{O}_2^{\cdot -}$ ) and that of holes on the valence band form singlet oxygen ( $^1\text{O}_2$ ). The valence band holes also react with surface adsorbed  $\text{H}_2\text{O}$  or  $\text{HO}^-$  and result in the formation of hydrogen peroxide ( $\text{H}_2\text{O}_2$ ), protonated superoxide radicals ( $\text{HOO}^{\cdot}$ ) and hydroxyl radicals ( $\text{HO}^{\cdot}$ ). The reaction of  $\text{H}_2\text{O}_2$  with  $\text{HO}^{\cdot}$  forms protonated superoxide radicals ( $\text{HOO}^{\cdot}$ ). These free electrons/holes, and reactive oxidizing species react with the surface adsorbed organic compounds that leads to their decomposition<sup>12</sup>.

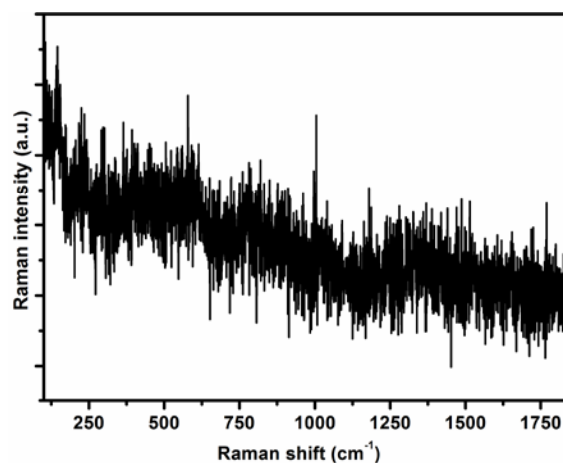


**Figure 4.14:** SERS spectrum of  $1 \times 10^{-5}$  M R6G molecule from as-prepared substrate after photodegradation

The SERS activity was again tested for  $10^{-5}$  M R6G. Figure 4.15 compares SERS activity of as prepared substrate and the recycled substrate. It is observed that the SERS intensity is regained completely which confirms the recyclable nature of Ag- $\text{TiO}_2$  based SERS substrate.

Hence the advantage of as fabricated substrate is that it can detect the organic species especially food adulterants, pesticides, pollutants, etc., at very low

concentrations and after that, it can degrade the molecules so that SERS substrate can be recycled.

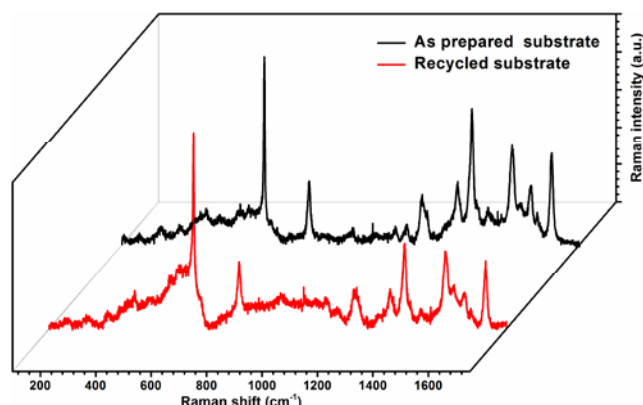


**Figure 4.15:** SERS spectra of  $1 \times 10^{-5}$  M R6G molecule from as-prepared substrate and recycled substrate

In contrast to previously reported 3D hybrid SERS substrate such as ZnO nanorods achieved via hydrothermal synthesis<sup>13</sup> and TiO<sub>2</sub> nanorods synthesized via hydrothermal method<sup>10</sup>, our Ag-TiO<sub>2</sub> hybrid substrate offers a large quantity of efficient SERS “hot spots” in the focused region. A detection limit of single-molecule is achieved successfully and in comparison with already reported one, our SERS substrates are at the top in detection limit.

#### 4.4 Conclusion

Fabrication of multifunctional Ag-TiO<sub>2</sub> based 3D hybrid SERS active substrate by a simple novel method is demonstrated. The TiO<sub>2</sub> nanorods are grown on fused silica in a single step hydrothermal method and AgNPs are assembled simultaneously, merely by simple chemical reduction. An inclined growth of TiO<sub>2</sub> nanorods lead to formation of different types of “hot spots”. As-prepared substrates exhibit excellent enhancement factor of about  $2 \times 10^8$  with single molecule detection capability. The recycling capacity of Ag-TiO<sub>2</sub> based SERS substrate is verified, which open a new opportunity to get rid of the traditional use and throw SERS substrates. The substrate can be a promising multifunctional sensor for detection of food adulterants, organic pollutants, pesticide, etc.

**References**

- [1] X. Yang, H. Zhong, Y. Zhu, J. Shen, and C. Li, Dalton Trans. **42**, 14324 (2013).
- [2] H. Tang, G. Meng, Q. Huang, Z. Zhang, and Z. Huang, Adv. Funct. Mater. **22**, 218 (2012).
- [3] X. Wang, C. Wang, L. Cheng, S.-T. Lee, and Z. Liu, J. Am. Chem. Soc. **134**, 7414 (2012).
- [4] Y.F. Chan, H.J. Xu, L. Cao, Y. Tang, D.Y. Li, and X.M. Sun, J. Appl. Phys. **111**, 033104 (2012).
- [5] J. Huang, F. Chen, Q. Zhang, Y. Zhan, D. Ma, K. Xu, and Y. Zhao, ACS Appl. Mater. Interfaces **7**, 5725 (2015).
- [6] H. Tang, G. Meng, Q. Huang, Z. Zhang, Z. Huang, and C. Zhu, Adv. Funct. Mater. **22**, 218 (2012).
- [7] B.X. Li, G. Chen, L. Yang, Z. Jin, and J. Liu, Adv. Funct. Mater. **20**, 2815 (2010).
- [8] P. Hildebrandt and M. Stockburger, J. Phys. Chem. **88**, 5935 (1984).
- [9] A.M. Michaels, M. Nirmal, and L.E. Brus, J. Am. Chem. Soc. **121**, 9932 (1999).
- [10] E. Tan, P. Yin, T. You, H. Wang, and L. Guo, ACS Appl. Mater. Interfaces **4**, 3432 (2012).
- [11] T. Ohno, K. Sarukawa, and M. Matsumura, New J. Chem. **26**, 1167 (2002).
- [12] P.P. Subha and M.K. Jayaraj, J. Exp. Nanosci. **10**, 1106 (2014).
- [13] C. Pacholski, A. Kornowski, and H. Weller, Angew. Chemie **116**, 4878 (2004).

## Chapter 5

# Investigation on electromagnetic and chemical enhancement mechanism of SERS

In this chapter, SERS enhancement mechanisms such as the correlation between excitation wavelength and LSPR wavelength to produce EM enhancement and the role of surface state energy level in producing chemical enhancement effect in metal oxide nanostructures are investigated. Gold nanotriangular arrays are employed for investigating electromagnetic enhancement mechanism. A correlation between excitation wavelength and LSPR wavelength has been observed in producing EM enhancement. Chemical enhancement mechanism is investigated in  $\text{TiO}_2$  nanorods and  $\text{TiO}_2$  nanoparticles. Photo-induced charge-transfer mechanism is observed in  $\text{TiO}_2$  nanostructures and it is seen that surface defect energy states mediate charge-transfer in  $\text{TiO}_2$  nanostructures.

### **5.1 Investigation on SERS electromagnetic enhancement mechanism**

Since the discovery of SERS in 1974, the origin and parameters affecting the total enhancement have been investigated. The major contribution to SERS is electromagnetic enhancement. However, the chemical enhancement also contributes to total enhancement upto some extent<sup>1</sup>. The electromagnetic enhancement mechanism is exhibited by coinage metals such as Ag, Au, Cu, etc. Even though the spatial dependence of enhancement factors is same for both silver and gold, the magnitude of EF is smaller for gold. Hence silver is more plasmonically active than gold and commonly used for ultra-sensitive detection and for single molecule SERS<sup>2</sup>. On the other hand, the importance of gold is that they are chemically more inert than silver and hence it is suitable for experiments, where the chemical stability of the colloid is more important than a maximum enhancement.

It is possible to maximize the electromagnetic enhancement by tuning excitation wavelength<sup>3,4</sup>. The wavelength-scanned SERS studies show that LSPR wavelength of the metal nanostructure should be close to the excitation wavelength used for SERS. Even though a systematic study of the relationship between the two has not been reported till date, McFarland *et al.*<sup>4</sup> has made a measurement Raman enhancement factor as a function of LSPR and the excitation wavelength. It is found that at the constant excitation wavelength, the enhancement factor is maximum when the position of LSPR is located at the red of the fixed excitation wavelength and at the blue of Stoke-shifted Raman band. Additional studies demonstrated that the largest SERS enhancement factor is observed when the LSPR falls within a 120 nm window that includes

both the excitation wavelength and the Raman-shifted wavelength<sup>5</sup>. In another study, the enhancement factor is calculated with various excitation wavelengths at constant LSPR position. In this study, a maximum enhancement factor is achieved when the excitation wavelength is positioned to the blue of LSPR. More detailed studies demonstrated that the maximum enhancement factor is observed when LSPR is roughly around the middle of the gap between excitation wavelength and Stoke-shifted Raman wavelength. These experiments illustrated the importance of optimizing LSPR and excitation wavelength to achieve maximum SERS enhancement<sup>5,6</sup>. A detailed study is still required to explore the relationship among LSPR, excitation wavelength and SERS enhancement factor.

### 5.1.1 Experimental details

#### Fabrication of gold nanotriangular arrays

Fabrication details of PMMA nanotriangular arrays by the nanoimprinting technique are given in chapter 3. In order to make PMMA nanotriangular arrays SERS active, gold film with 40, 60 and 80 nm thickness was deposited by electron beam evaporation. The experimental parameters are tabulated in table 5.1.

**Table 5.1:** Deposition parameters for gold over PMMA replicas

<b>Gold thickness</b>	40 nm	60 nm	80 nm
<b>Time</b>	2 min	3 min	4 min
<b>Power</b>	100 W	100 W	100 W

Rhodamine 6G (R6G) was taken as analyte molecule for SERS characterization of nanotriangular array. The SERS active substrate was

dipped in  $10^{-6}$  M aqueous solution of R6G for 3 hrs to distribute uniformly over the substrate. The SERS measurements were carried out on Horiba Jobin Yvon LabRAM HR microRaman spectrometer and excitation wavelength used was 514.5 nm of Ar ion laser and 632.8 nm of He-Ne laser. The scattering cross section of gold nanotriangles was calculated by Mie theory using 3D FDTD solution from Lumerical.

### 5.1.2 Results and discussion

The SERS activity of gold nanotriangular arrays of thickness 40, 60 and 80 nm using R6G molecule as Raman probe is shown in figure 5.1. The SERS measurement was carried out under non-resonant SERS condition using 632.8 nm as excitation wavelength. It is observed that as the thickness of nanotriangle increases from 40 to 60 nm, the Raman intensity boost up from 800 to 2080 counts. This value is almost same for 80 nm.

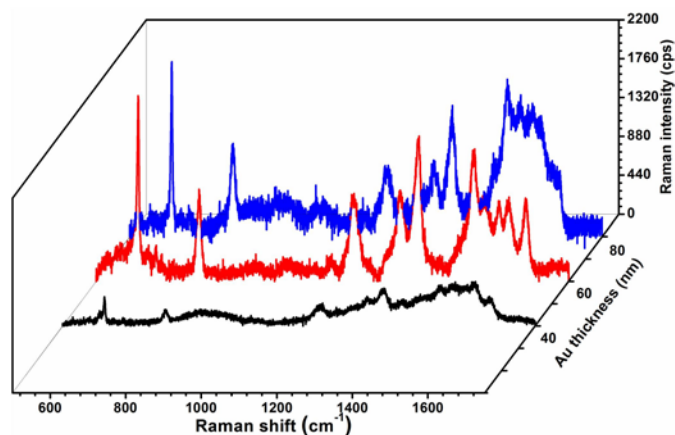


**Figure 5.1:** SERS spectra of R6G molecules using gold nanotriangles with various thicknesses under non-resonant excitation

Earlier reports suggest that LSPR position contributes a major role in SERS enhancement and hence scattering cross section of gold nanotriangles of thickness 20, 40, 60 and 80 nm were calculated by Mie theory and is given in figure 5.2. As the thickness increases from 20 to 80 nm, the LSPR position shifts to shorter wavelength, from 900 to 750 nm. The variation in SERS intensity with thickness can be thus attributed to variation in LSPR position whose values are moving towards the excitation wavelength (632.8 nm) as the thickness of nanotriangle increases to 80 nm.

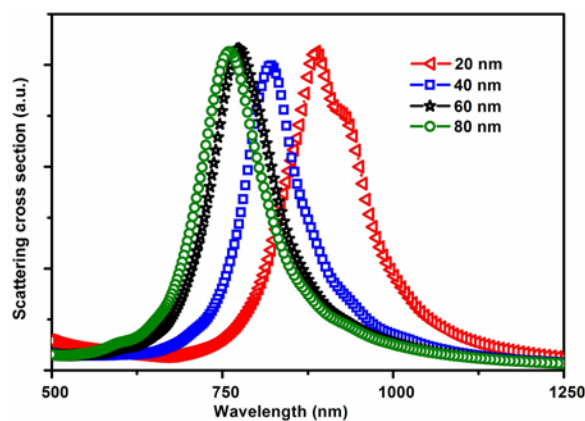


**Figure 5.2:** Scattering cross section of gold nanotriangles with different thickness

Compared to SERS, surface enhanced resonance Raman scattering (SERRS) has been known for producing very large enhancement factors of the order  $10^{11}$ – $10^{12}$ <sup>5</sup>. In SERRS, the Raman excitation wavelength is such that the molecule can make the electronic transition from the ground to some electronically excited state. When LSPR of the enhancing substrate is in the proper energy region, SERRS enhancement will be roughly the product of the enhancement factor for non-resonant SERS of

the substrate and the resonance Raman spectrum of the adsorbate. To investigate surface enhanced resonance Raman scattering (SERRS) in gold nanotriangles, SERS measurement was carried out using 514.5 nm as excitation wavelength. Surprisingly, the Raman intensity is smaller under resonant SERS condition than that under non-resonant condition. Under resonant SERS, the Raman intensity from gold nanotriangle of edge length 60 nm and thickness 60 nm is around 900 counts and is shown in figure 5.3. The Raman intensity under the non-resonant condition is 2080 counts (figure 5.1).

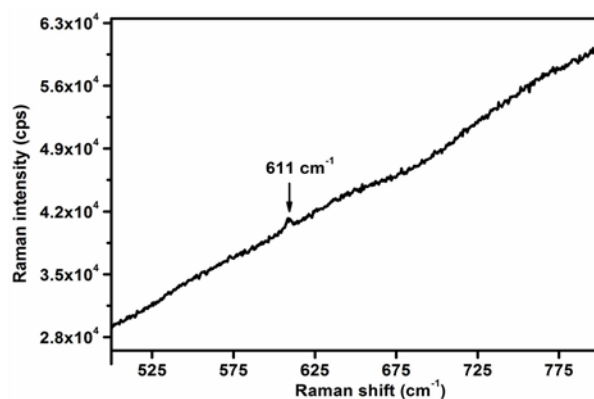


**Figure 5.3:** SERS spectrum of R6G molecules using gold nanotriangles of thickness 60 nm under resonant excitation

The SERS spectrum from non-patterned surface (flat) under non-resonant condition shows no Raman peaks and is clearly seen in figure 5.4. It is because, flat surface does not produce any electromagnetic enhancement and hence they cannot act as a SERS substrate. Raman measurement under identical condition was carried out on a flat gold surface under resonant condition also. Figure 5.5 shows resonance Raman of 10<sup>-6</sup> M R6G measured from non patterned surface (flat). The

corresponding peak intensity of  $611\text{ cm}^{-1}$  is around 600 counts which is comparable with SERRS intensity from nanotriangular arrays.

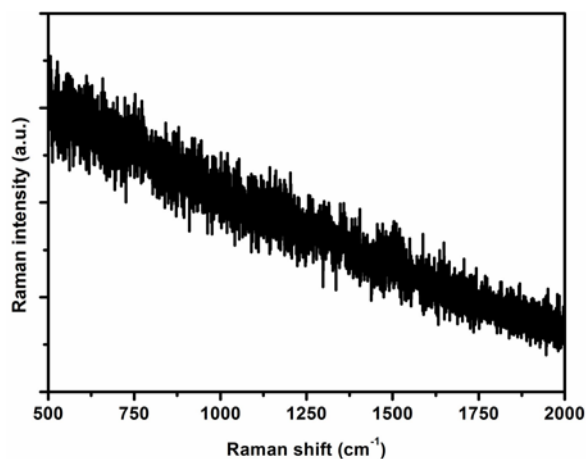


**Figure 5.4:** SERS spectrum of R6G molecules using flat gold film of thickness 60 nm under non-resonant excitation

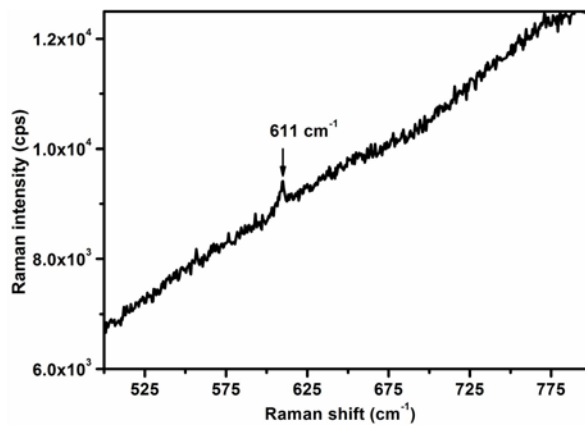


**Figure 5.5:** SERS spectrum of R6G molecules using flat gold film of thickness 60 nm under resonant excitation

On comparison, it is seen that under the non-resonant condition, patterned surface produces Raman signal of the intensity of 2000 cps and the flat surface doesn't produce any peaks, but under a resonant condition, Raman intensity from patterned surface and the flat surface is almost same. Therefore it can be concluded that under a resonant condition, nanotriangle does not contribute to Raman intensity, ie. no SERS electromagnetic effect. The observed Raman intensity is only due to resonance Raman effect. The enhanced SERS enhancement under the non-resonant condition as compared to that under resonant condition can be attributed to the variation in the gap between LSPR and excitation wavelength. Hence it is proposed that the presence of metal nanostructure alone does not ensure SERS effect. It is required that position of LSPR wavelength and excitation wavelength should be within a range to produce SERS effect.

## **5.2 Investigation on SERS chemical enhancement mechanism in metal oxide nanostructures**

Even though fabrication of SERS active substrate is initially focused on noble coinage metals and transition metals, nowadays considerable research have been centered on semiconductor materials based SERS active substrates. Oxides such as NiO<sup>7</sup>, ZnO<sup>8</sup>, TiO<sub>2</sub><sup>9</sup> and Cu<sub>2</sub>O<sup>10</sup> were demonstrated as SERS active substrates. SERS effect from semiconductor nanostructures has importance in the field of nanodevices because performance and reliability of nanodevices strongly depend on the surface and interfacial properties of the constituent nanomaterials<sup>11,12</sup>. Quagliano *et al.*<sup>13</sup> is the first in observing SERS on a semiconductor and the semiconductor under study was epitaxial InAs quantum dots. A new Raman band appeared corresponding to chemisorption of the molecule to

the semiconductor surface. Zhao's group proposed charge-transfer mechanism for SERS from ZnO<sup>14</sup>, ZnS<sup>15</sup> and TiO<sub>2</sub><sup>16</sup> based substrates by investigating Raman enhancement of 4-mercaptopyridine (4-Mpy) molecule.

Zhu *et al.*<sup>17</sup> verified metal semiconductor contact induced charge-transfer mechanism of SERS. In order to identify enhanced Raman modes by chemical enhancement effect, the metal and ZnO surfaces were inter-connected through PATP molecule. They have succeeded in providing a rather complete picture of dependence of excitation wavelength as well as Fermi energy on charge-transfer mechanism associated with the metal-semiconductor-molecule-metal assembly. The dramatic role of metal semiconductor contact to the contribution of charge-transfer mechanism of SERS was verified. The studies on micro-nanoscale charge-transfer in such junction are important to both the frontier of fundamental science and applications in molecular electronics. Surface enhanced Raman spectroscopy is one of the well developed techniques for probing these CT processes in microelectronic devices. The Ohmic and Schottky contacts play an important role in electron transport properties of metal semiconductor interface and control of these contact plays an important role in (opto) electronic devices.

SERS studies using TiO<sub>2</sub> nanoparticle by Xue *et al.*<sup>18</sup> revealed that particle size is a critical parameter affecting SERS enhancement factor. The correlation of particle size of semiconductor with Raman intensity enabled to determine the configuration of the nanoparticle, that make advancement in the field of semiconductor based sensors as well as solar cells<sup>18</sup>. In order to design efficient solar cells, nanostructures that provide a high rate of charge-transfer are preferable whereas to design

a high sensitive sensor, nanostructure that provides excellent Raman enhancement property is desired. In the same report, the optimization of various parameters according to desired applications was explained. A charge-transfer mechanism was proposed by Yang *et al.*<sup>19</sup> for SERS effect in TiO<sub>2</sub> nanostructures and it was observed that surface defects promote this charge-transfer between adsorbate and surface. In order to improve the charge-transfer effect, Yang *et al.*<sup>20</sup> incorporated silver onto TiO<sub>2</sub> through a photoreduction method. In comparison between Ag-TiO<sub>2</sub> and pure TiO<sub>2</sub> surfaces, it is concluded that Ag-TiO<sub>2</sub> exhibits higher enhancement factor. The enhancement can be attributed to the fact that besides the intrinsic CT contribution of TiO<sub>2</sub> to a molecule, incorporation of Ag brings additional electrons into the molecules adsorbed on TiO<sub>2</sub> surface through the conduction band of TiO<sub>2</sub> nanoparticle due to the localized surface plasmon resonance of silver.

Xue *et al.*<sup>18</sup> proposed a photo-induced charge-transfer between the adsorbate and the substrate, for probe molecules adsorbed onto the colloidal TiO<sub>2</sub> quantum dots and also proposed that the frequency of light for charge-transfer resonance varies with particle size. Later Yang *et al.*<sup>19</sup> proposed TiO<sub>2</sub>-to-molecule charge-transfer mechanism for the Raman enhancement. Another important observation is that not only Raman signals of adsorbed species are enhanced but also the phonon modes of TiO<sub>2</sub> are enhanced due to adsorption of probe molecules. Tarakeshwar and group<sup>21</sup>, in their studies on Raman enhancement of formic acid and dopamine on TiO<sub>2</sub> nanoparticles showed that vibronic coupling strengthens the charge-transfer from the highest occupied molecular orbital (HOMO) of the molecule to the conduction band of the quantum dot and hence the SERS effect.

### 5.2.1 Experimental details

#### Synthesis of TiO<sub>2</sub> nanoparticles and TiO<sub>2</sub> nanorods

Pure anatase TiO<sub>2</sub> nanoparticles (TiO<sub>2</sub> NPs) were synthesized through a chemical route using the procedure as follows. 50 ml of distilled water was added to a mixed solution of 5 ml of titanium isopropoxide and 15 ml of isopropyl alcohol. The above mixture was kept at 100 °C until all the solvent gets evaporated. The precipitate was then taken out and washed well with 5 ml and then 10 ml of ethanol. Finally, the products were dried in air in a laboratory oven at 60 °C.

Pure rutile phase TiO<sub>2</sub> nanorods (TiO<sub>2</sub> NRs) were synthesized by hydrothermal condition using titanium isopropoxide (TTIP) as a titanium precursor and hydrochloric acid (HCl) as a peptizer. In a typical procedure, 3 ml of TTIP was added into 25 ml HCl and 25 ml de-ionized water along with magnetic stirring. The resulting solution was then sealed in teflon lined stainless steel autoclave and placed inside an oven. The furnace was maintained at a temperature of 180 °C for 3 hrs, after which it was naturally cooled to room temperature. Finally, solid products were taken out, washed well with distilled water, filtered and then dried in air in a laboratory oven at 60 °C.

4-mercapto benzoic acid (4-MBA) was used as a probe molecule for SERS characterization of TiO<sub>2</sub> nanostructures. Figure 5.6 provides a model for adsorption of 4-MBA on TiO<sub>2</sub> nanostructure. TiO<sub>2</sub> nanostructure surface modified by 4-MBA molecules was obtained as follows. 20 mg of TiO<sub>2</sub> nanostructures were dissolved in 20 ml of 4-MBA, ( $1 \times 10^{-3}$  M) ethanol solution, and the mixture was stirred for 2 hrs. Then, the precipitate was centrifuged and rinsed with purified water once more and made into 3 ml by adding ethanol. TiO<sub>2</sub> nanostructures modified by 4-MBA were obtained.

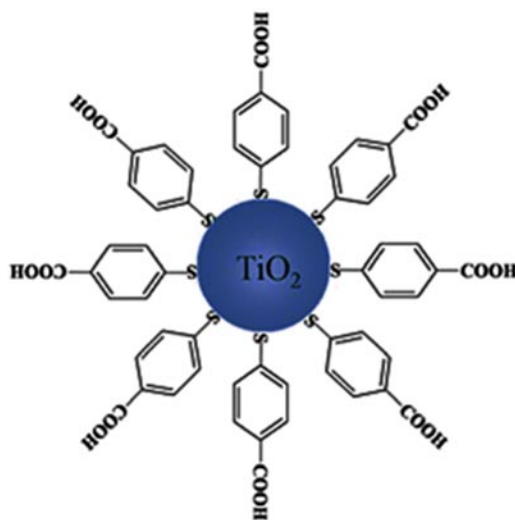


Figure 5.6: Model for 4-MBA adsorption on  $\text{TiO}_2$  nanostructures

### 5.2.2 Results and discussion

XRD (PANalytical X'pert PRO X-ray diffractometer) studies given in figure 5.7(a) and 5.7(b) show  $\text{TiO}_2$  nanoparticle growth with anatase phase of tetragonal structure (ICDD file no 03-065-5714) and  $\text{TiO}_2$  nanorod growth with rutile phase of tetragonal crystal structure (ICDD file no 03-065-1118) respectively.

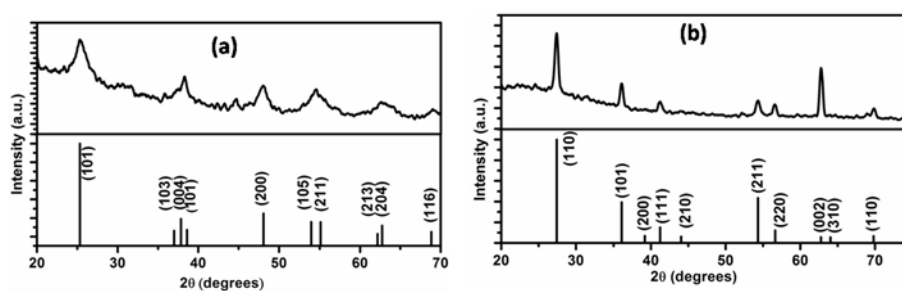
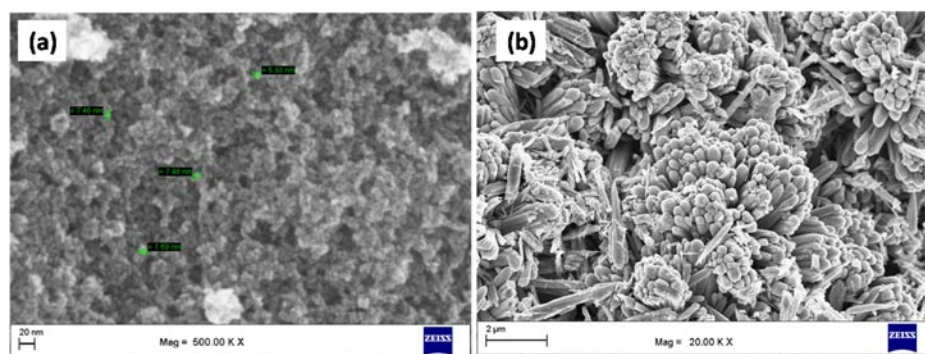


Figure 5.7: XRD spectra of (a)  $\text{TiO}_2$  nanoparticles and (b)  $\text{TiO}_2$  nanorods

The field emission scanning electron microscope (FESEM) images confirm the formation of nanoparticles by chemical route (figure 5.8(a)) and formation of flower-like TiO<sub>2</sub> nanorods by hydrothermal method (figure 5.8(b)).



**Figure 5.8:** FESEM image of (a) TiO<sub>2</sub> nanoparticles (b) and TiO<sub>2</sub> nanorods

To demonstrate TiO<sub>2</sub> nanoparticles and TiO<sub>2</sub> nanorods as SERS substrates, a well-known probe molecule, 4-mercapto benzoic acid (4-MBA) is used. This 4-MBA probe molecule forms a chemical bond with TiO<sub>2</sub> surface. Figure 5.9 shows the SERS spectrum of 10<sup>-3</sup> M ethanol solution of 4-MBA adsorbed on TiO<sub>2</sub> nanoparticles and nanorods. Normal Raman spectrum of solid 4-MBA is also given in figure 5.9 for comparison. The Raman peaks of 4-MBA adsorbed on TiO<sub>2</sub> match with those previously reported in literature<sup>16</sup>. The SERS spectra are dominated by bands at about 1581 and 1073 cm<sup>-1</sup>, which are assigned to  $\nu_{8a}$  (a<sub>1</sub>) and  $\nu_{12}$  (a<sub>1</sub>) aromatic ring characteristic vibrations, respectively<sup>19</sup>. The chemical bonding of 4-MBA with TiO<sub>2</sub> surface is confirmed by the presence of weak bands at about 1141 ( $\nu_{15}$ , b<sub>2</sub>) cm<sup>-1</sup> and 1172 ( $\nu_9$ , a<sub>1</sub>) cm<sup>-1</sup> corresponding to the C-H deformation modes. The significant variation of SERS spectrum of 4-MBA adsorbed on TiO<sub>2</sub> from

normal Raman spectra of bulk 4-MBA can be observed both in intensity and position of bands.

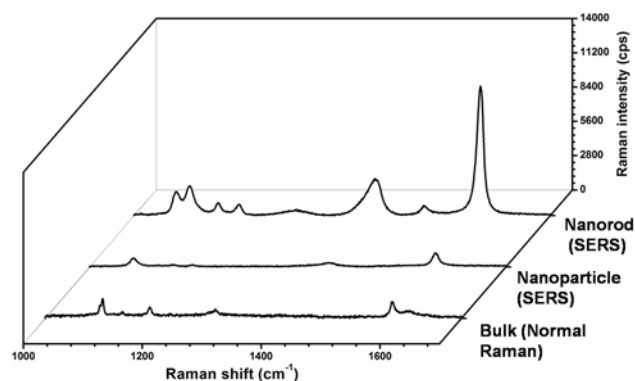


**Figure 5.9:** Normal Raman spectrum of bulk 4-MBA and SERS spectra of 4-MBA on TiO<sub>2</sub> nanoparticles and nanorods

From figure 5.9, it is also observed that SERS enhancement of 4-MBA from TiO<sub>2</sub> nanorods is higher than that from TiO<sub>2</sub> nanoparticles. In order to explore the reason for boosted SERS enhancement in nanorods as compared to nanoparticles, the effect of TiO<sub>2</sub> crystal phase was studied. As discussed in structural studies, TiO<sub>2</sub> nanorods are grown with rutile crystal phase and nanoparticles are with anatase crystal phase. So in order to confirm the effect of the crystal phase on SERS enhancement, the crystal phase of TiO<sub>2</sub> nanoparticle was transformed into rutile by annealing the samples at 800 °C for 1 hr. The transformation of TiO<sub>2</sub> nanoparticles from anatase to rutile was confirmed from the Raman spectra which are given in figure 5.10. As prepared TiO<sub>2</sub> nanoparticles show characteristic peaks of anatase crystal phase<sup>22</sup> and TiO<sub>2</sub> nanoparticles annealed at 800 °C show characteristic peaks of rutile crystal phase<sup>23</sup>.

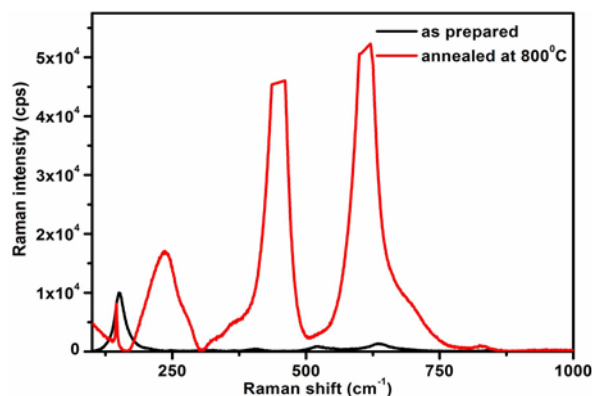


**Figure 5.10:** Raman spectra of as prepared and annealed TiO<sub>2</sub> nanoparticles

SERS activity of anatase and rutile phase of TiO<sub>2</sub> nanoparticles was compared and is given in figure 5.11. From figure 5.11, it is observed that change in crystal phase of TiO<sub>2</sub> nanoparticles did not bring any improvement in SERS activity; instead, it decreased the activity. So it is confirmed that higher SERS enhancement in nanorods is not attributed to rutile crystal structure of nanorods.

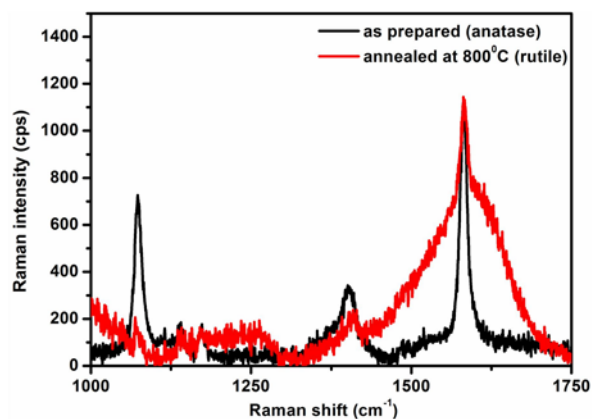


**Figure 5.11:** SERS spectra of 4-MBA using as-prepared TiO<sub>2</sub> nanoparticle and TiO<sub>2</sub> nanoparticles annealed at 800°C

It is reported that the chemical enhancement in  $\text{TiO}_2$  is due to the photo-induced charge-transfer mechanism due to the presence of surface defect states in the forbidden gap<sup>19</sup>. So to clarify the effect of surface defects, the photoluminescence (PL) measurements were carried out. Figure 5.12 shows the PL spectra of nanorods and nanoparticles under excitation of 514 nm. Both the samples showed emission at 565 nm which is due to the presences of trap levels or surface defects in the material. From PL intensity, it is seen that nanorods possess more surface defects as compared to nanoparticles since PL intensity is higher for nanorods. Hence it can be concluded that huge SERS activity of nanorods compared to nanoparticles is due the effect of surface defect states present in the material.

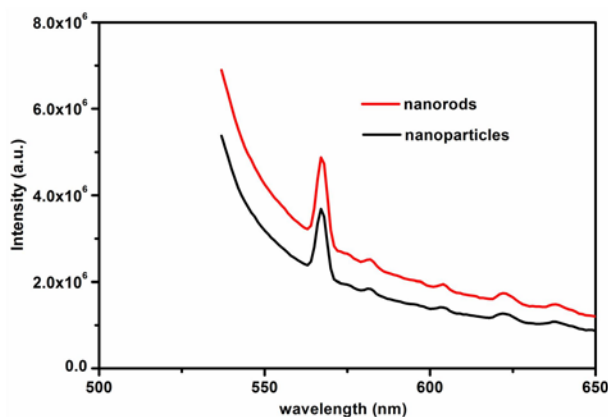


**Figure 5.12:** Photoluminescence spectra from anatase  $\text{TiO}_2$  nanoparticles and  $\text{TiO}_2$  nanorods under 514 nm excitation wavelength

To further confirm the effect of surface defect states on SERS enhancement,  $\text{TiO}_2$  nanoparticles and  $\text{TiO}_2$  nanorods were annealed at various temperatures from 200 to 600 °C. The SERS activity of

annealed anatase TiO<sub>2</sub> nanoparticles and TiO<sub>2</sub> nanorods were compared with that of pristine samples and the spectra are given in figure 5.13 and 5.14, respectively. The corresponding intensity variation of prominent peak, 1581cm<sup>-1</sup> of 4-MBA, as a function of annealing temperature is shown as inset of figure 5.13 and 5.14. From the figures, it is clearly seen that the samples annealed at 600 °C exhibit the lowest SERS activity which is due to the well-known phenomena that when a material is annealed in the presence of air, the oxygen vacancies are removed and hence the number of surface state is reduced<sup>24</sup>. Therefore the chemical enhancement mechanism in TiO<sub>2</sub> nanostructure is photo-induced charge-transfer mechanism (PICT) mediated by surface defect states.

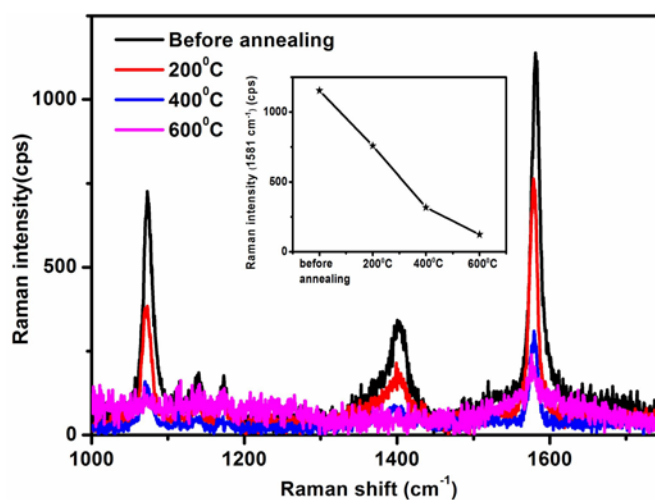


**Figure 5.13:** SERS activity of anatase TiO<sub>2</sub> nanoparticles annealed at various temperatures. Inset shows intensity variation of prominent peak, 1581cm<sup>-1</sup> of 4-MBA, as a function of annealing temperature

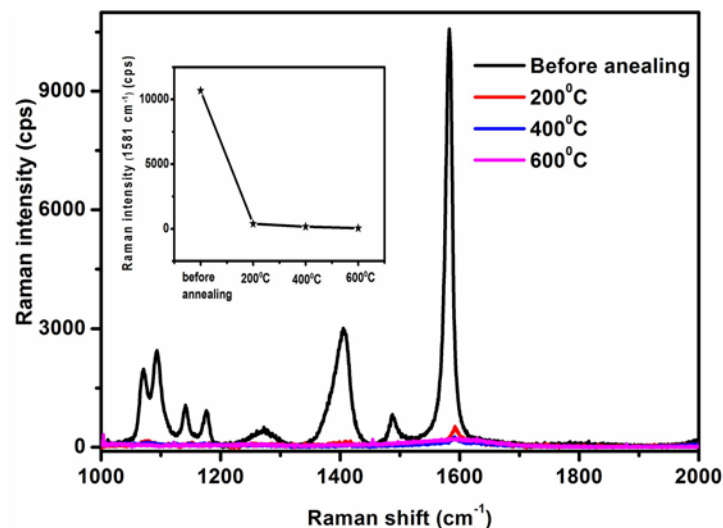


**Figure 5.14:** SERS activity of TiO<sub>2</sub> nanorods annealed at various temperatures. Inset shows intensity variation of prominent peak, 1581cm<sup>-1</sup> of 4-MBA, as a function of annealing temperature

### *PICT mechanism in TiO<sub>2</sub> nanostructures*

The two major enhancement mechanisms in SERS is described to electromagnetic enhancement mechanism (EM) and chemical enhancement (CE) mechanism. Since LSPR position of metal oxides lies in IR region of electromagnetic spectrum, it is impossible to obtain EM contribution from semiconductor under visible excitation. Hence the enhancement mechanism in semiconductor based SERS substrate is due to chemical enhancement mechanism. It is suggested that<sup>25</sup> when the molecule is adsorbed on the surface of the semiconductor, it interacts with the atoms of the substrate surface. As a result of such interaction, electron density distribution is varied that could affect the Raman scattering cross section of the molecular vibrational modes, which selectively enhances various vibrational modes of molecules. Different types of chemical

enhancement are a chemical-bonding enhancement, surface complexes resonance enhancement and photo-induced charge-transfer enhancement (PICT). The enhancement in Raman scattering intensity in all these mechanisms would depend on the change in molecular polarizability. In chemical bonding enhancement mechanism, when the molecule is adsorbed onto the surface of the substrate via chemical bonds, the partial charge-transfer process might increase the effective molecular volume as well as the ground state polarizability, and result in the magnification of Raman scattering cross section. In the second type of surface complexes resonance enhancement mechanism, a new highest occupied molecular orbital (HOMO) and lowest unoccupied molecular orbital (LUMO) levels are generated owing to new surface-complexes. A resonant enhancement can be produced in these surface complexes under suitable excitation. PICT enhancement mechanism is the most appropriate mechanism for metal oxide based SERS substrates. In the PICT enhancement mechanism, it is not necessary to have molecules to be chemisorbed onto the surface of the substrate. However, for the thermodynamically feasible CT, the HOMO and LUMO of the molecule should match the energy levels of the valence band (VB) and conduction band (CB) of the substrate. The possible routes for PICT are between the molecule and the semiconductor substrate. Thus, PICT transfer occurs either from the semiconductor substrate to molecule or from the molecule to semiconductor substrate.

The charge-transfer between  $\text{TiO}_2$  and 4-MBA is schematically represented in figure 5.15. The band gap of  $\text{TiO}_2$  nanoparticles and  $\text{TiO}_2$  nanorods are 3.16 eV and 3.43 eV respectively. Therefore, on excitation with 514.5 nm (2.4 eV), an electron in VB couldn't make the transition to

CB. The presence of defect level state at 2.4 eV in  $\text{TiO}_2$  nanostructures is confirmed through PL studies. Hence an electron in VB is transferred to defect states by stimulation of incident excitation light which creates an electron in defect states and a hole in the valence band. The excited electron is quickly tunneled to a matching energy level above the LUMO of the molecule through the resonant transfer process. The excited electron eventually transfers back to VB of semiconductor and recombines with the hole. Hence charge transfer between the metal oxide and adsorbate occurs and the SERS effect from metal oxide nanostructures.

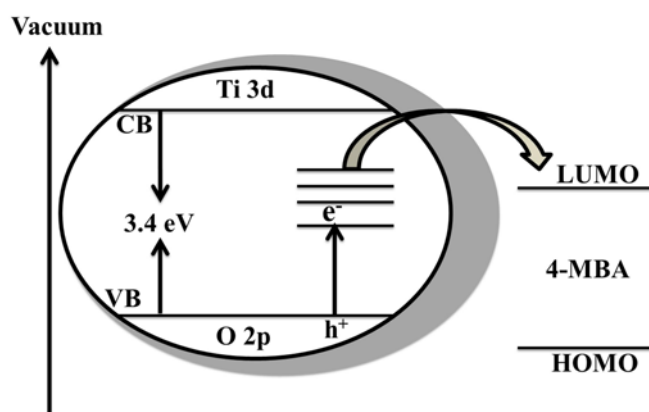


**Figure 5.15:** Model for PICT mechanism in  $\text{TiO}_2$  - 4-MBA complex

#### 5.4 Conclusion

The electromagnetic enhancement mechanism is investigated using gold nanotriangular arrays fabricated by nanoimprinting technique. It is observed that non-resonant SERS effect is higher than resonant SERS effect in the nanotriangles. Hence it is proposed that the position of LSPR and excitation wavelength should be within a range to produce SERS effect. Chemical enhancement mechanism is also investigated in

TiO<sub>2</sub> nanoparticles and TiO<sub>2</sub> nanorods. A photo-induced charge-transfer mechanism due to the presence of surface defect states is confirmed in TiO<sub>2</sub> nanoparticles and TiO<sub>2</sub> nanorods.

## References

- [1] D.P. Fromm, A. Sundaramurthy, A. Kinkhabwala, P.J. Schuck, G.S. Kino, and W.E. Moerner, *J. Chem. Phys.* **124**, 61101 (2006).
- [2] K. Kneipp and H. Kneipp, *Acc. Chem. Res.* **39**, 443 (2006).
- [3] P.L. Stiles, J.A. Dieringer, N.C. Shah, and R.P. Van Duyne, *Annu. Rev. Anal. Chem.* **1**, 601 (2008).
- [4] A.D. Mcfarland, M.A. Young, J.A. Dieringer, and R.P. Van Duyne, *J. Phys. Chem. B* **109**, 11279 (2005).
- [5] C.L. Haynes and R.P. Van Duyne, *J. Phys. Chem. B* **107**, 7426 (2003).
- [6] K. a Willets and R.P. Van Duyne, *Annu. Rev. Phys. Chem.* **58**, 267 (2007).
- [7] B. H. Loo, *J. Electroanal. Chem* **136**, 209 (1982).
- [8] H. Wen, *Mol. Phys.* **88**, 281 (1996).
- [9] H. Yamada and Y. Yamamoto, *Surf. Sci.* **134**, 71 (1983).
- [10] A. Kudelski, W. Grochala, J. Bukowska, A. Szummer, and M. Dolata, *J. Raman Spectrosc.* **4555**, 430 (2016).
- [11] X. Wang, W. Shi, G. She, and L. Mu, *Phys. Chem. Chem. Phys.* **14**, 5865 (2012).
- [12] A.G. Milekhin, L.L. Sveshnikova, T.A. Duda, N.A. Yeryukov, N. V. Surovtsev, S. V. Adichtchev, E.E. Rodyakina, A.K. Gutakovskii, A. V. Latyshev, and D.R.T. Zahn, *Optoelectron. Instrum. Data Process.* **49**, 504 (2013).

- [13] L.G. Quagliano, *J. Am. Chem. Soc.* **126**, 7393 (2004).
- [14] Y. Wang, W. Ruan, J. Zhang, B. Yang, W. Xu, B. Zhao, and J.R. Lombardi, *J. Raman Spectrosc.* **40**, 1072 (2009).
- [15] Y. Wang, Z. Sun, H. Hu, S. Jing, B. Zhao, W. Xu, C. Zhao, and J.R. Lombardi, *J. Raman Spectrosc.* **38**, 34 (2007).
- [16] L. Yang, X. Jiang, W. Ruan, B. Zhao, W. Xu, and J.R. Lombardi, *J. Phys. Chem. C* **112**, 20095 (2008).
- [17] Z. Mao, W. Song, L. Chen, W. Ji, X. Xue, W. Ruan, Z. Li, H. Mao, S. Ma, J.R. Lombardi, and B. Zhao, *J. Phys. Chem. C* **115**, 18378 (2011).
- [18] X. Xue, W. Ji, Z. Mao, H. Mao, Y. Wang, X. Wang, W. Ruan, B. Zhao, and J.R. Lombardi, *J. Phys. Chem. C* **116**, 8792 (2012).
- [19] L. Yang, X. Jiang, W. Ruan, B. Zhao, W. Xu, and J.R. Lombardi, *J. Phys. Chem. C* **112**, 20095 (2008).
- [20] L. Yang, X. Jiang, W. Ruan, J. Yang, B. Zhao, W. Xu, and J.R. Lombardi, *J. Phys. Chem. C* **113**, 16226 (2009).
- [21] P. Tarakeshwar, D. Finkelstein-Shapiro, S.J. Hurst, T. Rajh, and V. Mujica, *J. Phys. Chem. C* **115**, 8994 (2011).
- [22] T. Ohsaka, F. Izumi, and Y. Fujiki, *J. Raman Spectrosc.* **7**, 321 (1978).
- [23] T. Mazza, E. Barborini, P. Piseri, P. Milani, D. Cattaneo, A. Li Bassi, C.E. Bottani, and C. Ducati, *Phys. Rev. B* **75**, 045416 (2007).
- [24] S. Mathew, A.K. Prasad, T. Benoy, P.P. Rakesh, M. Hari, T.M. Libish, P. Radhakrishnan, V.P.N. Nampoore, and C.P.G. Vallabhan, *J. Fluoresc.* **22**, 1563 (2012).
- [25] X. Wang, W. Shi, and L. Mu, *Phys. Chem. Chem. Phys.* **14**, 5891 (2012).

---

**Chapter 6**

---

## **Detection of bio and chemical analytes by surface enhanced Raman Spectroscopy**

The demonstration of the possibility of fabricated SERS substrates in bio and chemical sensing applications is presented in this chapter. The chapter is divided into two sections. In order to check SERS as an inexpensive and easily processable food adulterant sensor, the fabricated SERS substrates are used for the detection of Sudan I and melamine. Applicability of SERS technique as a biosensor is investigated via label-free detection of DNA of various species. Label-free detection of DNA by SERS opens up the possibility of SERS towards cancer cell detection and barcoding using DNA.

Applications of surface enhanced Raman scattering (SERS) in biochemistry, food safety, environmental monitoring and particularly in biomedical fields are rapidly growing<sup>1,2</sup>. Discovery of surface enhanced Raman scattering (SERS)<sup>3,4</sup> explored as a platform for getting fingerprint information from a molecule with single-molecule detection capability<sup>5</sup>. Therefore in addition to the efforts on developing highly sensitive reproducible SERS active substrates, SERS field is also focusing on biosensing and chemical sensing applications<sup>1</sup>.

### **6.1 Detection of food adulterants by SERS**

Nowadays synthetic azo compounds are widely used as coloring agents in many commercial applications<sup>6</sup>. Azo dyes are mainly found in printing ink, color waxes, oils, petrol, solvents, plastics, polishes as well as in foodstuffs. These azo dyes are identified as significant carcinogenic and mutagenic agents and are included in third category carcinogen by international agency for research on cancer (IARC)<sup>7</sup>. Still, these azo dyes are widely used in foodstuffs. One of the most well-known food additives is Sudan I which is widely used in chili powder, chili oil, chicken fast foods, turnip pickles, etc<sup>8</sup>. These contaminated products are widely used as ingredients in numerous ready meals. They are also detected in several dried spices products. Concerns about food safety demands the need for a rapid, low cost and highly sensitive technique for the detection of food adulterants even at ultra low concentration. The extensive method that is available for detection of Sudan I in contaminated foodstuffs is high performance liquid chromatography (HPLC) based instrumentation which involves chromatographic separation of Sudan I from the food matrix and subsequent detection by various detectors. Examples include HPLC fluorimetry, HPLC-UV/Vis and

flow injection chemiluminescence<sup>9,10</sup>. Molecularly imprinted solid phase extraction method is also developed, in which a glass carbon electrode is used to detect Sudan I in food stuffs<sup>10</sup>. Though chromatography based methods are reproducible, highly robust, have very good detection limits, and have relatively high sample throughput through automation, they possess disadvantages such as labor intensive sample pretreatment and extraction method, time consumption, high cost, and lack of portability. Therefore direct analysis of food adulterants such as Sudan I within the food matrix without any sample treatment would be highly desirable<sup>11</sup>.

Melamine is another industrial chemical compound used mainly in the production of plastics, primarily for countertops, fabrics, etc<sup>12</sup>. It is also metabolites of the insecticide cyromazine. Though melamine is not an approved ingredient, it has been added illegally to dairy products and powdered milk to overestimate their nutritional values and to make them appear rich in protein. Uptake of melamine leads to kidney disease and even mortality in infants.

Surface enhanced Raman spectroscopy is a high sensitive technique which provides chemical information of molecules in a nondestructive approach. Another highlight of Raman spectroscopy is that little or no sample preparation is required. Since water is a weaker Raman scatterer, samples in aqueous solution can also be analyzed without any special accessories. Recently portable Raman spectrometers are developed which again make SERS a proper technique for detection of food adulterants. Hence SERS is realized as an ideal technique for qualitative and quantitative applications that involves the analysis of organic and inorganic chemicals. There are reports that combine SERS with chemometric

analysis for the detection and quantification of food adulterants from food matrix<sup>13</sup>. In this work, detection of Sudan I and melamine using as-prepared SERS substrates such as silver nanocube (Ag NC), Ag-TiO<sub>2</sub>, pyramidal arrays and silver nanotriangular arrays are demonstrated.

### 6.1.1 Experimental details

For detection of melamine, SERS substrates (Ag NC) were immersed in 10<sup>-10</sup> M melamine aqueous solution for 30 min and then the samples were removed and were rinsed with de-ionized water to remove unadsorbed melamine.

For the detection of Sudan I, 10<sup>-6</sup> M Sudan I solution was prepared in methanol and 40 μL of the solution was deposited onto the Ag-TiO<sub>2</sub> based SERS substrate and dried in air.

The SERS spectra were recorded on a Horiba Jobin Yvon LabRAM HR microRaman spectrometer through 100X (0.90 NA) microscope objective, coupled with a Peltier-cooled charge-coupled device (CCD) detector. He-Ne laser (wavelength: 632.8 nm) was used as excitation laser. The incident laser power was kept at 1 mW and total accumulation time of 5 s was employed during measurement.

### 6.1.2 Results and discussion

It is found that the SERS substrate shows strong SERS response for the detection of melamine. The normal Raman spectrum of bulk melamine is shown in figure 6.1 and all the peaks match well with reported values<sup>12</sup>. SERS spectrum of 10<sup>-10</sup> M melamine using silver nanocube based SERS substrate is given in figure 6.2. The most intense peak at 660 cm<sup>-1</sup> arises from ring breathing mode II of melamine and

involves in-plane deformation of the triazine ring in melamine molecule and the peak around  $982\text{ cm}^{-1}$  is assigned to the ring breathing mode I of the triazine ring. The detection limit for melamine is also found to be  $10^{-10}\text{ M}$ .

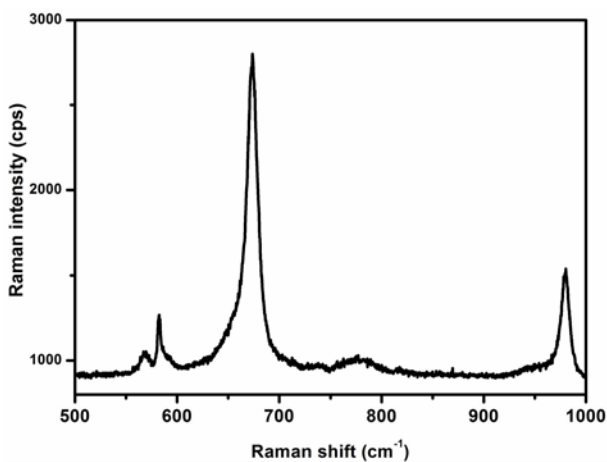


**Figure 6.1:** Normal Raman spectrum of bulk melamine

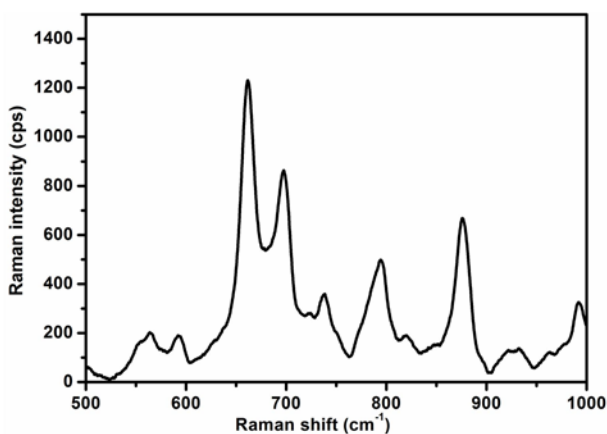


**Figure 6.2:** SERS spectrum of  $10^{-10}\text{ M}$  melamine using Ag NC based SERS substrate

SERS spectrum of Sudan I was carried out using Ag-TiO<sub>2</sub> based SERS substrate. The SERS spectrum of Sudan I with a concentration of  $1 \times 10^{-6}$  M is shown in figure 6.3 and the peaks at 464, 1450 and 1590 cm<sup>-1</sup> are assigned to out of plane -C=C- deformed vibration, C-N=N deformed vibration and C-O in plane deformed vibration respectively<sup>14</sup>.

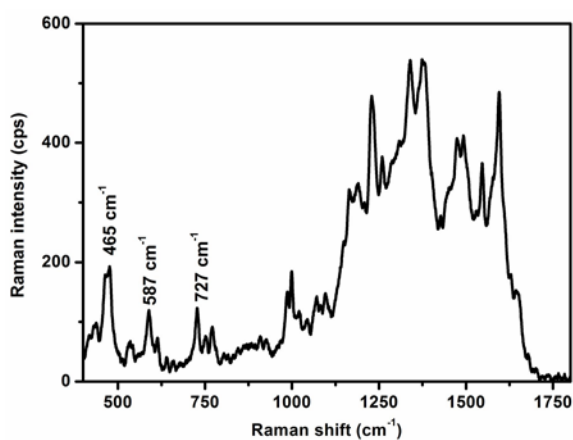


**Figure 6.3:** SERS spectrum of  $2 \times 10^{-6}$  M Sudan I using Ag-TiO<sub>2</sub> based SERS substrate

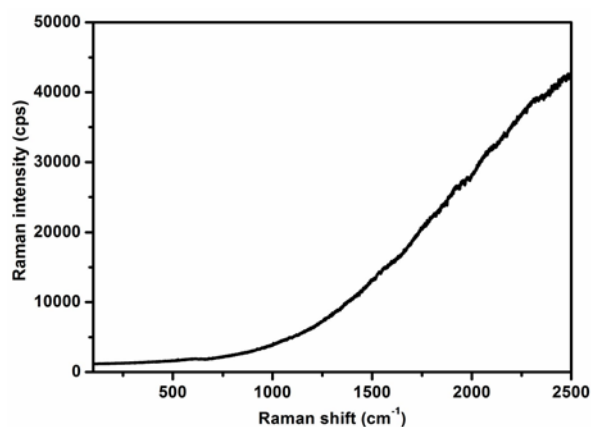


**Figure 6.4:** Normal Raman spectrum of bulk Sudan I

Even though the characteristic peaks of Sudan I is observed in SERS spectrum, bulk Sudan I doesn't produce any Raman signal and is dominated by fluorescent background. The normal Raman spectrum of bulk Sudan I is shown in figure 6.4.

The result proves the possibility for fast detection of additives in food matrix and proposes the *in vitro* analysis of food stuffs containing melamine and Sudan I.

## 6.2 Label-free detection of DNA by SERS

SERS is realized as an excellent platform for the development of diagnostic assays and optical imaging tools<sup>15</sup> with the following advantages. As compared with fluorescence peaks, Raman peaks have narrow spectral width. Fluorescence peaks are 10-100 times wider than Raman peaks. Hence SERS possesses excellent multiplexing capabilities of individual molecules. Additional advantages for SERS over fluorescence imaging is the possibility of using a single excitation source for the analysis of multiple probes, low photobleaching effect and low background from water due to very weak Raman signal from the water. As a result, research on bio and chemical analytical application of SERS have grown exponentially. Specific applications such as DNA sequence analysis<sup>16</sup>, diagnostics<sup>17</sup>, clinical transformation, biosensing<sup>18</sup>, etc., have been demonstrated successfully.

Various techniques such as identification of cancer biomarkers, *in vitro* and *in vivo* identification of DNA modifications, etc., have been employed to attain consistent and specific information regarding chemically modified base injuries present in the cancer cell. A SERS based method to detect chemical modifications in RNA and DNA both

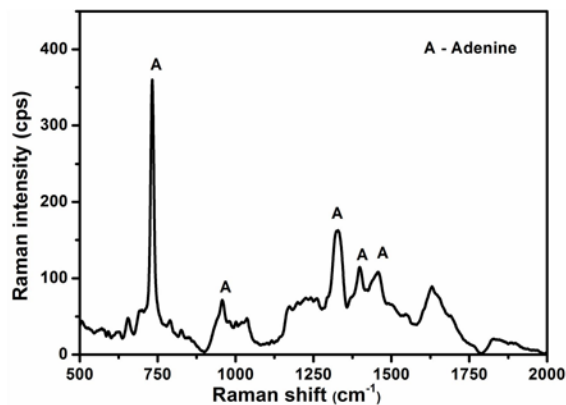
qualitatively and quantitatively is still a challenge. Nowadays, SERS is recognized as a powerful tool for detection of DNA which is the base of numerous technologies ranging from forensic testing in law-enforcement to diagnostic screening in clinical medicine. Although numerous SERS studies on DNA have been performed to date, development of more practical SERS substrates with sensitive and reliable detection strategies for label-free DNA detection is also a major hurdle for SERS based detection. Here an attempt to barcode the organism according to their DNA sequences is carried out by analyzing the Raman spectra of DNA of various species or organisms.

### 6.2.1 Experimental details

DNA of salmon fish with concentration 0.1 g/ml and DNA of *Escherichia coli* (*E. coli*) with concentration 80 ng/ml were used for the analysis. For the SERS analysis, DNA was uncoiled by heating its solutions in TE buffer [10x Tris ethylenediaminetetraacetic acid (EDTA) (TE), 100 mM Tris–Cl (pH 8.0), 10 mM EDTA (pH 8.0), and sterilizing solutions by autoclaving for 20 min at 15 psi (1.05 kg/cm<sup>2</sup>) on liquid] to 86°C for 10 min. The prepared SERS substrates (Ag NC, pyramidal arrays and nanotriangular arrays) were then immersed in DNA solutions for 12 h. Finally, the substrates were taken out and washed carefully with de-ionized water, followed by drying in N<sub>2</sub> flow.

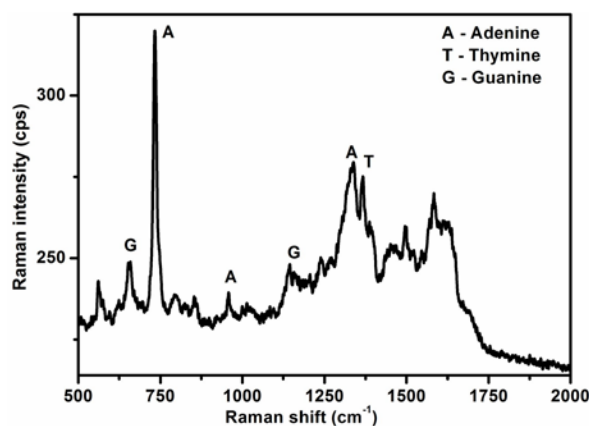
### 6.2.2 Results and discussion

Figure 6.5 shows SERS spectrum of uncoiled DNA of salmon fish using Ag NC based SERS substrate. The Raman peaks corresponding to the DNA are observed at 732, 956, 1331, 1397 and 1454 cm<sup>-1</sup>. These can be assigned to the peaks of adenine<sup>19</sup>.



**Figure 6.5:** SERS spectrum of salmon fish DNA using Ag NC based SERS substrate

SERS spectrum of DNA of salmon fish was again recorded using pyramidal array based SERS substrate. The corresponding spectrum is shown in figure 6.6. Here, in addition to peaks corresponding to adenine, guanine and thymine are also observed<sup>19–22</sup>. Nevertheless, both spectra of DNA of salmon fish are dominated by a peak at  $732\text{ cm}^{-1}$  which corresponds to adenine base.



**Figure 6.6:** SERS spectrum of salmon fish DNA using pyramidal array based SERS substrate

DNA detection was carried out for second organism, *E. coli* using the fabricated SERS substrates. SERS spectrum of *E. coli* DNA using pyramidal array based SERS substrate is shown in figure 6.7. The spectrum shows the peaks corresponding to adenine, thymine, and guanine<sup>19</sup>. It is also noticed that unlike SERS spectra of salmon fish DNA, the peak corresponds to adenine base located at  $732\text{ cm}^{-1}$  is not dominant here.

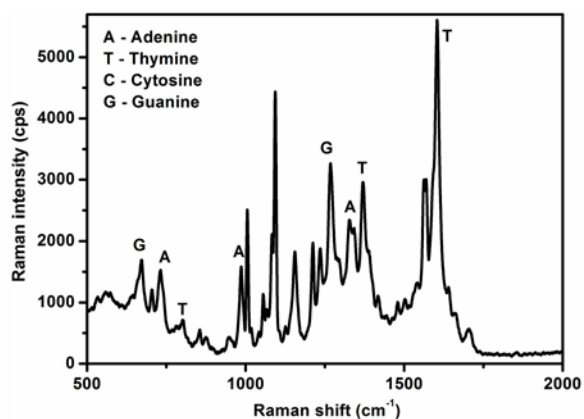


**Figure 6.7:** SERS spectrum of *E. coli* DNA using pyramidal array based SERS substrate

SERS spectrum of *E. coli* DNA using nanotriangular array based SERS substrate is given in figure 6.8. Raman signal is observed for a very low concentration of 80 ng/ml while bulk DNA doesn't show any signal. The peaks corresponding to all the bases adenine, thymine, cytosine and guanine are enhanced and match well with the reports<sup>20-22</sup>. It is observed that many of the peaks that obtained from nanotriangular array based SERS substrate are not observed in the spectra from pyramidal array based substrate (figure 6.7). These results demonstrate the sensitivity and potential of nanotriangular array based SERS substrates for label- free detection of DNA.

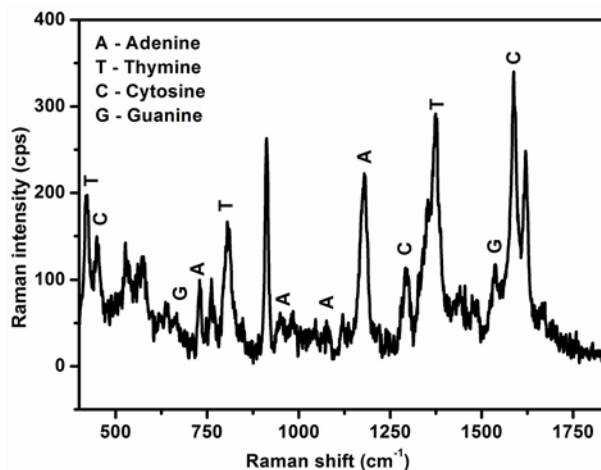


**Figure 6.8:** SERS spectrum of *E. coli* DNA using nanotriangular array based SERS substrate

All the DNA contain the four fundamental bases i.e. adenine, thymine, guanine, and cytosine. But the order of arrangement of these bases are different in different organisms and is always unique to the organism. Since Raman spectra are highly sensitive to chemical composition, their Raman spectra are also unique to each DNA. From the above analysis, it can be proposed that there is a probability of achieving unique SERS spectra corresponding to DNA of different organisms. Further studies are required for SERS based DNA based barcoding.

### 6.3 Conclusion

Detection of food adulterants and label-free detection by SERS is demonstrated using the fabricated SERS substrates. Sudan I with a concentration of  $10^{-6}$  M is detected using Ag-TiO<sub>2</sub> based SERS substrate and melamine with a concentration of  $10^{-10}$  M is detected using Ag NC

based SERS substrate. This demonstrate the possibility of food adulterant detection in an easy and inexpensive technique. DNA of salmon fish and E. coli are detected via SERS without the use of any labeling agents. DNA of E. coli with a concentration of 80 ng/ml is detected using nanotriangular array based SERS substrate. This study highlights the future possibility of label-free detection by SERS in cancer cell detection and DNA barcoding.

### References

- [1] S. Schlücker, *Angew. Chem. Int. Ed.* **53**, 4756 (2014).
- [2] X. Qian and S.M. Nie, *Chem. Soc. Rev.* **37**, 912 (2008).
- [3] M. Fleischmann, P.J. Hendra, and A.J. McQuillan, *Chem. Phys. Lett.* **26**, 163 (1974).
- [4] D.L. Jeanmaire and R.P. Van Duyne, *J. Electroanal. Chem. Interfacial Electrochem.* **84**, 1 (1977).
- [5] K. Kneipp, Y. Wang, H. Kneipp, L.T. Perelman, I. Itzkan, R.R. Dasari, and M.S. Feld, *Phys. Rev. Lett.* **78**, 1667 (1997).
- [6] J. Noonan, *Color Additives in Food*, vol. I, 2nd edn. (Florida: CRC Press, 1981).
- [7] M. Stiborová<sup>2</sup>, V. Martínek, H. Rýdlová, P. Hodek, and E. Frei, *Cancer Res* **62**, 5678 (2002).
- [8] V. Martinek and M. Stiborova, *Collect. Czech. Chem. Commun.* **67**, 1883 (2002).
- [9] R. Rebane, I. Leito, S. Yurchenko, and K. Herodes, *J. Chromatogr. A* **1217**, 2747 (2010).

- [10] W. Wardencki, M. Michulec, and J. Curylo, *Int. J. Food Sci. Technol.* **39**, 703 (2004).
- [11] C. V Di Anibal, L.F. Marsal, M.P. Callao, and I. Ruisánchez, *Spectrochim. Acta. A. Mol. Biomol. Spectrosc.* **87**, 135 (2012).
- [12] S. Ehling, S. Tefera, and I.P. Ho, *Food Addit. Contam.* **24**, 1319 (2007).
- [13] W. Wang, M. Xu, Q. Guo, Y. Yuan, R. Gu, and J. Yao, *RSC Adv.* **5**, 47640 (2015).
- [14] W. Cheung, I.T. Shadi, Y. Xu, and R. Goodacre, *J. Phys. Chem. C* **114**, 7285 (2010).
- [15] M. Vendrell, K.K. Maiti, K. Dhaliwal, and Y. Chang, *Trends Biotechnol.* **31**, 249 (2013).
- [16] K. Faulds, W.E. Smith, and D. Graham, *Analyst* **130**, 1125 (2005).
- [17] H.-W. Cheng, S.-Y. Huan, and R.-Q. Yu, *Analyst* **137**, 3601 (2012).
- [18] P. Negri and R. a Dluhy, *J. Biophotonics* **6**, 20 (2013).
- [19] S.E.J. Bell and N.M.S. Sirimuthu, *J. Am. Chem. Soc.* **128**, 15580 (2006).
- [20] T. Xu, J. Huang, L. He, Y. He, S. Su, and S. Lee, *Appl. Phys. Lett.* **99**, 153116 (2011).
- [21] K.F. Domke, D. Zhang, and B. Pettinger, *J. Am. Chem. Soc.* **129**, 6708 (2007).
- [22] A. Barhoumi and N.J. Halas, *J. Phys. Chem. Lett.* **2**, 3118 (2011).



## Concluding remarks

This chapter summarizes the results presented in this thesis and the future prospects of surface enhanced Raman spectroscopy.

### Summary of the thesis

A number of fundamental and applied researches are being undertaken in the field of surface enhanced Raman spectroscopy by different research groups. In this thesis, we have discussed the fabrication of an efficient SERS active substrate in an economic way, investigation of various SERS enhancement mechanisms and finally demonstration of its applications.

Since major contribution to the SERS enhancement is electromagnetic enhancement, great attention has been given to the fabrication of metal nanostructures that generate very large enhancement in a reproducible way by an economic technique. Anisotropic metal nanostructures exhibit large electromagnetic enhancement, hence silver nanocubes and silver nanotriangles are fabricated as SERS substrates. Initially, SERS substrate with an enhancement factor of about  $1.2 \times 10^8$  is fabricated using solvothermally synthesised silver nanocubes. To further improve the SERS enhancement factor and reproducibility of SERS

intensity, arrays of nanotriangular pillars are fabricated by a non-conventional lithographic technique, nanoimprinting lithography. The nanoimprinting technique facilitated successful fabrication of cost effective and highly reproducible SERS active substrate with an enhancement factor of  $2.9 \times 10^{11}$ . This nanotriangular pillar based SERS substrate is positioned as patterned SERS substrate with highest enhancement factor.

Like anisotropic metal nanostructures, metal nanostructures with 1-2 nm inter-particle distances also produce very large electromagnetic enhancement. Titanium dioxide nanorods are employed as a template for the growth of silver nanoparticle with "hot spots". Since titanium dioxide possesses photocatalytic activity, a recyclable SERS substrate with large enhancement factor is successfully fabricated by decorating silver nanoparticles onto titanium dioxide nanorods. The substrate shows an enhancement factor of  $7 \times 10^8$  and is used for detection of food adulterant, Sudan I.

In addition to the effect of shape, size and inter-particle gap of metal nanostructures on electromagnetic effect, the correlation between localized surface plasmon resonance wavelength of metal nanostructures and excitation wavelength for SERS measurement are investigated using gold nanotriangular arrays. Even though chemical enhancement contribution to the total SERS enhancement is small, significant research focused on the chemical enhancement of SERS in metal oxide nanostructures reveal the mechanism of chemical enhancement. A photo-induced charge-transfer enhancement is observed in titanium dioxide nanoparticles and titanium dioxide nanorods. It is confirmed that surface defect states mediate the charge-transfer in  $\text{TiO}_2$

nanostructures and SERS enhancement in TiO<sub>2</sub> nanorods is higher than in TiO<sub>2</sub> nanoparticles.

Highly sensitive detection capability at picomolar level is the significance of SERS to be applied in the field of bio and chemical analyte sensors. Food adulterants such as melamine and Sudan I are detected using the fabricated SERS substrate. Label-free detection of various DNA sequences is also demonstrated by SERS.

### **Future scope**

The incorporation of an array of nanotriangular pillars onto the facet of an optical fiber can act as a probe for in situ surface enhanced Raman scattering (SERS) detection. The surface plasmons in the nanotriangles resonate with the incident excitation wavelength that can produce SERS activity. The excitation light can be coupled to the probe through the other facet of fiber. Therefore it is possible to collect the enhanced Raman signal from multiple analytes simultaneously.

Silver nanotriangular arrays can be further used for other plasmonic applications which are described below. Plasmonic nanostructures have been widely applied in the field of energy conversion, photocatalysis, etc. In plasmonic solar cells, metallic nanostructures facilitate enhanced absorption of photons and thereby avoid the use of relatively thick absorber layer used in traditional thin film solar cells. With the advantage of metal nanostructures such as geometry dependent LSPR wavelength, they can be employed in high density optical data storage devices. LSPR wavelength is also sensitive to dielectric constant of surrounding medium and that can be exploited for sensing applications. Biomedical applications of metal nanostructures are that they are used

as contrast agents and label agents in diagnostics, imaging and in therapy.

In this thesis, only demonstration of bio and chemical analyte detection by SERS is carried out. So future works can be focused on other applications as biosensors and chemical sensors. The SERS substrate can be used for cancer cell detection. Early detection of genetic modifications is highly desirable for the successful treatment of cancer cell. The modifications in the cellular constituents are a consequence of reactive oxygen species (ROS), continuous exposure to the cellular constituents to carcinogenic chemicals and intense ionization radiations which ultimately result in various types of cancers. The traditional sensing methods exhibit drawbacks such as expensive and complex enzyme based target or signal amplification procedures. Surface enhanced Raman spectroscopy (SERS) have already received keen attention as a safe and reliable technique to detect cancer at the very early stages, in a simpler and relatively inexpensive way. With the support of Raman marker, the variations in the chemical environments and associated modifications in the molecular vibrations in DNA can be precisely detected. Thus it is possible to distinguish the cancer cell from a normal cell.

Recyclable Ag-TiO<sub>2</sub> based SERS substrate can be employed for both quantitative and qualitative detection of food adulterants, organic pollutants, etc. It can be employed as a promising online sensor capable of monitoring continuous flows in real time.

.....✪.....